THE RECOVERY OF PLATINUM GROUP METALS FROM LOW GRADE CONCENTRATES TO AN IRON ALLOY USING SILICON CARBIDE AS REDUCTANT

by

Willem du Toit Malan

Thesis presented in partial fulfilment

of the requirements for the Degree

of

MASTER OF ENGINEERING

(EXTRACTIVE METALLURGICAL ENGINEERING)

in the Faculty of Engineering

at Stellenbosch University

Supervisor

Professor G. Akdogan

Co-Supervisor

Professor S.M. Bradshaw

DecŜYōŜℕ 2014

Declaration

By submitting this thesis electronically, I declare that the entirety of the work contained therein is my own, original work, that I am the sole author thereof (save to the extent explicitly otherwise stated), that reproduction and publication thereof by Stellenbosch University will not infringe any third party rights and that I have not previously in its entirety or in part submitted it for obtaining any qualification.

21 November 2014

Abstract

In this study, SiC reduction of Rowland and Easterns LG (Low Grade) concentrates was investigated. The purpose of the study was to investigate the feasibility of SiC as reductant with respect to metal fall, PGM grade in the alloy, slag composition, Cr solubility and overall PGM recovery. The integration of such process in the current matte-based collection process was also investigated.

Currently, the matted-based collection process is most widely used for PGM recovery, but because PGM containing concentrates are becoming more enriched with UG2 (Upper Group 2) LG concentrates, it is expected to be integrated or replaced with an alloy collection process. This kind of process offers greater flexibility to the different types of ore that could be used. The process is chromium tolerant and environmentally friendly.

For this purpose Rowland and Easterns UG2 LG Concentrate samples from Lonmin Western Platinum Limited were analysed with XRD, XRF and ICP-MS and it was found that SiO_2 and MgO are the most abundant oxides and Pd is the most abundant element from the PGMs. Sulphide bearing minerals such as chalcopyrite were detected in low concentrations (below 1 %) and Cr_2O_3 concentrations are between 2 – 4 %. The FeO/SiO_2 ratio was lower in Rowland LG concentrate.

SiC reduction of Rowland and Easterns concentrate was done at 1600°C. Reductant to concentrate ratios for laboratory scale experiments were ranged from 2.5 to 3.5 kg SiC / 100 kg concentrate. SiC reduction of Rowland concentrate had different reduction times. The duration of reduction experiments ranged from 30 - 180 min.

PGM recoveries from SiC reduction of Rowland concentrate were very poor (below 10 %) and Fe recoveries were lower than 50 %. A slag viscosity at the end of the melt of more than 4 poise was responsible for poor phase separation. SEM images revealed metal prills entrained in the slag phase instead of settling and combining to the alloy globule at the bottom of the crucible. However, PGM recoveries from SiC reduction of Easterns concentrate was significantly better. More than 85 % of Ir and Pd and almost 60 % of Pt were recovered in a test with a reductant to concentrate ratio of 3.5 kg SiC / 100 kg Easterns concentrate. Fe recovery was also the highest at 66%. Cr and Si concentrations were below 5 % in total. The slag viscosity at the end of melt was calculated to be less than 4 poise and a SEM image of a slag sample revealed few entrained metal prills.

After the above findings on the importance of viscosity, it was decided to increase the FeO content in the initial concentrate charge in order to decrease slag viscosity, increase metal fall (PGM collecting phase) and further increase PGM recovery. Peirce-Smith converter slag was used for this purpose. A test was conducted with the addition of 10 kg converter slag / 100 kg Easterns concentrate. The reductant to concentrate ratio was kept at 3.5 kg SiC / 100 kg Easterns concentrate. The results revealed that Ir and Pd recoveries were more than 95%, while Pt recovery was almost 70%. Fe recovery increased to 76 %. On the basis of the results from the test, an optimum feed ratio between Easterns LG concentrate, Rowland concentrate and Peirce-Smith converter slag was calculated. Thermodynamic phase equilibrium calculations predicted that the concentrate charge should consist of 60 - 80% Easterns concentrate with a slag addition of 30 – 40 kg converter slag / 100 kg LG concentrate. SiC reduction of this optimum LG concentrate charge is expected to recover more than 90% of all PGMs. Cr and Si concentrations in the alloy will be below 1 % in total. The

amount of converter slag as an addition will be however limited by final PGM grade in the alloy, furnace slag quantities recycled and slag resistivity required in the alloy furnace.

The effectiveness of SiC as reductant was also compared to C reduction. C reduction of an optimum concentrate charge had a marginally higher metal fall at the same reductant to concentrate ratio than SiC reduction of an optimum concentrate charge. However, gas emissions are on average 3 times higher for C reduction of a concentrate charge and C reduction requires at least 300 MJ more to smelt 1 ton of LG concentrate than SiC reduction. This is mostly due to C reacting endothermically with FeO to produce Fe(l) and CO(g) in contrast to SiC reacting exothermically with FeO to produce Fe(l), SiO_2(l) and CO(g).

Integrating SiC reduction of LG concentrates into the existing smelting route at Lonmin was also proposed through a process flow diagram. From an economic point of view, it was found that SiC reduction of 1 ton of LG concentrate charge with a converter slag addition requires almost 700 MJ more than the smelting of a UG2 blended concentrate to produce a matte phase. However it must be taken into account that the sulphide rich layers in the Bushveld complex are being depleted rapidly and alternative processes such as SiC reduction and alloy collection process will be utilized faster than expected. Moreover, gas emissions from reductive smelting is considerably lower, hence it is a more environmentally friendly process. Finally, from the findings of this study, it could be said that base metals and PGMs could be recovered in an iron alloy from SiC reduction of LG concentrate with converter slag additions. Therefore integrating such a process into the matte-based collection process could be considered as a future alternative to smelting UG2 LG concentrates.

Opsomming

In hierdie studie, word SiC reduksie met Rowland en Oostelikes LG (Lae Graad) konsentrate ondersoek. Die doel van die studie was om die doeltreffendheid van SiC as reduktant te ondersoek met betrekking tot metaalval, PGM graad in die allooi, slaksamestelling (spesifiek word daar gekyk na Cr oplosbaarheid) en algehele PGM herwinning. Die integrasie van die proses in die huidige mat-gebaseerde versamelingproses word ook ondersoek.

Tans word die mat-gebaseerde versamelingproses die algemeenste gebruik om PGM'e te kollekteer, maar omdat PGM konsentrate al hoe meer verryk word met UG2 (Upper Group 2) LG konsentrate, word daar verwag dat dit geïntegreer of vervang gaan word met 'n allooi-versamelingproses. Hierdie tipe proses bied groter buigsaamheid om die verskillende reekse van erts wat gebruik kan word. Die proses kan ook chroom hanteer en is omgewingsvriendelik.

Vir hierdie doel was Rowland en Oostelikes UG2 LG konsentraatmonsters van Lonmin Western Platinum Limited ontleed met XRD, XRF en ICP -MS en met die ontleding was daar gevind dat SiO_2 en MgO die volopste oksides was en dat Pd die volopste elemente van die PGMe was. Sulfiedminerale soos chalkopiriet is in lae konsentrasies opgespoor (minder as 1%) en Cr_2O_3 konsentrasies is tussen 2-4 %. Die FeO/SiO_2 verhouding was laer in Rowland konsentraat.

SiC reduksie van Rowland en Oostelikes konsentrate is teen 1600 °C uitgevoer. Die reduktant tot konsentraat verhouding vir laboratoriumskaal eksperimente het gewissel van 2.5 – 3.5 kg SiC / 100 kg konsentraat. SiC reduksie van Rowland LG konsentraat het verskillende reduksie tye gehad. Die duur van die reduksie eksperimente het gewissel van 30-180 min.

PGM herwinning van SiC reduksie met Rowland konsentreer was baie laag (onder 10 %) en Fe herwinning was minder as 50%. 'n Slakviskositeit aan die einde van die smelt was hoër as 4 poise en was verantwoordelik vir die swak skeiding van fases. SEM beelde het gewys dat fyn metaalstukkies opgehou was in die slakfase in plaas daarvan dat dit vestig en kombineer met die allooibolletjie aan die onderkant van die smeltkroes. In teenstelling was die PGM herwinning van SiC reduksie met Oostelikes konsentraat aansienlik beter. Meer as 85 % van Ir en Pd was herwin en byna 60% van Pt was herwin tydens 'n toets met 'n reduktant tot konsentraat verhouding van 3.5 kg SiC / 100 kg Oostelikes konsentraat. Fe herwinning was 66% en was ook die hoogste van al die eksperimente. Cr en Si konsentrasies was minder as 5 % in totaal. Die slakviskositeit aan die einde van smelt was bereken en is minder as 4 posie. 'n SEM beeld van 'n slakmonster het baie min vasgevangde metaalstukkies getoon.

Na afloop van die bogenoemde bevindinge oor die belangrikheid van viskositeit, was daar besluit om die FeO inhoud van die aanvanklike konsentraat te verhoog. Dit was gedoen om die slakviskositeit te verminder, die metaalval (PGM kollektering fase) te verhoog en sodoende die PGM herwinning verder te verbeter. Vir die doel was Peirce -Smith omskakelaarslak gebruik. ’n Toets was uitgevoer met die toevoeging van 10 kg omskakelaarslak / 100 kg Oostelikes konsentraat. Die reduktant tot konsentraat verhouding was behou by 3.5 kg SiC / 100 kg Oostelikes konsentraat. Die resultate het getoon dat meer as 95 % van Ir en Pd herwin was, terwyl byna 70 % Pt herwin was. Die Fe herwinning het toegeneem tot 76%. Op grond van die resultate van die toets, is 'n optimale verhouding tussen Oostelikes konsentraat, Rowland konsentraat en Peirce -Smith omskakelaarslak bereken. Termodinamiese modellering voorspel dat die begin LG konsentraat voer uit 60 – 80 % Oostelikes

konsentraat moet bestaan, met 'n slak toevoeging van 30 – 40 kg omskakelaarslak / 100 kg LG konsentraat. Daar word verwag dat meer as 90 % van PGM'e herwin sal word vanaf SiC reduksie met ’n optimum LG konsentraat voer. Cr en Si konsentrasies in die allooi sal minder as 1% in totaal wees. Die hoeveelheid slak wat bygevoeg kan word sal egter beperk word deur die finale PGM graad in die allooi, oond-slak hoeveelhede wat herwin kan word en slakweerstand wat benodig word in die allooi-oond.

Die effektiwiteit van SiC as reduktant is ook vergelyk met C reduksie. C reduksie van ’n optimale konsentraatvoer het 'n effens hoër metaalval wanneer dieselde reduktant tot konsentraat verhouding behou was vir SiC reduksie van 'n optimale konsentraatvoer. Gas hoeveelhede van C reduksie is gemiddeld 3 keer meer en vereis te minste 300 MJ meer om 1 ton LG konsentraat te smelt. Dit is hoofsaaklik te wydte aan C wat endotermies reageer met FeO om Fe (l) en CO (g) te produseer, in teenstelling met SiC wat eksotermies reageer met FeO om Fe (l), SiO2(l) en CO (g) te produseer.

Integrasie van SiC reduksie met LG konsentrate in die bestaande smeltroete by Lonmin Western Platinum Limited is ook voorgestel deur 'n proses vloeidiagram. Uit 'n ekonomiese oogpunt, is daar gevind dat SiC reduksie van 1 ton LG konsentraatvoer met 'n omskakelaarslak byvoeging ongeveer 700 MJ meer benodig as om 1 ton UG2 gemengde konsentraat te smelt en 'n mat-fase te produseer. Dit moet wel in ag geneem word dat die sulfied ryk lae in die Bosveld-kompleks vinnig uitgeput word en dat hierdie alternatiewe prosesse soos SiC reduksie en ’n allooiversameling proses vinniger as verwagtend benut sal word. Verder, gas hoeveelhede van SiC reduksie is laer en daarom is dit 'n meer omgewingsvriendelik proses. Ten slotte, vanaf die bevindinge van hierdie studie, kan dit gesê word dat basismetale en PGM'e in 'n ysterallooi herwin kan word deur middel van SiC reduksie met LG konsentrate en die toevoeging van omskakelaarslak. Daarom kan die integrasie van so 'n proses in die huidige mat-gebaseerde versameling proses beskou word as 'n alternatief vir die toekoms om UG2 LG konsentrate te smelt.

Acknowledgements

As the Author of this dissertation, I would like to thank my head supervisor, Prof Guven Akdogan for guiding me with his knowledge and infectious enthusiasm though the course of the project. Without him the project would not have been possible. I would also like to thank Prof J.J. Eksteen for funding the project from the beginning.

Next, I would like to thank Harry Delport for assisting me with the modification of the furnace and all that was required to conduct pyrometallurgical experiments.

I am grateful to Lonmin Western Platinum Limited for their financial support and for the opportunity to conduct such a study, and especially to Riaan Bezuidenhoud from Lonmin Western Platinum Limited who assisted me in various aspects of the project. Many other people were involved in the analysis of the samples, especially the staff from the central analytical facility of Stellenbosch and Goldenpond 67. There contributions to the project are greatly appreciated.

Lastly, I would like to thank my co-supervisor Prof. S.M. Bradshaw for his contributions to the project.

Table of Contents

List of Figures

List of Tables

Nomenclature

Abbreviation	Explanation
UG2	Upper Group 2
PGM	Platinum Group Metals (for the purposes of this paper Ir, Pt, Pd, Rh, and Ru)
LG	Low Grade
PMR	Precious Metal Refinery
BMR	Base Metal Refinery
PSC	Peirce-Smith converter
XRD	X-Ray Diffraction
XRF	X-Ray Florescence
ICP-MS	Inductively Coupled Plasma Mass Spectrometry
SEM	Scanning Electron Microscope
EDX	Energy Dispersive X-Ray
AC	Alternating Current
DC	Direct Current
STF	Split Tube Furnace
Wt. %	Weight percentage
PPM	Parts Per Million
MLA	Mineralogical Analysis
P_{O_2}	Oxygen partial pressure
TGA	Thermogravimetric Analysis
STDEV	Standard deviation

*Some symbols are not shown here and is identified in the respective sub-sections of the report.

1. Introduction

Background

South Africa is the leading supplier of platinum group metals (PGM) in the world and these PGMs are mostly found in nickel-copper bearing ores. Most of the PGMs are contained in the Merensky and UG2 Reefs of the Bushveld Igneous Complex and need to be treated in order to extract these PGMs. In Merensky ore, the major base-metal sulphide mineral is pyrrhotite, with pentlandite, chalcopyrite, pyrite and minor amount of other sulphides also present. In UG2 (Upper Group 2) ore the major base-metal sulphide present is pentlandite. Pyrrhotite is found in moderate amount, and millerite and pyrite in minor amounts. To reduce mining costs, platinum mining is becoming more UG2 based and the resulting concentrates contain high levels of chromite, unless the UG2 LG ore is blended with Merensky ore. Therefore it is critical that new and improved extraction methods need to be developed and exploited. The methods used in the recovery of the PGMs from these ores consist of physical concentration techniques, pyro-metallurgical processing and hydrometallurgical extraction of the base metals followed by the PGMs [1, 2].

During pyrometallurgical processing, the nickel-copper concentrates acquired from the mill-float concentration step are smelted to bring about physical and chemical changes that enable recovery of base metals, PGMs and other valuable metals in crude form. In general, the idea is to melt a concentrate in a furnace to produce a matte which contains all the sulphides below a carefully maintained slag layer. This matte, which still contains large amounts of iron and sulphur, is oxidized in a converter (known as a Peirce Smith converter) in order to lower the iron and sulphur concentrate, while at the same time increasing the PGM grade. Conventional PGM matte smelting essentially requires the presence of a certain quantity of base metal sulphides in order to collect the PGMs in a molten sulphidic phase in the smelting furnace. However, the quantity of chrome oxide in the feed materials (particularly UG2 related) need to be strictly controlled to avoid the build-up of high melting chromite spinels [1, 2].

Currently, the matte-based collection process is most widely used for PGM recoveries, but because PGM containing concentrates are becoming more enriched with UG2 concentrates, it is expected to be integrated or replaced with an alternative processes. Mintek (Randburg, South Africa) has developed an alternative process for smelting PGM-containing oxide feed materials that contain low amounts of sulphur, and often high amounts of chromium oxide, known as the Conroast process. The process involves the extraction of the sulphur content from a LG concentrate in a very well enclosed fluidized-bed roaster. There after the dead-roasted sulphide concentrates are smelted, in order to generate a small amount of an iron alloy in which PGMs and base metals are collected. A slag is also produced, which mostly contain unwanted materials and very low levels of residual PGMs. The desired degree of reduction is controlled by adjusting the carbon addition. However, it is known that highly reducing conditions provided high recoveries of the valuable metals, but also, high iron collection diluted the grade of the alloy, resulting in unacceptable PGM recoveries. In order to have high PGM recoveries, mild reducing conditions should be maintained [1, 2].

Hypothesis

It is hypothesized that it is possible to sustainably produce a PGM-containing alloy and discardable slag from the reaction of low grade concentrates and **silicon carbide** as reducing agent. It is known that silicon carbide would react exothermically with the low grade concentrate, rather than endothermically as for instance coal or coke. Further it is known that only a third of the amount of gases that are normally produced will be generated with SiC as reducing agent. The following simplified reactions have been proposed to illustrate this.

$$FeO(s) + C(s) = Fe(l) + CO(g) \quad \text{(Eq.1.1)}$$

$$3FeO(s) + SiC(s) = 3Fe(l) + SiO_2(l) + CO(g) \quad \text{(Eq.1.2)}$$

It is further postulated that a more acidic slag and moderate reducing conditions should aid in Cr_2O_3 reduction in the slag to CrO and increased Cr-solubilities.

Project plan

In this study, Rowland and Easterns UG2 LG concentrates were smelted with SiC as reductant. Before lab scale experiments could be conducted, high temperature phase equilibrium calculations were required and done with the commercial software package, FactSage 6.2. The results from the thermodynamic evaluation will give an idea on what experimental parameters will be most influential. The effect of process parameters such as reductant to concentrate ratio, temperature and different reductants on metal fall, alloy composition, slag composition and gas composition will be investigated. However, modelling physical properties of the melt with thermodynamic modelling can only be investigated in a limited paradigm. These physical characteristics could significantly influence phase separation. These include, viscosity, interfacial tension, entrainment of alloy or matte in the slag phase and size of matte/alloy droplets. Once it was established which parameters from thermodynamic modelling are most influential, an experimental matrix was set-up.

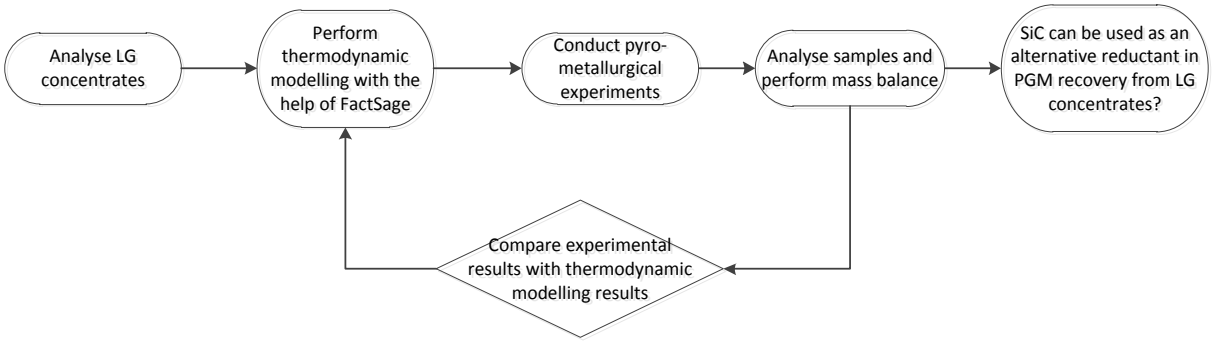

Figure 1.1 – The framework and key question of the project

These experiments were conducted in a Carbolite STF 1800 tube furnace in the Department of Process Engineering, Stellenbosch University. The alloy button and slag was separated afterwards and sent for analysis. A mass balance is performed to conclude on PGM recoveries and SiC as an effective alternative reductant.

Primary objectives

- To determine the optimum experimental conditions using thermodynamic evaluation. This will involve the calculation of thermodynamic equilibrium with the help of FactSage.
- The detailed chemical and mineralogical characterization of all feed and alloy, slag and dust produced using XRD, XRF, SEM and ICP analysis.
- To study the major factors that could distinguish between the reducibility of the low grade concentrates at various experimental conditions including the oxidation state of iron, various feed elemental ratios, particle size and the concentrate/reductant ratio.
- To understand the reducing conditions to produce the minimum alloy whilst maintaining a high as possible recovery of PGMs.
- To quantify the deportment of the various elements to the alloy and slag phase and to establish which factors will affect the solubility of PGMs
- To look at the costs of smelting experiments and additional revenue that can be made by the recovery of PGMs at the concentrator. The importance of finding the optimal SiC concentrate ratio, with regard to economic constraints is critical.

Advantages of the recovery of PGMs from a Fe alloy

- There would be no constraints on the minimum quantity of base metals required in the feed material, as the collection of the PGMs is done in an iron based alloy.
- It is perhaps more practical to integrate the relatively large quantities of the alloy product into an existing smelter complex, possibly through a converter. As the alloy makes up a small fraction of the total feed, the effect on the existing smelting process would be small.
- Would also allow for the possibility of hydrometallurgical refining of the alloy. Therefore the amount of alloy that would require further downstream treatment should be minimized.
- The process would most likely be chromium tolerant, efficient in the collecting of PGMs and significantly reduces sulphur emissions compared to current matte-smelting processes in use in the PGM industry along the Bushveld Complex.
- The process could also become an economic incentive for treating other waste materials in a similar manner.

Thesis layout

The thesis document is structured in the following manner:

- Chapter 1 contains an introduction explaining the background of PGM refining, hypothesis, scope and the approach of the project. Along with this, it also contains the primary objectives of the study, benefits of the process and why it will be relevant.
- Chapter 2 contains a literature study into current PGM collection processes and which factors contributed in the recovery of base metals or PGMs during smelting.
- Chapter 3 describes the materials and methods that were used and produced during the study.
- Chapter 4 discuss the thermodynamic modelling and experimental results.
- Chapter 5 contains a proposed optimum integrated flow diagram.
- Chapter 6 contains a conclusion.

- Chapter 7 contains recommendations for future work.
- Chapter 8 contains references used in the thesis.
- Appendix A contains additional graphs and tables from analytical results.
- Appendix B contains example calculations.
- Appendix C contains TGA methodology and results.

2. Current trends in PGM smelting processes

There is an abundant literature dealing with reductive smelting of base metals with carbon as reductant, embracing the fields of copper and nickel smelting and converting, as well as PGM recovery. In all papers reviewed none have dealt with SiC as reductant, however many similarities are expected to arise from previous work and also shortcomings will be addressed.

The first part of the review deals with conventional matte-based PGM collection process used at Lonmin Western Platinum Limited, which in such will be subdivided into a description, of the process and limitations of it. An alternative process known as the ConRoast process has been developed to collect PGMs in an alloy [3, 4]. The benefits of this process will be explained. The second part of the review deals with reduction of base metals and factors such as oxygen partial pressure, temperature, slag chemistry and slag physical characteristics will be examined and the effect of such on **metal fall, PGM recovery** and **Cr solubility**.

After the review has been completed, a summary of the main findings are listed and how it will be relevant to this study.

2.1 Process descriptions

In this section of the review, the matte based collection process used at Lonmin Western Platinum Limited and alloy collection process known as ConRoast process that was introduced by Mintek will be examined. For each process, a block flow diagram and a description of the process is included. The limitations of the matte based collection process are listed as well as to overcome these limitations by means of the ConRoast process is also listed.

2.1.1 Matte-based collection process

Description of the process

The dried concentrate from a flash or spray drier is pneumatically transferred from the drier into the furnace for smelting (See Figure 2.2). Smelting is intended to separate the gangue (oxide and silica) minerals from the minerals which are considered valuable. The aim is to form phases which are immiscible in each other, known as a matte and slag. In practice, a matte-fall of at least 15 % is required to assure good collection of and a higher recovery of PGMs [2]. Figure 2.1 shows PGM recovery as a function of matte fall. Matte fall is defined as follow:

$$matte\ fall\ \% = \frac{Mass\ of\ matte\ at\ end\ of\ melt}{Initial\ UG2\ blend\ concentrate\ mass} \times 100\% \qquad \text{(Eq. 2.1)}$$

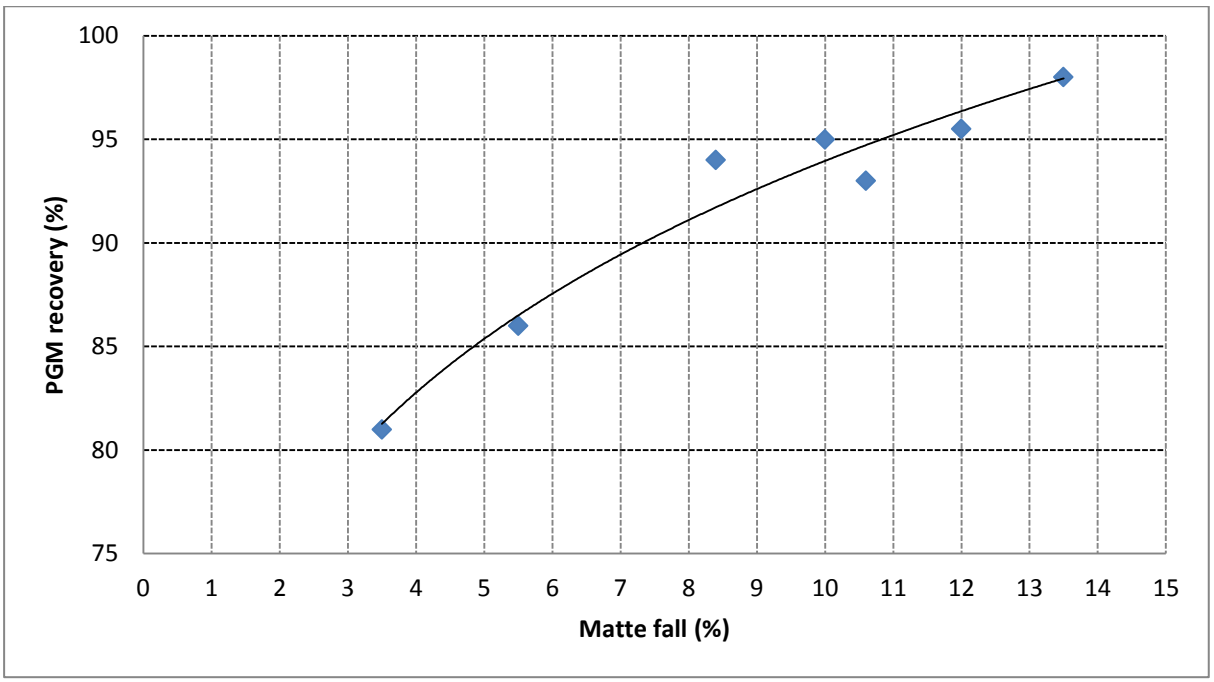

Figure 2.1 – Relationship between PGM recovery and the amount of matte phase formed during melting. The solid line is a visual guide. Redrawn from [2].

However, during smelting, some magnetite and chrome spinels form an intermediate viscous zone between the matte and slag layers, causing insufficient coalescence and settling of matte droplets from the slag and will also decrease the operational volume of the furnace. This will then ultimately cause an increase in entrainment, which should be avoided, as some valuable materials such as PGMs could be lost [5, 6].

The dry concentrate feed to the furnace is either a Merensky HG concentrate or a UG2 LG concentrate and Merensky HG blend. Table 2.1 displays a typical Merensky and blend concentrate composition [2].

Table 2.1 – Feed composition to the furnace (Adapted from [2])

Feed	Al_2O_3	CaO	Cr_2O_3	Cu + Ni	Fe	MgO	S	SiO_2	PGM (ppm)
Merensky	1.8	2.8	0.4	5.0	18	18.0	9.0	41.0	130
Blend	3.6	2.7	2.8	3.3	15.0	21.0	4.1	47.0	340

The slag from the arc furnace typically contains less than 5 ppm PGM + Au and is usually discarded. The matte leaving the furnace is further treated in converters (Peirce-Smith converters at Lonmin Western Platinum Limited), where air is blown through tuyeres located at a lateral position of the converter in order remove much of the iron and sulphur (mostly FeS) by oxidation. The iron oxide reacts with the silica to produce a fayalite slag. The chemical reactions present are as follow:

$$2FeS(l) + 3O_2(g) \rightarrow 2\ FeO(l) + 2SO_2(g) \qquad \text{(Eq.2.1)}$$

$$FeO(l) + SiO_2(l) \rightarrow FeO.SiO_2(l) \qquad \text{(Eq.2.2)}$$

The converter matte is skimmed off in time intervals, once it has reached a desired level of iron concentration (1-3 %). The slag is not discarded, since it still contains some prills of valuable converter matte due to the turbulent conditions caused by the air injected at high velocities. This will also cause some of the base metals (especially cobalt and Nickel) to be oxidized [5].

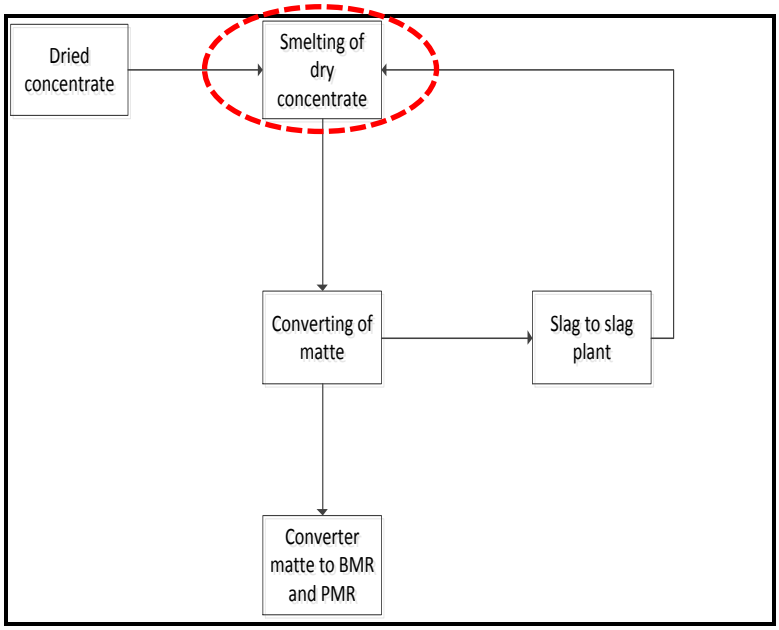

Figure 2.2 – Block flow diagram of the classical matte based smelting route. The area of focus of this study is highlighted.

Sulphur entering the smelter distributes as follow[5]:

- 60% leaves in the converter gases
- 20% leaves as furnace gases
- 15% leaves in the converter matte
- 5 % leaves in the furnace slag

The sulphur leaves the converter as SO_2 and is sent to the acid plant for further processing. The converter matte is usually milled prior to treatment in the base metals refinery, where the copper and nickel are extracted using a sulphuric-acid leach process. The leach residue makes up the high-grade PGM concentrate and is then sent to the precious metal refinery for final separation of the precious metals.

Limitations of process

The matte-based process does have some limitations, which constrains this process to specific concentrates that can be fed to the furnace. Some of the limitations involved are now pointed out.

Environmental concerns have focused on the problem with SO_2 emissions, especially at the mouth of the Peirce-Smith converter. Some methods and techniques have been developed to reduce emissions, but have been found to be ineffective as a lot of converter gas still escaped.

An increasing amount of **UG2 concentrate** is processed, so the quantity of base metal sulphides decreases as is shown in table 2.1. It is critical that the matte-based collection process produce sufficient matte ($\pm$15% of the total mass) to allow for effective coalescence of droplets in order to collect valuable metals. Therefore a limitation is placed on the mining of the ore, as ore has to contain a certain amount of nickel and copper for acceptable processing [3].

One of the main problems associated with LG based concentrates are the chromium content, due to the low solubility of Cr_2O_3 in the slag phase – typically below 2 %. Depending on the chromium content of the feed and the detailed operating conditions of the furnace, it frequently happens that the slag phase becomes saturated with a chromium-rich spinel phase. The main consequences are [2, 65]:

- The spinel tends to be accumulated at the slag-matte interface (known as mush), hence clean separation between the matte and slag phases is not sufficient.
- It increases the effective slag viscosity and causes emulsification of slag and matte.
- The spinel freezes onto the sidewalls (known as build-up), therefore decreasing the operating furnace volume and also brings about changes in the hearth profile.
- It contaminates the matte with chromium (as $FeCr_2O_4$). Spinel in furnace matte causes problems with slag-matte separation and increases the chromite content in the slag. The high chromite concentrate in the slag hinders it from being recycled, causing PGM losses. In order to recover PGMs, the chromium-rich converter slag must either be melted in a slag-cleaning furnace or treated in a minerals processing plant.

The importance of limiting the formation of chromite-rich spinel phase is clear and certain parameters (temperature, reductant to concentrate ratio, pO_2 and CO/CO_2 ratio) need to be controlled to avoid it. Factors influencing Cr solubility in the slag will be discussed in section 2.2.2.

Many of the South African platinum producers have moved towards the processing of ore from the UG2 reef to supplement the previous production from the Merensky reef; however there have been numerous furnace failures and explosions in industry. Even with the introduction of water-cooled copper cooling systems in recent years, the highly superheated and corrosive molten matte in traditional smelters is inherently difficult to contain [3].

2.1.2 The ConRoast process

Description of the process

The ConRoast process developed by Mintek for the treatment of nickel and PGM concentrate has been developed as an environmentally friendly process in contrast to the traditional matte-smelting process. It also offers greater flexibility as it can handle more UG2 orientated ores. The ConRoast process is based on reductive smelting in a DC are furnace in the effective absence of sulphur, where an **iron-based alloy** is used to collect the valuable metals [5]. A process flow diagram of the ConRoast process is shown in figure 2.3.

Before any of the ore is sent for smelting in the furnace, it will undergo roasting in some sort of fluidized-bed roaster to remove most of the sulphur present in the ore. The feed stream will have a

typical composition of a low grade concentrate, high in chromium oxides and low in base metal sulphides. Table 2.2 displays a typical UG2 LG concentrate composition 1 [4, 5].

Table 2.2 – Typical feed composition of the ConRoast process. Adapted from [4, 5].

Al_2O_3	CaO	Cr_2O_3	Cu + Ni	FeO	MgO	S	SiO_2	PGM (ppm)
5 - 6	2.5 – 3.5	3 - 5	< 1	20 - 25	20 - 25	< 1	40 - 50	200 - 400

During roasting, the sulphide is converted to an oxide, and sulphur is released as sulphur dioxide. For example, the ore Cu_2S (chalcocite) balanced equation for roasting is:

$$2Cu_2S(s) + 3O_2(g) \rightarrow 2Cu_2O(s) + 2SO_2(g) \quad \text{(Eq.3.3)}$$

The roasting process has several effects [4]:

- Drying the concentrate
- Oxidizing a part of the iron present
- Decreasing the sulphur content by oxidation
- Partially removing volatile substances/impurities, for example arsenic
- Preheating the concentrate to lower the energy requirement of downstream processing.

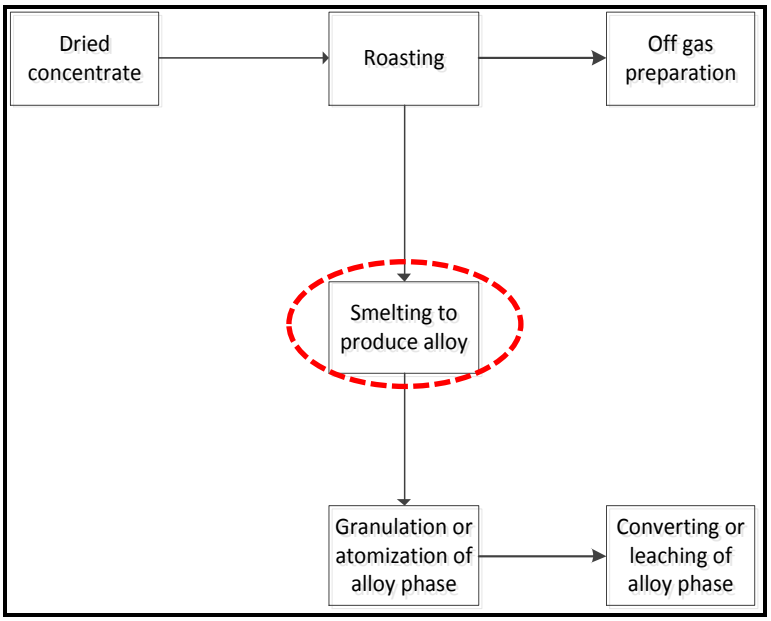

Figure 2.3 – Block flow diagram of the Conroast process. The area of focus of this study is highlighted.

The remaining SO_2 is removed from the fluidized-bed roaster which is a well enclosed vessel that produces a steady continuous stream of SO_2 that can be used for the production of sulphuric acid.

The ConRoast Process produces an iron-rich alloy from the DC arc furnace. The alloy product needs to be produced in a physical form that is conductive to further processing. Currently, granulation is routinely carried out on the alloy produced from the DC arc furnace; however other methods such as water atomisation can be used as an effective intermediate step between the production of a molten

alloy from a DC arc furnace and a converting or leaching process. The reason for the proposed technique is that not all alloys are readily crushable. In that sense, very fine particles are produced by the impingement of high-pressure water jets on a molten alloy stream. These very fine particles will decrease residence time and reactor volume and will also lower power consumption of the leaching process [3].

The molten alloy produced from the DC arc furnace requires iron removal. The two principal options that have been explored are converting (explained in matte-based collection process) or leaching. Both methods have been successfully carried out; however converting is more frequently used in the ConRoast process [3].

Improvements on conventional matte-based process

The ore concentrate sent to the furnace has been treated for sulphur by the fluidized-bed roaster and this allows the furnace to essentially smelt a sulphur-free material. The valuable metals are then collected in an iron alloy. Compared to the traditional matte smelting process, emissions of SO_2 can be an order of magnitude lower if the ConRoast process is used [5].

The strict legislation implied at industry to control SO_2 emissions has also contribute to the development of the ConRoast process, which was initially developed as an environmental friendly process. It is expected that pollution control legislation will become even stricter, making the ConRoast process an appropriate alternative process to replace the conventional matte based process.

The traditional matte-smelting process enforces strict limits on the amount of chromite (prevalent in the UG2 reef) that can be present in the smelter feed, due to the possibility of the formation of high melting chromite spinel. This restricts the recovery of the PGMs in the production of ore concentrates. The dead-roasted concentrate fed into the furnace, is already at a high temperature, reducing the amount of energy required for the smelting process. The furnace operates under high **reducing conditions** at very high temperatures [4]. This eliminates the chromium constraint, by hindering the formation of high melting chrome spinel, and so opens up opportunities in the types of materials that can smelted, ultimately PGM recovery will be more efficient.

The ConRoast process is able to use a simple and robust design of furnace, because of the melting temperature of the slag and alloy that are almost the same. Benefits resulting from the implementation of the ConRoast process could be summed up as follow [5]:

- Significant improvement on environmental, safety and health associated problems.
- Sulphur emissions are well regulated and captured and sent for further processing to sulphuric acid.
- The ConRoast provides great flexibility to the different ranges of ore that could be used in the process.
- The reductive smelting conditions eliminate the constraint of the amount chromite present in the concentrate feed, increasing PGM recoveries, because the slag phase can be recycled and prepared for smelting again. Almost all of the incoming chromite reports to the slag phase.

- The ConRoast process produces a metal alloy, in contrast to the sulphide matte produced. The alloy, mostly consisting of iron, nickel, copper, cobalt and traces of PGMs can be water-atomized to produce fine particles (with an average particle size that could be controlled anywhere between 20 and 100 µm)

Overall the ConRoast process has a high base metal and precious metal recovery.

2.2 Factors influencing the recovery of base metals and PGMs

The UG2 LG concentrates under investigation will consist of elements in its oxide form. That is it will consist of some metal oxides. Some of these oxide compounds will be reduced to pure elemental form, while others will not. The relative ease of reduction is governed by the thermodynamic equilibrium state.

Thermodynamics indicate what is recoverable but gives no timeframe. It is most likely that losses will be driven by kinetics such as settling time and residence time as well as by physical properties such as, **viscosity of slag, interfacial tension, entrainment of alloy or matte in the slag phase** and **size of matte/alloy droplets**.

Many studies have been done on such physical characteristics and will be investigated in order to minimize losses of base metals and PGMs in this study.

2.2.1 Carbon as reductant

Normally, the metal is found in a concentrate in its oxide form and needs to be directly reduced (removal of oxygen) to the metal. A variety of reducing agents are used, **carbon** being the one most widely employed. Al, Si and hydrogen are other reducing agents currently in use. However, the preferred reducing agent is carbon because of its availability and inexpensive production costs.

Since carbon is the reducing agent, which occurs in nature in large quantities, it has been used on a large scale to reduce metal oxides. Carbon burns in oxygen at temperatures below 710 ℃ to form carbon dioxide, but at higher temperatures it produces carbon monoxide as product [7].

$$C(s) + O_2(g) = CO_2(g) \quad \text{(Eq.2.1)}$$

$$2C(s) + O_2(g) = 2CO(g) \quad \text{(Eq.2.2)}$$

Carbon can also react with CO_2 (g) to form CO (g), which is favoured at high temperatures.

$$C(s) + CO_2(g) = 2CO(g) \quad \text{(Eq.2.3)}$$

Carbon reaction mechanisms of Chromite and other ores close related to UG2 ore

The chromite ores have a spinel structure that can represented by the general formula (Fe, X)O(Cr, T)$_2$O$_3$. Here, X and Y are elements that dissolve in the two different cationic sublattices. The two lattices are the octahedral and tetrahedral sites in the structure, respectively. This will cause the divalent cations such as Mg^{2+} to occupy the tetrahedral sites, and trivalent cations, such as Al^{3+}, Fe^{3+} etc. to occupy the octahedral sites. However, iron can also occupy the tetrahedral sites. Iron is reduced before chromium and forms the carbide Fe_3C, which acts as reducing agents to improve the reduction of chromium. From previous work done [8, 9], it is known that a higher (Fe/Cr) ratio will cause reducibly to increase. This is attributed to the formation of Fe_3C, which also acts as a reducing agent. The presence of carbon is essential for reduction and reduction might occur by direct contact between the oxide and carbon. The reaction present, in general, is as follow [8]:

$$MxOy + yC = xM + yCO \qquad \text{(Eq.2.4)}$$

Alternatively, the carbon is oxidized to carbon monoxide, which in turn can reduce the oxides. The reactions are represented by the following:

$$C(s) + CO_2\,(g) = 2CO(g) \qquad \text{(Eq.2.5)}$$

$$MxOy + yCO = xM + yCO_2 \qquad \text{(Eq.2.6)}$$

Generally it is believed that the reduction of chromite ores follow the latter mechanism. Various possible mechanisms controlling the rate of reaction have been discussed in literature [8-11].

Haque et al. [9] investigated direct and indirect reduction of iron oxide with carbon. From their work it is known that direct reduction can only occur when the gaseous products of reaction, namely, CO and CO_2 are removed from the system as they are produced. For direct reduction to occur, solid-solid reaction is necessary, which requires oxide-carbon contact. It was then also required to avoid gas-oxide contact, which can cause indirect reduction. Experiments were carried out by studying the reaction of a bottom layer of reductant and a covering iron ore using a fixed particle size, weight ratio and temperature. The layers were in contact with each other for some of the experiments while in some other experiments they were separated by a thin stainless steel mesh. The results indicated that direct contact (no mesh) enhances reduction significantly when coal or coal char were used, however some reductants such as coconut char or activated charcoal showed no difference, because they are known to gasify rapidly. Therefore, it was concluded that the difference observed in the case of coal or coal char is entirely due to the catalytic effect only and indirect reduction plays the major role in the reduction of iron oxide by coal.

Murti et al. [10] studied the reduction of synthetic chromite by carbon at 1423 to 1573 K. In this study it was concluded that reduction was controlled by diffusion of oxygen in the chromite. The same authors studied the reduction of chromite ore at 1513 to 1583 K. In this case, the reduction process was found to be controlled by the diffusion of oxygen in the ore to the gas/solid interface. However, in both experiments, the authors did not detect the formation of carbide during reduction. During the reduction of synthetic chromites with Al and Mg in the spinel structure, analysis shown that reduction progressed through the formation of carbide, either Cr_3C_2 or Cr_7C_3. FeO reduction occurred at temperatures less than 1423 K.

Nafziger et al. [11] investigated the reduction of chromite ores, by using different reducing agents, in the temperature range 1100℃ - 1500℃. The reductants that were used were coal char, coke breeze,

metallurgical coke, petroleum coke and shell carbon. It was found that coal char provided the highest degree of reduction. However, in the temperature range 1400℃ - 1500℃, metallurgical coke provided the highest degree of reduction and in all cases, the highest degree of reduction was obtained in the first 15 minutes. The authors also argued that the formation of a mixed (iron, chromium) carbide acted as an effective reducing agent.

Chakraborty et al. [8] studied the carbothermic reduction of chromite ore under different flow rates of inert gas. At a lower flow rate, the reaction proceeds through the oxidation of carbon to carbon monoxide, followed by the reduction of the oxide by carbon monoxide. An increase in the flow rate of argon diluted and swept away the CO_2 so that the carbon in the mixture is starved of CO_2 to get oxidized to CO. Therefore reduction occurs primarily through interaction of solid carbon and the ore. The authors also investigated the effect of ore/coke ratio and founded that it was highly dependent on the inert gas flow rate, however a lower ore/coke ratio did achieve better reduction of chromite.

2.2.2 The effect of slag chemistry on base metal and PGM recoveries

In any successful pyrometallurgical process, the ability to form a good slag is of great importance, therefore Nell [2] suggested the following characteristics need be maintained for a PGM concentrate:

- A low viscosity to allow clean slag-matte separation.
- A low liquidus temperature to avoid excessive superheating of the matte.
- The ability to dissolve all the chromium present in the concentrate to avoid the formation of refractory chromium-bearing spinel and to avoid the transfer of chromium to the matte.
- A limited solubility of nickel, copper and cobalt as oxides.
- Chemical compatibility with refractory lining in the furnace (in modern, water-cooled furnaces this is not as important as it was).

However, it is not entirely possible to have all these characteristics associated with the slag, because the slag composition is largely determined by the composition of the concentrate fed to the furnace and there is very little freedom to manipulate the slag composition. The only fluxing agent regularly used in different amounts by Lonmin Western Platinum Limited and other PGM producers is lime. The concentrate in turn depends on amounts of ore that are being processed. A blend of Merensky and UG2 ore is typically used for the Lonmin Western Platinum Limited operations. The UG2 ore will increase the concentrations of MgO and Cr_2O_3, which will increase the liquidus temperature of the slag (typical operating slag operating temperatures vary between 1350 ℃ (low UG2 concentrate) and 1600 ℃ (high UG2 concentrate). The higher silica content, will cause the viscosity of the slag to increase, causing some matte entrainment and PGM losses to the slag phase[2].

Effect of slag composition of Cr solubility

There has been some disagreement in this area, particularly on melt basicity, most likely because slag composition is dependent on the **feed of the concentrate**. Melt basicity is defined as follows [2, 38]:

$$\left(\frac{wt.\%\ CaO + wt.\%\ MgO}{wt.\%\ SiO_2}\right) \qquad \text{(Eq. 2.7)}$$

Some of the previous work does not deal with UG2 LG concentrates; however it is still important to take note of because slag composition has a major effect on recovery of all valuable metals.

Work done by Eric et al. [12] and Choi et al. [13] found that by increasing the basicity by adding MgO or CaO to the slag, increases the base metal dissolution and MgO is more effective at increasing solubility then CaO. In copper smelting and converting, however this was not the case, and adding MgO and CaO does not affect copper dissolution in the slag. This was confirmed by Ruddle et al. [14]. A study done by Fontana et al. [15], and Chen et al. [16] showed that the amount of cobalt dissolving in silicate slag decreases with increasing CaO addition. By adding silica to the slag decreases base metal dissolution [12, 17], as was found with the addition of alumina [18, 19].

The effect of slag composition on chromium solubility is not entirely known. Experimental work done under reducing conditions by Nell [2] (Figure 5 in the study), indicated a strong dependence on melt basicity. However, it was reported that the solubility relationship depends on the redox conditions and that it is less pronounced under more oxidizing conditions. It is expected that Cr solubility in air would be less dependent on melt basicity than at an pO_2 of $10^{-9.75}$ bar. Operating temperatures were at 1500℃. The effect of slag composition on Cr solubility in a multi-component slag system is, largely undocumented. Some plant observations from Mintek indicated that the solubility of Cr might depend on the concentrations of both silica and lime, however more data are required to verify these initial findings [2]. The effect of temperature and pO_2 on Cr solubility is now further investigated.

Effect of temperature on Cr solubility

Many previous works report on the effect of temperature on base metal solubility in slag. Yet again the base metal solubility in the slag is highly dependent on the type of concentrate fed to a furnace. Some authors state that increasing the temperature reduces base metal solubility in slag [13, 20, 21], however others claim that it has a reverse effect [22, 23]. Work done by Holzheid et al. [24] showed that the solubility of cobalt in silicate melts are little dependent on temperature in the 1300 ℃ to 1600 ℃ range, however it was found that nickel solubilities increased significantly with increasing temperature and also increasing pressure. For the purpose of this study, chromium is required to be soluble in the slag and according to Nell [2] solubility is little dependent on slag temperature increase. Figure 2.4 shows how Chromium solubility slightly increases for an increase in slag temperature.

As the temperature increases from 1300 ℃ to 1500℃, there is an almost threefold increase in the solubility of Cr_2O_3 in silicate liquid with compositions to a typical furnace slag. However, even at 1500 ℃ the solubility is still only about 0.6 % Cr_2O_3 and from the slope of the curve it is evident that under relative oxidizing conditions, an increase in temperature will not have a significant effect on the solubility of chromium in the slag phase [2, 65].

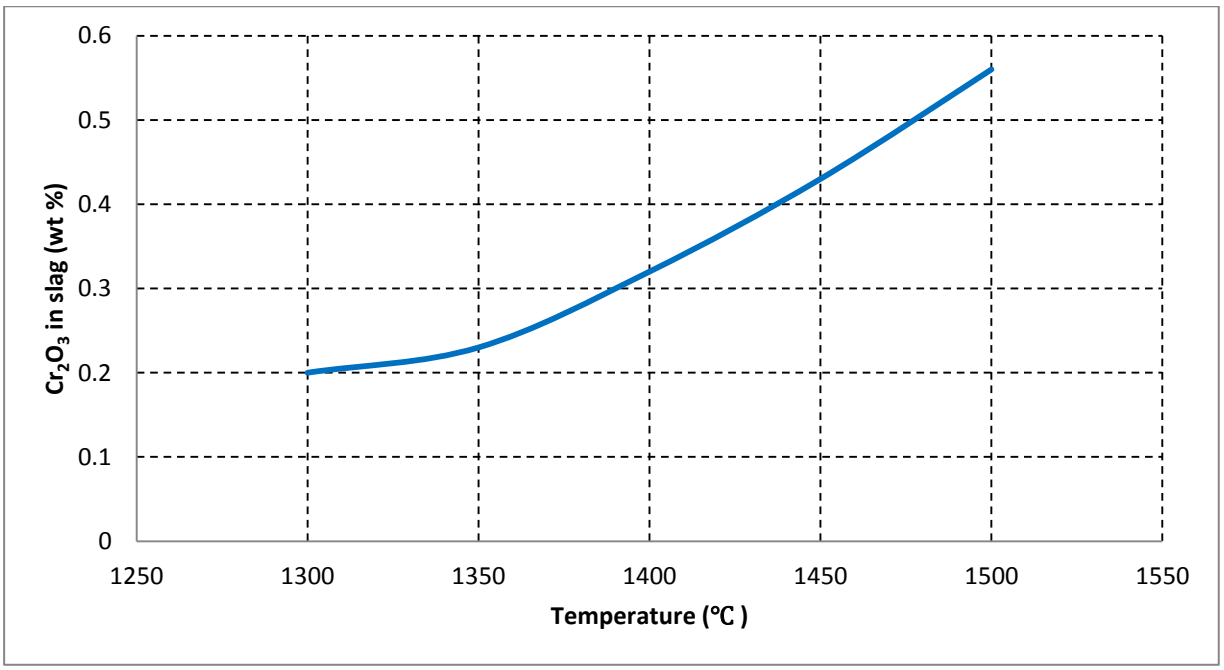

Figure 2.4 – Chromium solubility in a komatiite liquid (45.1 % SiO2, 6.4 % Al2O3. 10.4 % MgO, 5.9 % CaO as a function of temperature). Redrawn from [2].

Effect of oxygen potential on Cr solubility

Many studies have been conducted on the effect of oxygen partial pressure on base metal dissolution in slag, consequently many authors agree that increasing oxygen partial pressure in the slag of a slag-matte system increases the dissolution of the base metals [13, 14, 20, 25-27]. The work done by Wang et al. [20] has shown that nickel and cobalt dissolution in slag increases linearly with the square root of the oxygen partial pressure ($pO_2^{0.5}$) and at a lower oxygen partial pressure Ni is less soluble in slag than Cu. Also, it was found that the trend reversed at higher values of pO_2.

During converting, a high pO_2 in a converter slag will increase the amount of magnetite (Fe_3O_4) that forms. Ultimately, this will increase the levels of base metals partitioning into the slag, however this may be somewhat due to entrapment of sulphide or matte phases [23].

Moving on to studies more closely related to this one, Nell [2] has conducted a study on UG 2 concentrates and the effect of pO_2 on chromium solubility in the slag. It was found that in the case of base metals with multiple valences, it is generally true that at lower valence states, the metal oxide becomes more soluble in a silicate liquid than the higher valence states. Chromium, in addition to this, is no exception and will become miscible in a slag phase when reduced to CrO. From the study, it is evident that at a very low oxygen partial pressure (10^{-9} bar) it is possible to dissolve between 2 % and 3 % chromium oxide in the furnace slag. By even further lowering the oxygen partial pressure (10^{-10} bar), it will be possible to increase chromium solubility to 6% Cr_2O_3 [2].

From the work done by Nell [2] (Figure 3 in the study), it was found that an adjustment in the oxygen partial pressure will increase the chromium solubility; however this has to be done with utmost care and under conditions of tight control in order to avoid over-reduction of iron oxide from the slag. Another consequence associated with the lowering of oxygen partial pressure, is an increase in the deportment of chromium to the matte phase. It is important to maintain moderate reducing

conditions because the high solubility of chromium in the slag is a result of the reduction of Cr^{3+} to Cr^{2+} and as previously stated, CrO is more soluble in the slag [2, 65].

2.2.3 Matte/metal entrainment in slag

Base metal losses to slag can occur through entrainment as shown by many studies [12-49]. The work done by Andrews [28], has shown that over half of base metal losses in a six-in-line furnace at Anglo-platinum are as dissolved phases, which are not recoverable. The prediction of such base metal losses is not easy, because of the complex slag composition. During the study, measured distribution of the base metals was compared with an equilibrium model developed through thermodynamic evaluation in FactSage, in order to identify problems and to recommend actions for prediction improvements of base metal dissolution in slag.

Entrained matte can be responsible for 25 to 75 % of total copper losses to slag [29]. However from many studies it is clear that physical calculation of entrained matte cannot be done accurately. Andrews [28] concluded however that new electron microbeam techniques that have recently been developed can quantify base metal distribution in slag.

The next sections will include a discussion on the factors influencing matte/alloy entrainment in slag.

Effect of settling

From many previous studies [28-33] it has been concluded that the settling of either matte or metal alloy is greatly influenced by slag properties, i.e. composition, viscosity, density and interfacial tension. The settling rate is been found to be mainly size dependent and fine matte or alloy droplets can require very long settling times under quiescent bath conditions. From laboratory scale experiments [30], it was confirmed that droplets smaller than 2 μm did not settle. These smaller droplets may either settle very slowly or may be trapped as 'rafts' of droplets floating on the top surface of the slag or as droplets suspended below small gas bubbles [31].

Also, a sufficient amount of alloy or matte fall is required for settling, in South African platinum melting, a matte fall of at least 15 % is required to assure adequate collection and high recovery of PGMs [2].

Effect of coalescence

The ability of a matte droplet to settle is highly dependent on the droplet coalescence to form larger drops. The chance of coalescence can be increased by stirring, or, in DC furnaces, by electromagnetic fields. In a PGE smelting six-in-line furnace, coalescence is increased by stirring driven by buoyancy forces, which depend on the temperature and the electrode immersion in the slag. By lowering the slag viscosity, the drops will continue to coalesce, however this is limited by slag conductivity requirements [38].

A few studies have been done on factors influencing efficiency of coalescence [39-41]:

- Gas bubbles rising through the slag can enhance drop growth through drop-to-drop coalescence.

- The time required for drops to coalesce is largely the time required for film drainage, therefore when the film ruptures, coalescence will occur instantaneously.

- Gravity-induced coalescence is greatly affected by the drop size and drop-to-drop size ratio. A decrease in both will cause a decrease in coalescence.

- Collision frequency for neutrally-buoyant drops decreases as the kinematic viscosity of the slag increases.

- Sufficient matte/metal fall is required for successful coalescence to occur.

- Agitation and bubble injection can be used to enhance fine droplet recovery.

Matte/metal behaviour in industrial furnaces

The behaviour of matte or metal entrained in industrial furnaces has been investigated by many authors. One factor that will continue to influence the settling of matte or metal drops is the **slag viscosity**. All matte or metal particles need to settle through the slag at a settling rate which is dependent on the slag viscosity. The relationship between particle diameter and settling time in reveberatory slags has indicated that a larger particle will settle faster [42, 43].

A study done on copper flash smelting concluded that copper loss to slag is affected by **slag depth**, **viscosity**, and **slag tapping location**. The settling rate was inferred by measuring mass vs. depth and Stokes law was employed (Eq. 2.12). In addition, the effect of particle size vs. time to settle was estimated [44] and plotted (Figure 2.5).

$$U = \frac{2}{9} \cdot \frac{G(\rho - \rho')D^2}{\mu} \qquad \text{(Eq. 2.12)}$$

Where, U = Sedimentation velocity of matte particle

D = Radius of matte particle of matte particle

μ = Coefficient of viscosity of slag

ρ, ρ' = Matte and slag density

G = Gravitational Acceleration

In addition, a graph was constructed with the help of equation 2.12:

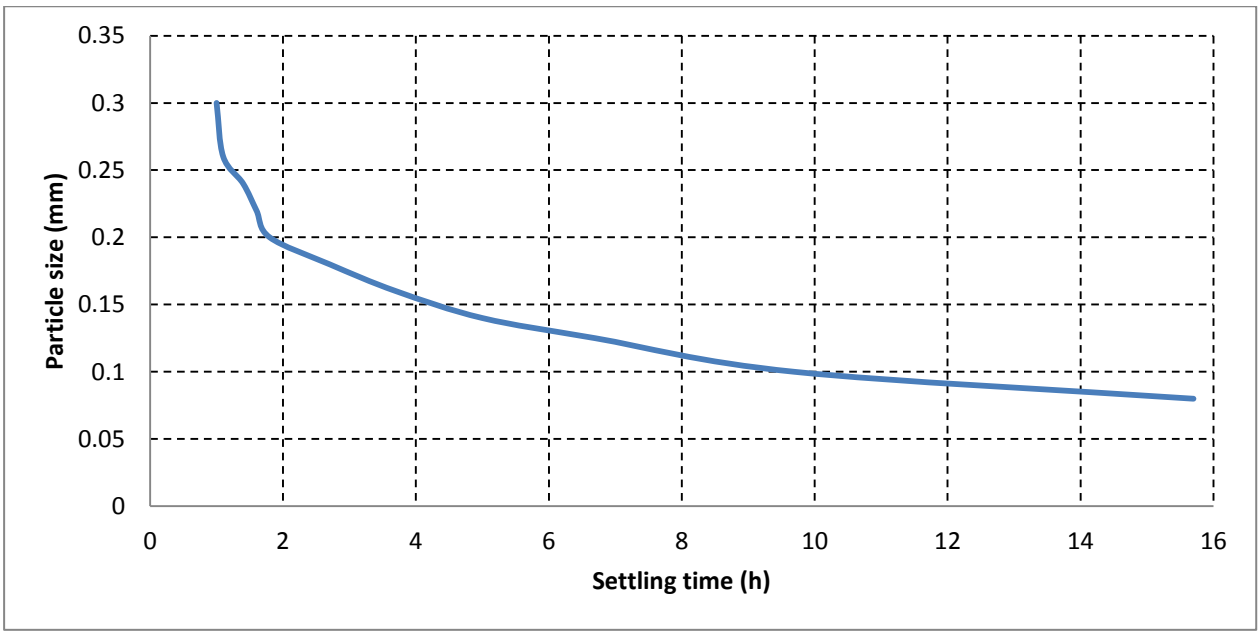

Figure 2.5 – Relationship between settling time and particle size in copper flash smelting (Redrawn from [44]).

Clearly, from the graph it is distinctively evident that a smaller particle will find it hard to settle and very small particles will take an infinite time to settle when only the force of gravity is applied. A further study was done on nickel-copper smelters and copper converters. Representative slag samples were taken from the smelters and converters. Microscope photos were taken and the matte droplet size from the photos processed using a standard quantitative metallography technique. Many entrained matte droplets were observed and only a small fraction of drop-to-drop collisions resulted in coalescence, concluding that recovery must be achieved through means other than gravitational settling. The main conclusions made from this important study were[45]:

- Large matte particles will settle easily to the bottom, whilst the very fine micron-sized droplet will inevitably be trapped in the slag phase.

- A settling model from a computer simulation indicated that varying the slag viscosity and density difference between slag and matte only has a limited influence on the separation of the matte from the slag when very small particles (<2 μm) are involved, however this can improve matte/slag separation significantly for larger drops.

- Better methods need to be utilized to improve coalescence and ultimately improve matte/slag separation.

The effect of slag-matte density differences and slag viscosity on the settling velocity of the matte droplets was determined from studies by Andrews [28] and Ip et al. [35]. It was reported that settling speed of matte droplets increased with slag-matte density differences and decreased with increased slag viscosity. Alloy droplets are denser than matte droplets and will settle faster through a slag.

Careful control of the slag viscosity can either improve or prevent settling matte or alloy particles. Since slag viscosity changes with temperature and composition, it may become harder to control. PGM smelting slags have a viscosity of **0.15 – 0.4 PaS** [38, 46] at 1400 ℃ and under these conditions particles have to be larger than 15 μm to settle. The FeO content of such a slag seems to have a major influence on the viscosity. Therefore increasing the FeO/SiO_2 ratio will decrease the viscosity and increase settling of smaller particles, while a higher basicity ratio (CaO/MgO ratio) reduces metal losses [38, 46]. However unfortunately, the conductivity and viscosity properties of the slag are opposite to each other. So the decrease in conductivity would be beneficial from a smelting point of view, but at the same time the increase in viscosity tends to diminish the gains that would arise from the increase in the resistivity [38]. Figure 2.6 shows that many phases are possible for different relationships in SiO_2-MgO-FeO. The area indicated by the arrow and circle is a typical content of a slag in smelting of PGM concentrates. It is important to keep slag viscosity low and at the same time have a good resistance of the slag. The viscosity and slag resistivity is greatly influenced by the composition of the feed [38].

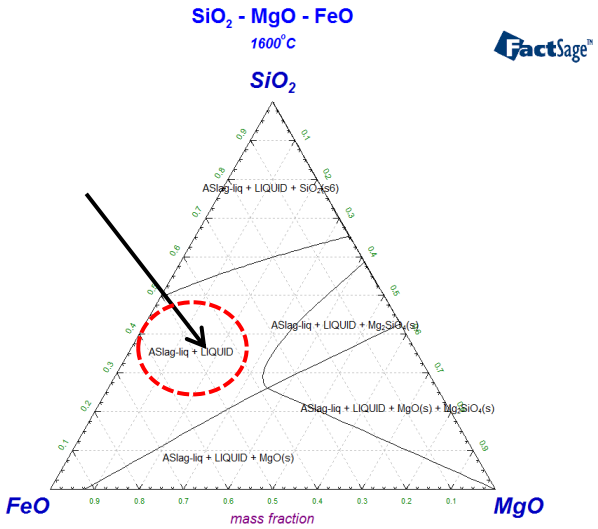

Figure 2.6 – The effect of FeO/SiO2/MgO ratio on liquidus temperature at 1600 ℃ (Generated in FactSage 6.2).

The heat in the electric furnace (DC) is generated by the current passing through the slag and is best described by the following equation:

$$Q = I^2R \qquad \text{(Eq. 2.13)}$$

Where, Q = Heat

I = Current through the electrodes

R= Resistance of the slag

Thus the slag resistivity is of great importance in the operation of an electric furnace.

Other factors contributing to settling of particles in furnaces are briefly outlined:

- **Tap-hole location:** The position of the tap holes around the furnace can also affect losses. For a six in line furnace, those close to the electrodes would be less quiescent than those between the electrodes. The height at which a tap hole is located will also affect losses, because more particles are suspended in the slag closer to the matte/slag interface[38]. However, moving these tap holes could impose difficulties, because of constraints such as cooler geometry and slag granulation layout[28].

- **Liquidus temperature:** The liquidus temperature of the slag is determined by its composition and a high MgO content in PGM concentrates will result in relatively high liquidus temperature. However the liquidus temperature of the slag should be as low as possible to diminish radiation heat losses but must also result in acceptable viscosities[28, 38].

- **Slag-matte surface tension:** The rate of settling can also be influenced by the interfacial tension between the matte and slag. When the surface tension between matte and slag is low, the matte is wet by the slag and settling velocity of matte/alloy prills is reduced. Therefore it is expected that coalescence of matte/alloy prills should increase with increasing interfacial tension. From previous work [38], it was stated that the magnitude of surface tension in matte slag systems are between 420 and 460 dynes/cm (0.42-0.46 N/m) and then to increase with total iron, MgO, CaO and basicity ratio. Increasing SiO_2 content in agreement with literature, decreases the surface tension. Differences in matte-slag and alloy-slag surface tension also need to be considered. The sulphur in mattes (also entrained matte droplets in recycled converter slag) significantly lowers the interfacial tension, leading to smaller matte droplets compared to the low sulphur alloy droplets, which tend to form larger droplets [65]. Limited amount of data is however available on surface tensions from alloy and matte-slag systems.

- **Residence time:** The smaller the particle the longer it takes to settle and some very small particles (i.e. $2\mu m$) will never settle under the force of gravity. However, a longer residence time will greatly improve the recovery of entrained particles in the slag.

- **Electric and magnetic fields:** Electrocapillary motion (the movement of an alloy or matte droplet in slag due to an electric field) is caused by the interaction between the electric field and the interfacial tension of a matte droplet. The speed and direction at which a droplet moves are dependent on the composition of both matte/alloy and slag. The effect of electrocapillary motion on entrained matte droplets will be more prominent in DC furnace than in AC furnaces [28, 47-49]. Conclusions drawn with regard to interaction between the electric field and surface tension forces that will effect motion yielded the following results:

    - The migration direction of a droplet (towards the anode or the cathode) was found to be dependent on both matte and slag composition, which will also determine the sign of the surface charge.

    - Cu_2S-FeS matte droplets migrated towards the anode and Ni_3S_2-FeS matte droplet towards the cathode, however this may vary with slag composition.
    - Migration rate was independent of droplet size in the 1 – 3 mm range.

- Migration rate increase with both applied potential and temperature.
- As the Cu concentration in the Cu_2S-FeS matte increased above 40%, migration rate increased.
- As the Ni concentration in the Ni_3S_2-FeS matte droplets increase, migration rate decreased.
- The migration rate was affected by the slag composition.
- The mobility of Fe-Cu matte is strongly affected by the FeO concentration in the slag

The coalescence of droplets would be far greater in a slag cleaning DC furnace than in an AC furnace due to the magnetodyhrodynamic (MHD) stirring. Therefore slag cleaning operations in a DC furnace would accelerate recovery of entrained matte/alloy from slag. Figure 2.7 illustrates how some of the respective parameters are dependent on each other and what need to be considered during a design of a typical electric furnace.

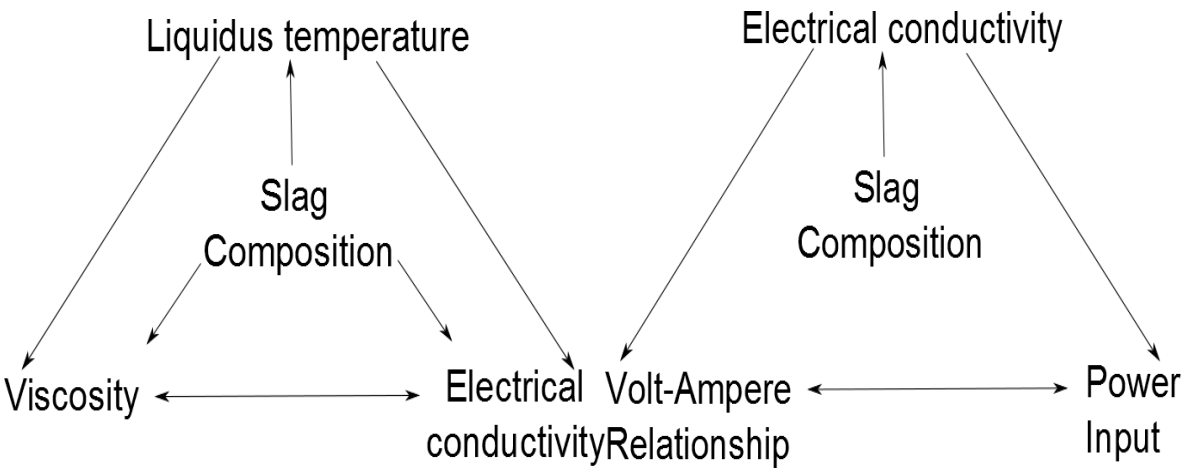

Figure 2.7 – Correlation of various parameters in the operation of an electric furnace (Redrawn from [38]).

2.3 Summary of findings from literature

Based on the review, follow a concise summary of the major conclusions, which is relevant and will aid in thermodynamic equilibrium calculations and clearing up experimental unknowns:

- The ConRoast process has been developed to collect PGMs in an alloy. The ConRoast process overcomes limitations from the matte-based collection process i.e. less gas emissions because of concentrate being roasted in a well enclosed vessel before it is smelted, no constrain on Cr content in the concentrate because of Cr_2O_3 being reduced to CrO, which is miscible in the slag phase and overcomes problems associated with containment.

- Carbon is the most frequently used reductant and may follow more than one reaction mechanism to reduce a metal oxide i.e. solid-solid reduction or solid-gas reduction. The base metal oxide Fe_xO_x will be reduced before the base metal oxide, Cr_xO_x.

- Cr solubility in the slag is most influenced by pO_2 and less influenced by temperature. Lowering the pO_2 will cause Cr_2O_3 (spinel) to be reduced to CrO, thereby increasing Cr solubility in the slag. However, over-reduction should be avoided in order to minimize reduction of FeO and CrO as this could decrease PGM grade in a matte or alloy phase.

- Factors that could influence phase separation during any smelting process include slag viscosity, matte/alloy – slag interfacial tension, settling time, entrainment of alloy or matte in the slag phase and size of matte/alloy droplets.

- Electrocapillary motion is caused by the interaction between the electric field and the interfacial tension of a matte/alloy droplet in a DC furnace and assists in the coalescence of matte/metal prills.

- Slag viscosity is greatly influenced by FeO/SiO_2 ratio. A higher FeO/SiO_2 ratio will decrease slag viscosity, however slag resistivity is lower at the same time. MgO content in the slag raises the slag liquidus temperature which increases the slag viscosity once again. Thereby, careful control of slag content is required for good phase separation and furnace operation.

3. Materials and method

3.1 Overview

This chapter presents the principle, methodology and materials employed in the reductive smelting of low grade concentrates. The smelting was done in the pyro-metallurgical laboratory in the Process Engineering building, Stellenbosch University. The chapter will also outline the thermodynamic simulation procedures. The UG2 low grade concentrates were derived from flotation tailings that have been subjected to gravity (spirals) recovery from operations at Lonmin Western Platinum Limited. SiC were also acquired from Lonmin Western Platinum Limited. The LG concentrates and SiC were analysed with various analytical techniques including XRD, XRF and ICP-MS, respectively.

3.2 Experimental set-up

Pyrometallurgy experiments were conducted in the department of Process Engineering, Stellenbosch University. In total 13 different experiments were carried out in a Carbolite 1800 STF with a programmable controller and thereafter samples were analysed. The procedure and other important aspects of these are experiments are outlined in this section of the report.

A Carbolite STF 1800 tube furnace with a programmable Carbolite controller is used for all pyrometallurgical experiments. The alumina tube is heated by five surrounding elements. The temperature is easily adjustable by the controller and a temperature fail-safe has also been fitted on the controller. If the temperature for any reason should exceed 1770 ℃, the furnace will be shut down and all current program settings need to be reset in order for power to return to the elements.

Before any experiments were conducted, major modifications to the furnace were required. The image on the left shows the tube furnace on its original bracket supports (Figure 3.1 A). During an experiment the idea is then to attach a crucible to a wire and then hang it in from the top of the furnace, at the tube outlet and lowering it down to the marked hot spot. The hot spot was identified with an external k-type thermocouple as the area within close proximity ($\pm$ 5℃) of the set temperature of the furnace. Hanging a crucible from the top was found to be difficult in terms of safe experimental operations. In order to ease the operation, the furnace was removed from its original supporting brackets and fitted on to a fork lifter capable of supporting 1 ton (Figure 3.1 B). After the adjustment, the furnace could easily be moved up and down in vertical direction. The movement is carefully controlled by a hydraulic lever or foot pedal.

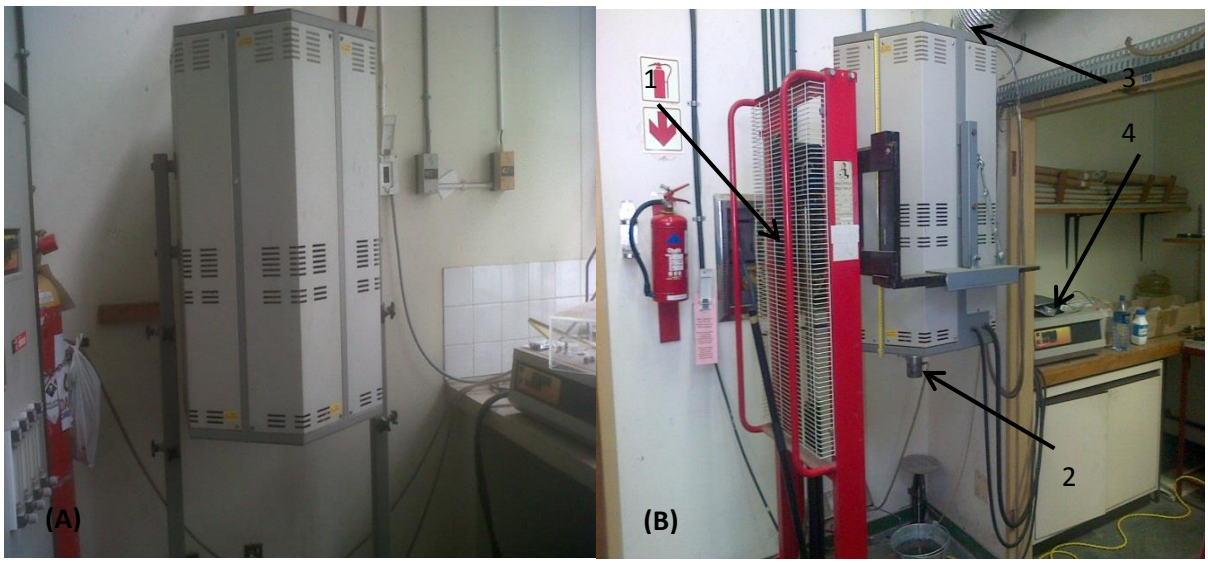

Figure 3.1 – (A): A Carbolite STF 1800 tube furnace with controller before being modified with a fork lifter. (B): A Carbolite STF 1800 tube furnace with controller after being modified with a fork lifter (1) – Fork lift, (2) – Argon gas inlet, (3) – Gas outlet with extraction fan, (4) – Temperature controller.

Raw materials

The two LG concentrates, Rowland and Easterns, were used for smelting purposes and the chemical composition of both respective concentrates is found in Section 3.4. In reductive smelting experiments, SiC was utilized as a reductant. High purity SiC (99 % purity) acquired from H.C. Strark GmBH was also used in an experiment. The chemical composition of the reductant received from Lonmin Western Platinum Limited is found in section 3.4.3.

To contain a concentrate charge, high purity MgO crucibles (see figure 3.2) were used to minimize interaction with slags produced by melted concentrates that are saturated in MgO. The crucible has an ID of 40 mm and a height of 70 mm. Therefore roughly 10 g of concentrate could accumulate in a crucible; however some frothing was expected to take place and no more than 8 g of concentrate was used at any time in order to leave room for frothing.

Figure 3.2 – High purity MgO (99%) crucible used in tests.

General smelting set-up

An alumina pedestal with a support made out of a refractory material was required for supporting the crucible and lowering the furnace upon the pedestal until the tube protrudes at least 3 mm into the water. This will insure that no further air can enter the furnace, other than the high purity Argon gas (99.99%).

A flow diagram for the experimental set-up is shown in Figure 3.3. The Argon flow is manually controlled through an attached valve on the cylinder. The Ar atmosphere was maintained by submerging the tube into water and continuously flushing the tube with Ar at a rate of 500 – 1000 ml/min. This was done to avoid atmospheric interaction of the melt. The temperature was externally carefully controlled. A set point of 1600 ℃ was set on the controller and the measured temperature is recorded by a thermocouple located in the furnace. Once the measured temperature had reached the set point temperature of 1600 ℃, the electric supply to the elements of the furnace was cut for a short time, until the temperature read below 1600 ℃ again. Power to the elements was then supplied once again to keep the temperature constant at 1600℃.

The tube furnace also has a second thermocouple located in the hot zone for record and furnace shutdown. If a temperature exceeds 1770 ℃ all electric supply to the elements of the furnace will be cut. This will assure that the furnace does not exceed its maximum design temperature of 1800 ℃.

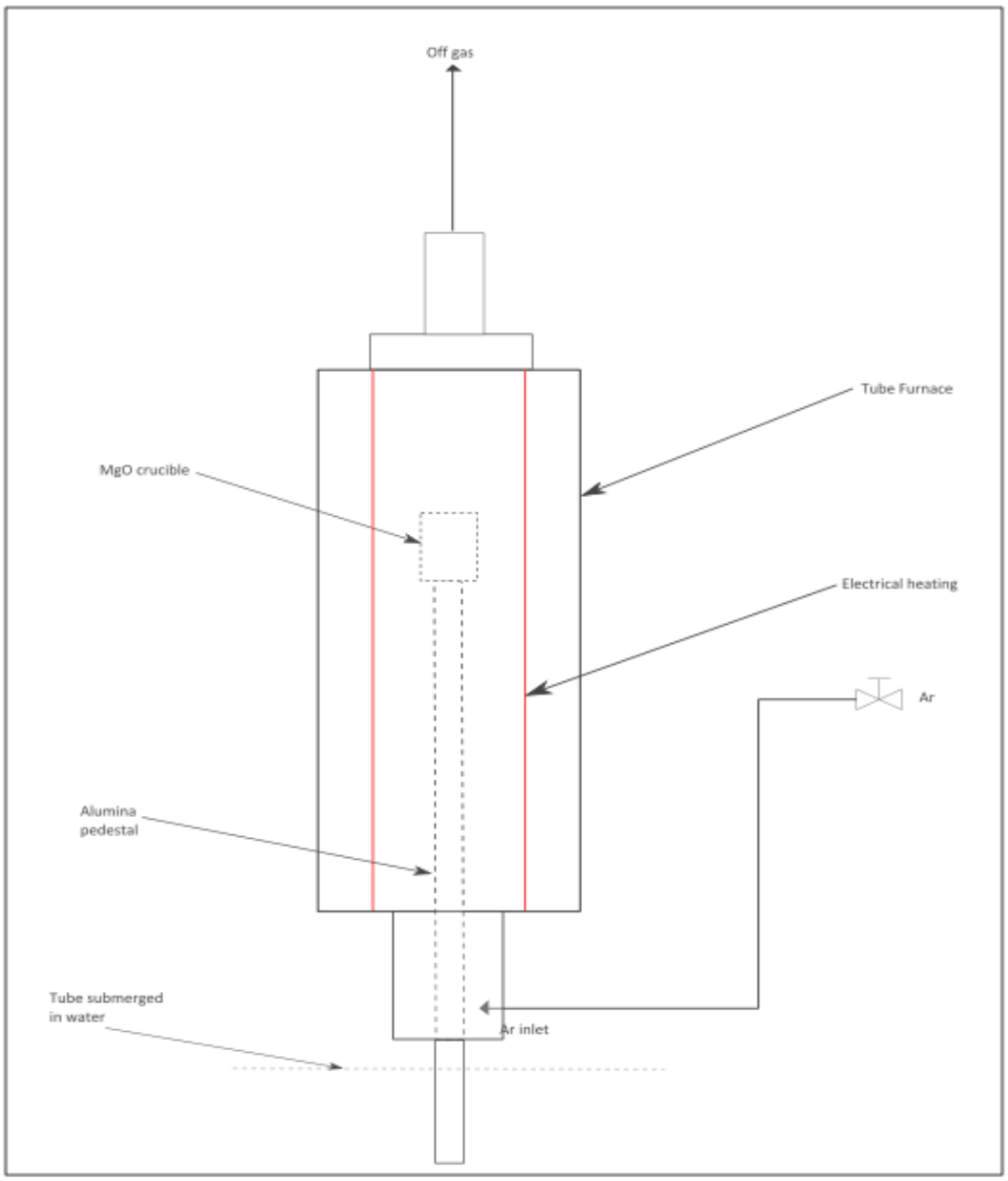

Figure 3.3 – Schematic drawing of the experimental set-up

3.3 Experimental procedure

Establishing the hot zone

The first step involved finding the hot spot in the tube furnace and is required to be done only once. A calibrated thermocouple (K-type) was inserted at the top of the furnace and readings were taken at different areas of the tube. The furnace was set at 1600℃. Once temperatures close to 1600 ℃ was measured, a small hot zone could be marked on the furnace. Figure 3.4 shows the temperature profile of the furnace.

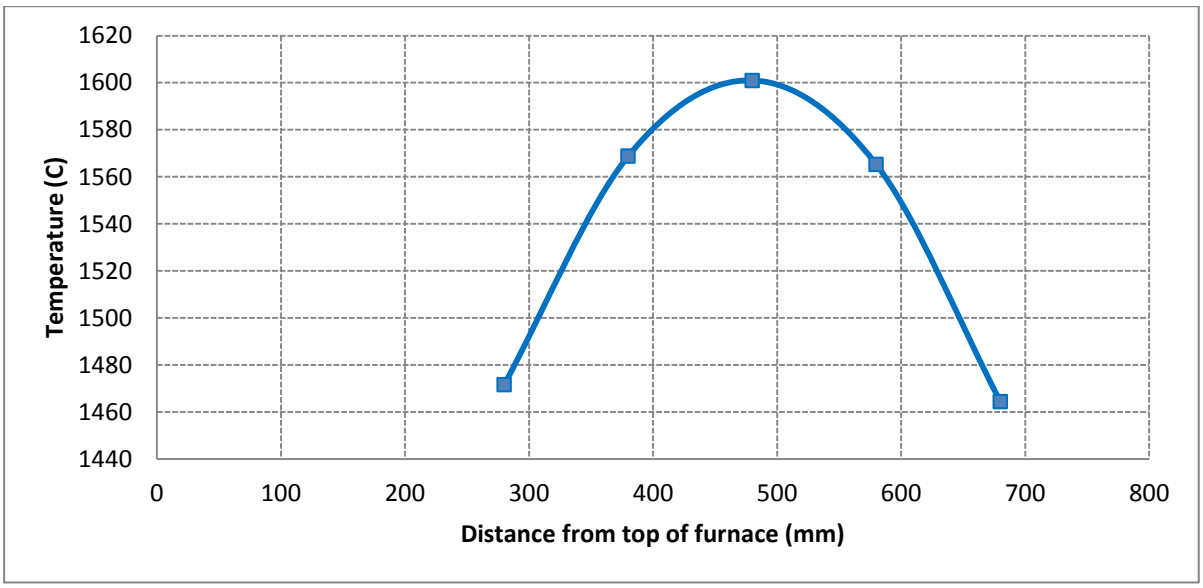

Figure 3.4 – Temperature profile of the tube furnace.

As it is seen, at about 490 mm from the top of the furnace, there is a well-developed hot zone. Therefore all specimens were placed within close proximity of this hot zone.

Preparing the mix

The second step involved the preparation of a mixed concentrate and reductant sample. A sample was taken from one of the low grade concentrates. However, the sample must be an actual representation of the large batch of concentrate; therefore riffle and sectorial splitting were used to acquire a small representative sample. A sample of the SiC reductant was also prepared in similar manner.

Next, the tube furnace and scales were turned on followed by entering a set point temperature on the temperature controller. Thereafter the furnace temperature was allowed to stabilize for 120 minutes at this temperature. The scale was allowed to stabilize for at least 30 minutes. Once the scale had stabilized, a concentrate sample and a SiC sample according to a required ratio were weighed in a glass sample holder and the mass was noted accurately. The concentrate/reductant blend was mixed properly by stirring vigorously with a stainless steel wire by hand inside the glass sample holder for at least 1 minute. Thereafter, the concentrate/reductant mix was added into the crucible and place on the scale pan and the mass was noted again.

Smelting the mix

After the preparation of the sample and time allowance for the furnace to reach its set temperature, the crucible containing the sample was placed into the tube furnace. The sample support pedestal holding disk was placed in the bucket of water, followed by placing the crucible onto the crucible refractory support. The high purity Argon vessel was opened at a flow rate of 5 L/min and allowed to purge into the Al tube inlet for 5 min. After 5 minutes, the Ar flow rate was reduced to less than 600

mL/min and the furnace was lowered until the Al tube protruded at least 3 mm into the water seal. The starting time was noted and the sample was left in the furnace for a designated time.

When the sample had been in the furnace for its designated time, the Ar flow rate was increased to 5 L/min. The furnace was raised until the crucible was directly opposite the Ar inlet in the Al tube and purged for additional 10 minutes. After the elapsed 10 minutes, the furnace was raised fully; the crucible was removed and was inserted into a glass sample holder previously purged with Ar to prevent any oxidation of a possible alloy phase. When the sample cools down, it is weighed.

Preparing alloy samples for different analytical techniques

In order to prepare samples for different analytical techniques, different approaches needed to be followed. For SEM preparation a sample was cut into thin slices ($< 10\ mm$) with a diamond coated cutter. After a sample had been produced and cooled down, it needed to be cut through the centre of the crucible (assuming that the alloy button had formed on bottom centre of the crucible) for SEM sample preparation. A cutter with a diamond coating blade was used to cut through this hard alloy button. A thin slice with a portion of the alloy as well as a portion of the slag from the original crucible was the desired end-product.

For XRF, ICP-MS and XRD preparation the crucible was broken with a hammer. The alloy button should easily separate from the small broken pieces of slag and was weighed after separation. The metal fall was then calculated as follow:

$$Metal\ fall\ \% = \frac{Alloy\ button\ mass}{Initial\ concentrate\ mass} \times 100\% \qquad \text{(Eq. 3.1)}$$

Slag samples were grinded and milled down to a fine powder ($< 70\ \mu m$) and analysed with XRD and XRF, whilst the alloy button was dissolved in an acid solution (66.67 % HCl and 33.33 % HNO_4) and analysed with ICP-MS (see section 3.4).

3.4 Analytical techniques

3.4.1 Overview

Two UG2 LG (low grade) concentrates, as well as silicon carbide were received from Lonmin Western Platinum Limited. The samples were already pulverised and were split for chemical analysis. Riffle and sectorial splitting were used respectively. Samples of different sieve sizes, 25/ 38/ 45/ 53/ 75/ 90/ 106/ 125/ 150/ 180/ 212/ 250/ 300/ 355/ 425/ 500/ 600 μm were analysed with XRF, XRD and ICP-MS to mainly detect crystal structure, major oxide content and PGMs.

After smelting, the MgO crucible was broken and the alloy button formed at the bottom of the slag layer was carefully separated. Respective slag samples were analysed with XRF and XRD, at the same time the alloy button was analysed ICP-MS for major base metal elements and PGMs. Some alloy buttons were polished and mounted for SEM-EDX.

3.4.2 Sampling and screening of LG concentrates and SiC

Methods used

In order to obtain a representative sample for analytical work, riffle and sectorial splitting techniques were used. Although these sampling techniques are not ideal and could contribute to sampling error, no other techniques could be conceived that would eliminate sampling error on the LG concentrates and SiC reductant. Therefore it is assumed that some small inconsistencies could appear in results, however it should not overshadow the major factors influencing PGM recovery results.

Particle size distribution

A screen analysis was conducted on each of the concentrates, as well as the SiC reductant. The screen sizes varied from 25 - 600 microns. The cumulative percent passing graphs are presented in Figure 3.5 and Figure 3.6. In other words, the percentage of mass of particles increases with increasing screen size.

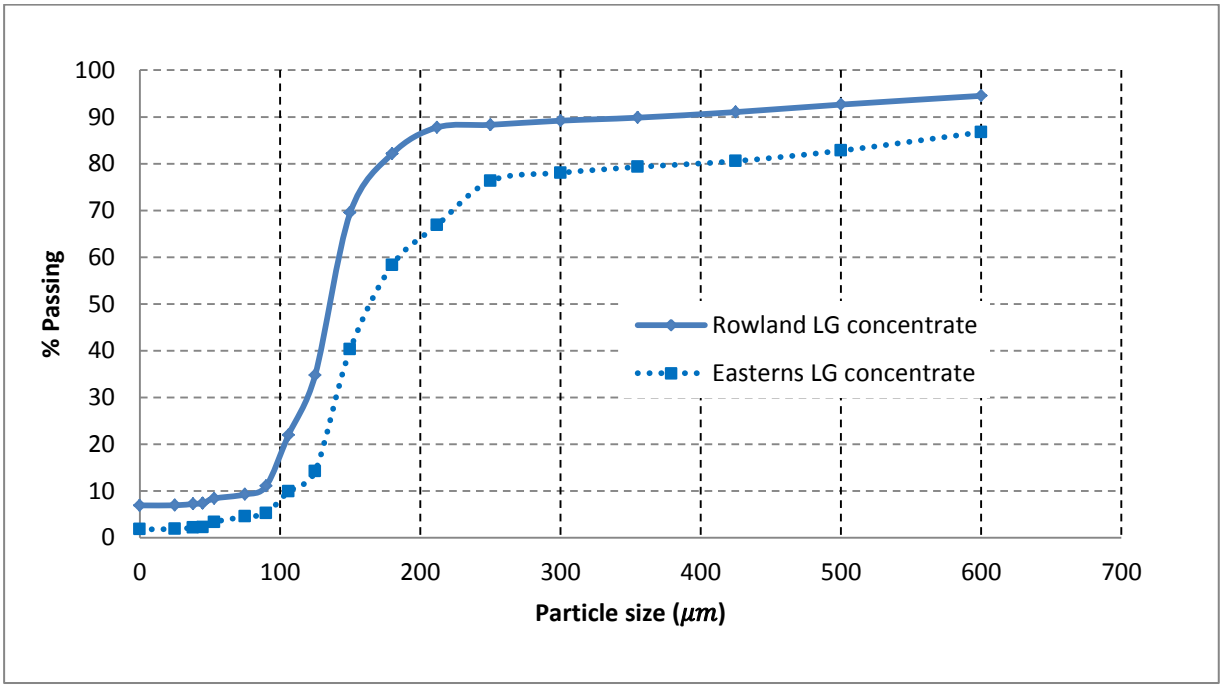

Figure 3.5 – Cumulative percentage of particles passing a size faction as a function of the particle size from particles of Rowland and Easterns LG concentrate.

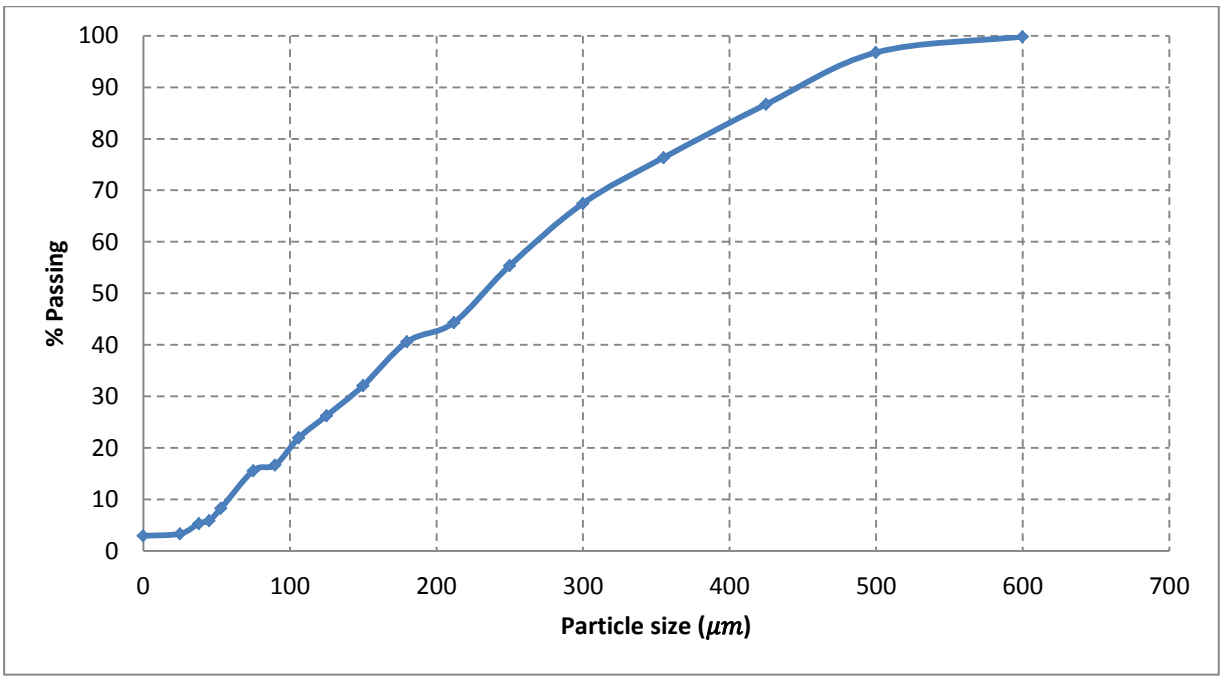

Figure 3.6 – Cumulative percentage of particles passing a size faction as a function of the particle size from particles of SiC reductant.

The P50 and P80 values for Easterns LG concentrate are $\pm 170\ \mu m$ and $\pm 420\ \mu m$, respectively. The P50 and P80 values of Rowland LG concentrate are $\pm 140\ \mu m$ and $\pm 180\ \mu m$, respectively. Particle size distribution for SiC reductant is more evenly distributed among the screen sizes. The P50 and P80 values for SiC reductant are $\pm 230\ \mu m$ and $\pm 380\ \mu m$, respectively. Particle sizes are coarser then UG2 flotation concentrates, which has a typical P80 below 50 μm. It is therefore clear that these flotation tailings will take longer to melt than flotation concentrates. However, the influence of reaction kinetics are expected to be minimal, given the high operating temperature and particle sizes being below 600 .

3.4.3 XRD

Methodology

Bulk samples and samples of different screen sizes from Rowland and Easterns LG concentrates along with SiC reductant were analysed at XRD analytical and consulting cc, Lynwood Glen, South Africa. The coarse samples were milled down in a swing mill. Thereafter, the samples were prepared for XRD analysis using a backloading method or a zero background holder, depending on amount of material available. The samples were analysed with a PANalytical X'Pert Pro powder diffractometer with X'Celerator detector and variable divergence- and fixed receiving slits with Fe filtered Co-Kα radiation. The phases were identified using X'Pert Highscore plus software and the relative phase amounts (weight %) was estimated using the Rietveld method. Only the results of the bulk samples along with the errors are shown in Table 3.1 and Table 3.2. The results for the different screen sizes, along with chemical formulas of minerals can be found in the Appendix.

Results from analysis

Table 3.1 – XRD results of Rowland and Easterns LG concentrates bulk samples

Mineral	Wt % - Rowland LG concentrate	3 sigma error	Wt% - Easterns LG concentrate	3 sigma error
Actinolite	3.33	0.63	0.91	0.24
Augite	4.5	0.51	5.44	0.6
Biotite	6.91	0.69	5.03	0.63
Calcite	0.57	0.3	0.15	0.57
Chalcopyrite	0.33	0.13	0.16	0.07
Chlorite	4.88	0.84	5.31	0.75
Chromite	4.68	0.3	7.57	0.42
Enstatite	43.63	1.23	48.22	1.2
Kaolinite	4.84	0.57	4.26	0.66
Plagioclase	5.82	0.57	4.38	1.5
Quartz	1.11	0.18	1.07	0.51
Talc	19.42	1.47	17.5	1.05

The two abundant minerals, Enstatite and Talc, are composed of SiO_2 and MgO. The results also highlight the high chromite and low sulphide mineral content. The only sulphide mineral detected is chalcopyrite in very low concentration; however from previous MLA of Lonmin Western Platinum Limited LG concentrates [50], it is possible that sulphide minerals may not have been detected. These include pentlandite and pyrite, which are Ni and Fe bearing minerals. Some factors contributing to the non-detection of these minerals are that peak intensities could not be allocated to certain minerals because of detection limitations of the XRD apparatus. Also it could be that the concentrates does not occur in a natural form, therefore a peak intensity of a natural occurring mineral could be harder distinguishable. Peak intensity graphs can be found in the appendix.

Errors associated with each mineral are also shown and found to be relatively small, although these indicated that there may be a small variation in weight percentages. Errors were calculated as part of the minimization of the residual function that utilizes a non-linear least squares algorithm [51].

Table 3.2 – XRD results of SiC reductant bulk sample

Mineral	Wt %	3 sigma error
Hibonite	3.56	0.51
Corundum	1.64	0.36
Cristobalite	1.13	0.25
Graphite C	9.22	1.05
4H-SiC	60.32	1.14
(α)6H-SiC	24.13	0.9

Referring to table 3.2, t is noticeably clear that the SiC is not pure and that some other minerals are present in relatively high percentages. Also, SiC is present in more than one crystal structure form, with 4H-SiC crystal structure being the more abundant of the two crystal structures. Both these two forms of SiC have hexagonal crystal structures and have only very small property differences. The (β)3C-SiC with a cubic crystal structure is known to have a larger surface and could support reduction reactions. However this form of SiC has not been detected and the effect of crystalline structures is assumed to be small during reduction [52].

3.4.4 XRF

Methodology

Bulk samples and samples of different screen sizes from Rowland and Easterns LG concentrates along with slag samples from smelting experiments was sent to the central analytical facility, Stellenbosch University, South Africa for XRF analysis. The samples were crushed and then milled into a fine powder (particle size < 70 µm) with a jaw crusher and milled in a tungsten-carbide Zibb mill prior to the preparation of a fused disc for major and trace elements analysis. The jaw crusher and mill were cleaned with clean uncontaminated quartz between 2 samples to avoid cross contamination. Glass disks were prepared for XRF analysis using 10 g of high purity trace element and Rare Earth Element-free flux ($LiBO_2$ = 32.83%, $Li_2B_4O_7$ = 66.67%, Li = 0.50%) mixed with 1g of the powder sample.

Whole-rock major element compositions were determined by XRF spectrometry on a PANalytical Axios Wavelength Dispersive spectrometer. The spectrometer is fitted with an Rh tube and with the following analyzing crystals: LIF200, LIF220, PE 002, Ge 111 and PX1. The instrument is also fitted with a gas-flow proportional counter that uses a 90% Argon-10% methane mixture of gas and a scintillation detector. Major elements were analyzed on a fused glass disk at 50 kV and 50 mA tube operating conditions. Matrix effects in the samples were corrected for by applying theoretical alpha factors and measured line overlap factors to the raw intensities measured with the SuperQ PANalytical software. The concentration of the control standards that were used in the calibration procedures for major element analyses fit the range of concentration of the samples. Amongst these standards were NIM-G (Granite from the Council for Mineral Technology, South Africa) and BE-N (Basalt from the International Working Group).

Results from analysis

Only the results of the bulk samples along with the relative standard deviation of each oxide are shown in Table 3.4. The results for the different screen sizes can be found in the Appendix. Analysis of slag samples are found in the main results section of the report.

Table 3.3 – XRF results for Rowland and Easterns LG concentrate bulk samples

Oxide	STDEV	Wt % - Rowland LG concentrate	Wt % - Easterns LG concentrate
Al_2O_3	0.20	5.41	5.00
CaO	0.04	2.72	3.03
Cr_2O_3	0.00	2.94	4.31
Fe_2O_3 *	0.14	12.73	14.24
K2O	0.06	0.10	0.10
MgO	0.04	22.79	23.05
MnO	0.01	0.15	0.18
Na_2O	0.18	0.38	0.30
P_2O_5	0.01	0.02	0.02
SiO_2	0.54	49.40	47.81
TiO_2	0.02	0.31	0.32
LOI *	0.05	3.08	2.32
Sum Of Conc.	**0.71**	**100.05**	**100.66**

* LOI includes the total of volatiles content of the rock (including the water combined to the lattice of silicate minerals) and the gain on ignition related to the oxidation of the rock (mostly due to Fe), therefore Fe_2O_3 need be converted to FeO. After the conversion, wt. % is normalized in order for the total sum of concentrates to be 100%. The new values of the respective oxides are found in the section 3.6 of the report.

The compositions of both concentrates are as expected, particularly the high Cr_2O_3 concentration, which corresponds to the high percentage of Chromite detected from XRD analysis. Also, the high SiO_2 and MgO concentration is consistent with XRD results because of an abundant of MgO and SiO_2 bearing minerals that were detected. The higher SiO_2 and lower FeO, Cr_2O_3 concentration in Rowland LG concentrate will cause slag viscosity at the beginning of the melt to be higher than slag viscosity of Easterns LG concentrate at the beginning of the melt. This could already be an indication that PGM recovery should be higher for SiC reduction of Easterns LG concentrate.

3.4.5 ICP-MS

Two LG concentrates were received from Lonmin Western Platinum Limited. During smelting of the concentrates under mild to high reducing conditions, alloy buttons were formed and afterwards separated from a slag phase (Refer to section 4 on results and discussion of SiC reduction).

ICP-MS sample preparation

LG Concentrates were prepared with sodium peroxide fusion followed by dissolution. Alloy buttons were dissolved in an acid solution (33.33 % HCl and 66.67 %HNO_4) followed by sodium peroxide fusion. ICP-MS makes use of isotopes identified in the plasma phase. Where multiple isotopes exist, the redundancy in data allows the elimination of plasma-isotope combinations that may cause false spectral analyses. Single isotopes may occasionally give rise to false combinations of lighter elements with plasma gases. Silicon may lead to inaccurate results when the silicon has not been completely dissolved, as particles may spend an insufficient time in the plasma to volatilise.

ICP-MS results

The ICP-MS results of Rowland and Easterns LG concentrates are shown in Table 3.4, respectively. The results were provided by Golden Pond 67. The results of alloy buttons can be found in the main result and discussion section of the report (section 4).

Table 3.4 – PGM weight % in the respective LG concentrates. Both samples were analysed at Golden Pond 67.

	Au %	**Ir %**	**Pd %**	**Pt %**	**Rh %**	**Ru %**
Rowland LG Concentrate	<0.005	0.057	0.100	0.059	<0.005	<0.005
Easterns LG concentrate	<0.005	0.064	0.110	0.083	<0.005	<0.005

The weight % of Pd, Pt and Ir form the bulk of PGM total weight %, with Rh and Ru below the detection limit of 0.005 %. Some traces of Au was also detected, however no traces of Os was detected.

3.4.6 SEM-EDX

Sample preparation

A thin slice, which includes a part of the alloy and slag, was sent to the sample preparation laboratory at the Central Analytical Facility at the Stellenbosch University. The samples were polished and mounted. Figure 3.7 is a sample after it has been mounted.

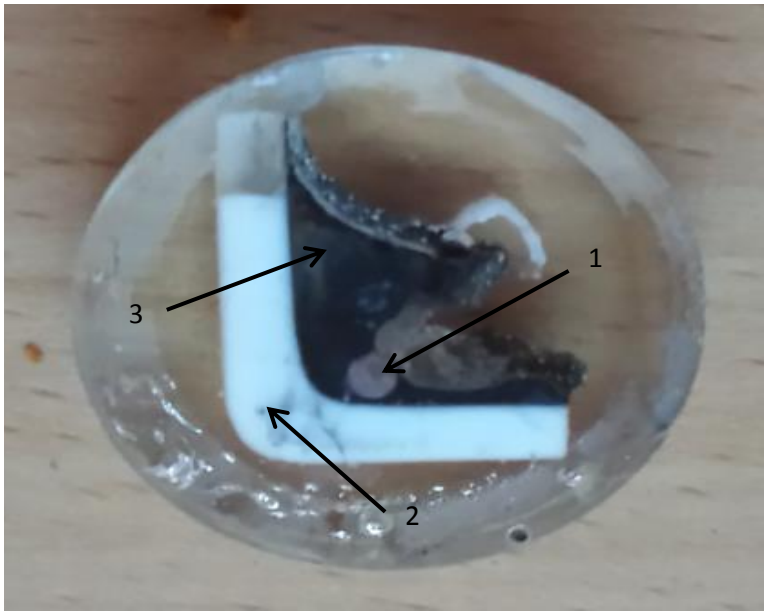

Figure 3.7 – A mounted sample - Top view: (1) – Alloy button, (2) – Crucible wall, (3) – Slag

SEM-EDX to identify phases and analyse elemental composition of phases

A scanning electron microscope (SEM) focuses a beam of electrons on a specimen to acquire information as to its structure and composition. Figure 3.8 is a typical modern SEM fitted with EDX (Energy dispersive X-Ray) found at the Central Analytical Facility, Stellenbosch University.

Figure 3.8 – Scanning electron microscope (model EISS EVO MA15VP) at the central analytical facility, Stellenbosch University, South Africa.

The SEM is equipped with the following detectors:

1.) Secondary Electron Detector (SED)
2.) Variable Pressure Secondary Electron Detector (VPSED)
3.) Backscattered Electron Detector (BSD)
4.) Energy Dispersive X-ray Spectrometer (EDS or EDX: “GENESIS XM2”)
5.) Cathodoluminescence detector
6.) Wave Dispersive X-ray Spectrometer (WDS) for more quantitative, in-situ elemental analysis.

3.5 Thermodynamic modelling methodology

Thermodynamic equilibrium modelling was performed with a commercial software package FactSage, version 6.2 [64].

Thermodynamic modelling (FactSage) approach

The analysis of chemical reactions forms the central part in any chemical/metallurgical engineering environment. There is an infinite amount of products and arrangements that can be formed from a certain set of reactants. Therefore it is important to determine which products are favoured given specified elemental composition, temperature and pressure. This phenomenon is known as chemical

reaction equilibria and will form the basis during the reduction of all metal oxides. The constraints [6] associated with reaction equilibria need to be considered at all times since it will determine if a metal oxide will be reduced or not. During the reduction of any concentrate or ore the final product will be a combination of product species with the lowest Gibbs energy from a reactant input [6, 64]. FactSage equilib module employs the Gibbs energy minimization algorithm for treating complex heterogeneous equilibrium using compound and solution databases.

System selection

Within the FactSage equilib module, it is possible to calculate equilibrium according to a normal and open system. The normal system calculates equilibrium products of the entire input feed streams, including gaseous, liquid and solid. The open system allows for the gaseous products to be continually removed in a number of steps and a new gas addition is done upon which equilibrium is calculated again. The equilibrium products, with the exception of the gas phase, are seen as the feed to the next step, with the number of steps being specified.

However, in this evaluation, a normal system is a suitable selection to calculate equilibrium compositions, since the concentrate and reductant is feed into a furnace and contained, with the gas phase being slowly extracted. Therefore, only one equilibrium state could be calculated.

Databases description used in the thesis

The FactSage databases utilized in this study are the largest set of evaluated and optimized thermodynamic databases for inorganic systems in the world and used extensively in metallurgical and chemical applications. The solution databases (for solutions of oxides, salts, metals, etc.) have all been developed by evaluation and optimization obtained from literature.

Based on proper thermodynamic models for every phase, all available thermodynamic and phase equilibrium data for a system are evaluated simultaneously in order to acquire one set of model equations for the Gibbs energies of all phases as functions of temperature and composition. During optimization, all the data are condensed self-consistent, discrepancies in the data can often be resolved, and the data can be properly interpolated and extrapolated. For example, the properties of multicomponent solutions can normally be estimated with very good accuracy from the optimized model parameters of their binary and ternary sub-systems. The resulting databases of model parameters can be used for calculating phase equilibria and thermodynamic properties using the FactSage Gibbs energy minimization software [64].

The FactSage thermodynamic databases are developed as follow:

1.) A mathematical model for G (T, P, composition) is developed for each phase.
2.) The model parameters are optimized simultaneously by using all available thermodynamic and phase equilibria data from the literature.
3.) Use models and database to estimate properties of multicomponent systems.
4.) Through the minimization of Gibbs energy, thermodynamic properties and phase equilibria is calculated.

In the Fact 53 database more than 4500 compounds are enlisted. It contains selected data for thousands of compounds taken from standard compilations as well as most of the data for those compounds which have been evaluated and optimized to be thermodynamically consistent. All individual thermodynamic extensive properties for elements and compounds can be extracted from the Fact 53 database. During evaluation of a multicomponent system, data from the gas phase is generally found from the Fact 53 database, while the solid and liquid data are found in other databases. The following databases are utilized to model these solid and liquid phase [64].

Slag phases

In a multicomponent system it is most likely that more than one phase will be present. For instance, during smelting a slag phase that contains elements in its oxide form will be formed and the FToxid databases that contain data for pure oxides and oxide solutions can be initiated. Some of the major compounds that are has been fully evaluated and optimized are Al_2O_3, CaO, FeO, Fe_2O_3, MgO and SiO_2 [64].

Matte phases

This database is particularly useful for matte/alloy/slag/gas equilibria in conjunction with Fact 53 and FT oxide databases. The principal phase in this group is the **liquid matte [FTmisc-MATT].** It is designed for calculation of matte/slag/metal equilibria and is consistent with FToxid-SLAG, FTmisc-CuLQ, FeLQ and FTmisc-PbLQ [64].

Alloy phases

A molten metal phase is likely to occur during smelting of a concentrate with high iron content. The FeLQ from the FTmics database is suitable for diluted solutions (used in steel industry); however in the presence of other base metals, the FeLQ may give inaccurate results. The SGTE LIQUID phase will give more accurate results when the metal phase contains iron and other base metals.

In general, there are 78 elements included in this database and from these elements, there are some 350 completely assessed binary alloy systems, of which over 40 are newly assessed systems and many others have been reviewed or amended on the basis of newly published experimental information. The database also includes about 120 ternary and higher-order systems for which assessed parameters are available for phases of practical relevance. The systems now integrate approximately 180 different solution phases and 600 stoichiometric intermetallic compound phases [64].

3.6 FactSage input and initialization

Normalized concentrate inputs

The two low grade concentrates, along with the SiC reductant that were received from Lonmin Marikana, were analysed (See section 3.4 for results). Peirce-Smith converter slag was analysed at Lonmin Western Platinum Limited therefore no further analysis was required. Minor Oxides (<1 %), including Na_2O, TiO_2, MnO and K_2O were neglected in order to reduce total number of species in FactSage output. The major oxides will include **CaO, MgO, Al_2O_3, FeO, SiO_2** and **Cr_2O_3**, respectively and all composition percentages are normalized to acquire a total weight percentage of 100%. Neglecting these minor oxides is assumed to have no major impact on the final slag, metal or gas chemistry. This assumption does not need to be checked afterwards, since the idea of the thermodynamic modelling prior to laboratory scale experiments is to only estimate a range of optimum experimental conditions.

Table 3.5 – Normalized wt. percentages of major oxides and elements of Rowland LG concentrate, Easterns LG concentrate and Lonmin converter slag.

Concentrate	CaO	MgO	Al_2O_3	FeO	SiO_2	Cr_2O_3	Ni	Cu
Rowland	2.868	24.063	5.712	12.095	52.153	3.109	0	0
Easterns	3.155	24.008	5.204	13.346	49.801	4.486	0	0
Converter slag	0	0	0	64.560	29.994	2.219	2.048	1.179

From Table 3.5 it is apparent that an abundantly high amount of SiO_2 and MgO is present in the concentrates. The relatively high amount of FeO is expected to be sufficient for acceptable metal fall and PGM collection during SiC reduction of Rowland and Easterns LG concentrate. However, during reduction, FeO content decreases, causing slag viscosity to increase. Thereby, phase separation could become insufficient.

The base metals Ni and Cu, were not detected during XRF analysis, however it is known from literature [50] that Ni and Cu were present in these concentrates as sulphides, but due to these base metal oxides ease of reduction and low concentration, it were neglected in the thermodynamic modelling. Neglecting Ni and Cu will have a very small effect on metal fall, since FeO is in abundance and will form the bulk of the alloy when reduced. Also, since PGMs are in trace amounts and databases have not been fully optimized with noble metals, only base-metal databases were included for simulations.

From Table 3.5 it is also apparent that the converter slag has a very high FeO wt. %, which can be used as an additional source to increase metal fall and improve slag properties for improve PGM recovery.

Final settings

The final settings before thermodynamic equilibrium were calculated in FactSage are summed up in table 3.6:

Table 3.6 – Selection of databases, species and phases in FactSage 6.2

Databases selected	FACT 53, FToxide, FTmisc and SGTE
Species involved	CaO, MgO, SiO_2, FeO, Al_2O_3, Cr_2O_3, SiC, C, Ni, Cu and $CuFeS_2$
Phases selected	Gas, pure solids, matte, alloy and slag

The databases, along with the phases selected had remained selected throughout all FactSage simulations; however species involved had changed in composition due to two concentrates being simulated. Also pure Cu and Ni will only be included if the converter slag is included and simulated along with one of the respective concentrates. Also, chalcopyrite was only included in one simulation as a variable to verify if a separate matte phase could possibly form.

Figure 3.9 is a simple schematic on how a model is set-up and evaluated in FactSage. It involves 6 basic steps that are required to build any thermodynamic model in FactSage.

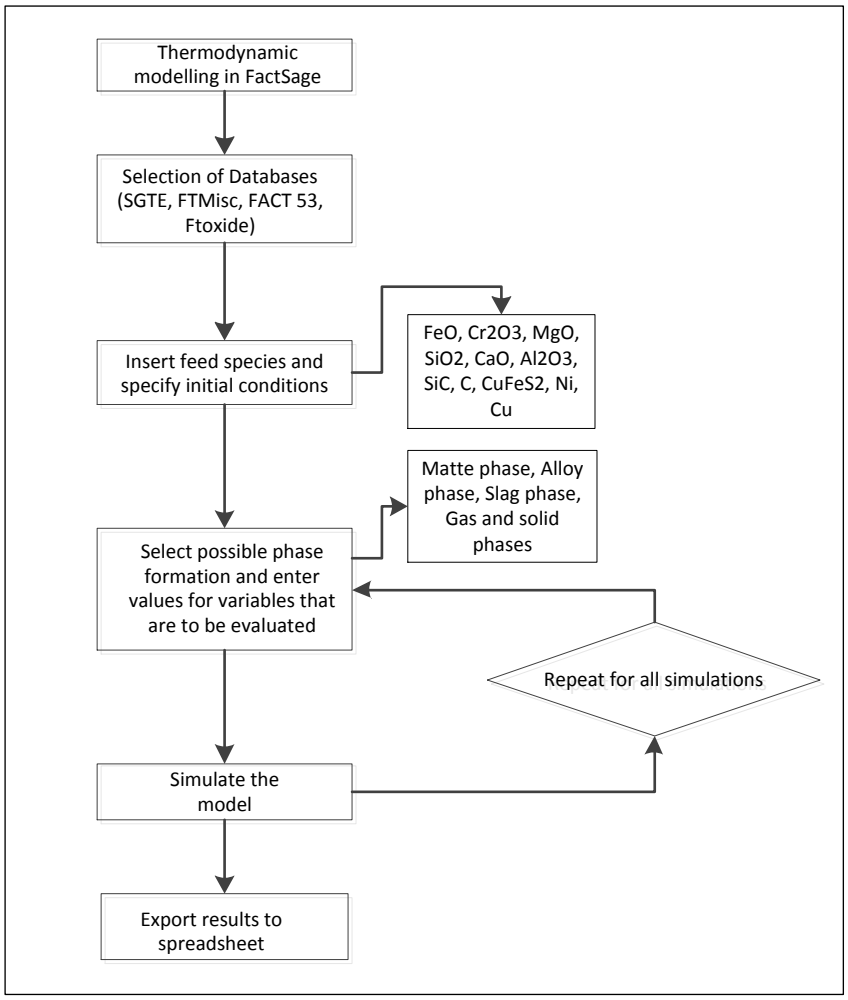

Figure 3.9 – 6 basic steps for setting up and simulating a thermodynamic model in FactSage.

Assumptions made for FactSage simulations

Compounds or elements that have a mass percentage of less than 1% were neglected in order to reduce possible stable products in equilibrium. FactSage has limited the number of possible products to 1500 and if all compounds are to be included, the number of products will exceed 1500.

However, it is expected that minor compounds will have negligible effect on gas, slag and alloy/matte formation and composition.

Thermodynamic equilibrium results did not consider any physical properties of the molten slag, metal or matte. These include, viscosity of slag, interfacial tension, entrainment of alloy or matte in the slag phase and size of matte/alloy droplets. Since the purpose of FactSage is to only thermodynamically evaluate reduction of LG concentrates with SiC, physical characteristics were not included in the analysis.

Moreover FactSage does not take kinetics of reactions into account, however due to a very high experimental temperature all reactions were assumed to precede fast; hence the effect of kinetics is likely to be diminished.

4. Results and Discussion

4.1 Overview

After the furnace has been modified for pyrometallurgical experiments and the tests were conducted. Along with the completed thermodynamic equilibrium simulations in FactSage, the metal fall, alloy composition, slag composition, gas composition (only FactSage) and PGM recovery were determined. The results are given in this chapter. Initial FactSage simulations were conducted prior to lab scale experiments in order to find a range of optimum conditions. Experimental results (when available) are then compared with thermodynamic equilibrium results and discussed. Images from SEM is also included and discussed in the chapter. After evaluation of experimental results, the optimum conditions for PGM recovery were attained. Lastly, the economic feasibility of reductive smelting vs. classical matte based smelting is evaluated.

4.2 Thermodynamic equilibrium analysis to find optimum conditions for experimental matrix

In this section, thermodynamic evaluation is conducted on properties expected to have an influence on reductive smelting. A range of optimum conditions for experiments were therefore predicted from thermodynamic modelling. Temperature and reductant to concentrate ratio were expected to be most influential with regard to metal fall, alloy composition and slag viscosity. Thermodynamic equilibrium with the presence of chalcopyrite is also determined in order to evaluate for a possible matte phase separating from the slag and alloy phase.

Effect of temperature

In this section, the effect of temperature was investigated. The metal fall together with Fe, Cr, C and Si concentrations in the alloy phase are shown in Table 4.1. Without any reductant in the system, an $MgCr_2O_4$(s) spinel forms, therefore a reductant mass of 3 kg SiC / 100 kg LG concentrate was chosen as a default state. For a prediction on optimum temperature range, Fe concentrations should remain high, while Cr and Si should remain low, preferably less than 10 % in total. Results from SiC reduction of Rowland LG concentrate and Easterns LG concentrate are shown in Table 4.1 and Table 4.2 at 1400, 1450, 1500, 1550, 1600 and 1650℃, respectively. A Metal fall of 8 - 15 % is required to recover most of base metals and PGMs.

Table 4.1 – Thermodynamic equilibrium prediction on metal fall and alloy composition as a function of temperature (values of Cr, C, Fe and Si expressed as wt. %) for Rowland LG concentrate.

Temperature	Metal fall %	Cr	C	Fe	Si	*Minor elements	Total
1400℃	9.78	6.67	2.14	90.65	0.54	~0	100
1450℃	9.76	6.33	1.83	90.85	1.00	~0	100
1500℃	9.75	6.19	1.46	90.88	1.47	~0	100
1550℃	9.73	6.01	1.14	90.90	1.96	~0	100
1600℃	9.68	5.79	0.87	90.90	2.44	~0	100
1650℃	9.63	5.57	0.66	90.87	2.89	~0	100

*The alloy mass balance being made of some minor elements (Al, Ca and Mg) found in trace amounts in the alloy.

Table 4.2 – Thermodynamic equilibrium prediction on metal fall and alloy composition as a function of temperature (values of Cr, C, Fe and Si expressed as wt. %) for Easterns LG concentrate.

Temperature	Metal fall %	Cr	C	Fe	Si	*Minor elements	Total
1400℃	9.85	4.49	1.26	94.08	0.16	0.01	100
1450℃	9.83	4.44	1.25	94.11	0.20	~0	100
1500℃	9.83	4.56	1.08	94.08	0.29	~0	100
1550℃	9.80	4.68	0.88	94.01	0.43	~0	100
1600℃	9.76	4.77	0.71	93.92	0.61	~0	100
1650℃	9.71	4.82	0.57	93.80	0.82	~0	100

*The alloy mass balance being made of some minor elements (Al, Ca and Mg) found in trace amounts in the alloy.

From the thermodynamic modelling in FactSage it was found that the liquidus temperatures for SiC reduction of Rowland LG and Easterns LG concentrate are 1420 ℃ and 1410℃, respectively. Below the liquidus temperature, MgSiO3 (s) proto-enstatite is formed (Figure 4.1, shows the binary phase diagram of MgO-SiO_2). The results indicate that Fe concentration decrease and at the same time; Cr concentration will decrease when the system temperature is increased from 1400 ℃ to 1650℃. However, Si concentrations systematically increase with an increase in temperature, signifying that conditions become more favourable for SiO_2 reduction at higher temperatures. The solubility of C in the alloy decreases when the temperature is increased. This indicates that C assisted in the reduction. The metal fall is to not significantly affected, however it does slightly lower when the temperature is increased.

Temperatures converging towards 1600 ℃ should yield a good metal fall (8 – 15%) and avoid formation of solid phases like $MgSiO_3$ (s) proto-enstatite likely to occur at temperatures below the respective liquidus temperatures. At the same time Cr, C and Si concentrations need to be kept low.

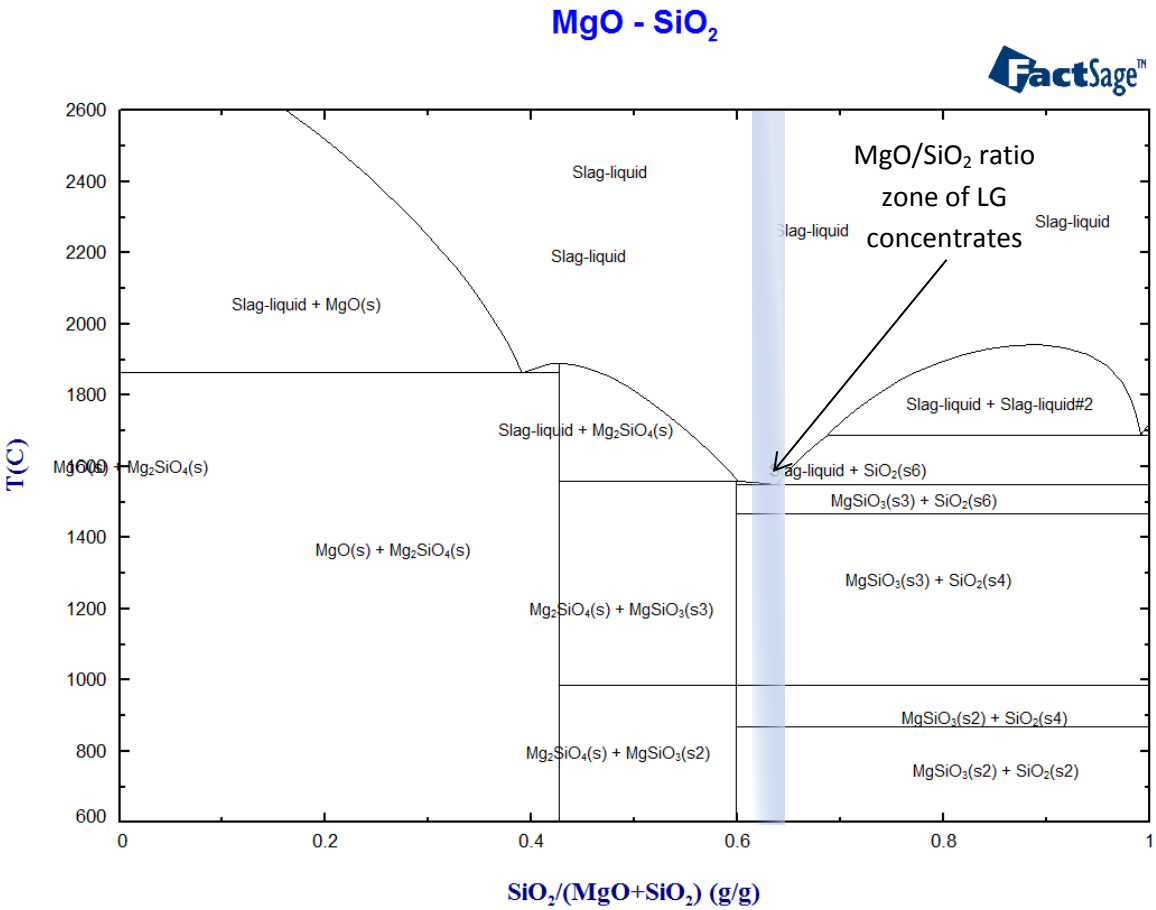

Figure 4.1 – Binary phase diagram of MgO-SiO_2 (generated in FactSage phase diagram module). The MgO/SiO_2 ratio of Rowland and Easterns LG concentrate is highlighted.

Effect of reductant to concentrate ratio

In this section, both LG concentrates were evaluated at various SiC / concentrate ratios. Thermodynamic equilibrium results are given in 100 kg concentrate per mass of reductant. It is also assumed that a temperature close to 1600 ℃ will yield the best results. Therefore a system temperature of 1600 ℃ was chosen to understand the effect of reductant to concentrate ratio. Results from SiC reduction of Rowland LG concentrate and Easterns LG concentrate are shown in Table 4.3 and Table 4.4 at stoichiometric amount of SiC / 100 kg LG concentrate and 0.5,1, 1.5, 2, 2.5, 3, 3.5,4 kg SiC / 100 kg LG concentrate, respectively.

Table 4.3 – Thermodynamic equilibrium prediction on metal fall and alloy composition as a function of reductant mass (values of Cr, C, Fe and Si expressed as wt. %). The evaluation is done for Rowland LG concentrate.

$\frac{SiC}{Concentrate}\ ratio\ (\times 10^2)$	Metal fall %	Cr	C	Fe	Si	*Minor elements	Total
0.27	~0	0.43	0.09	99.41	0.01	~0	100
0.50	0.92	0.48	0.09	99.41	0.01	~0	100
1.00	2.87	0.64	0.12	99.21	0.03	~0	100
1.50	4.81	0.92	0.17	98.85	0.06	~0	100
2.00	6.71	1.51	0.28	98.04	0.17	~0	100
2.50	8.41	3.04	0.52	95.70	0.73	~0	100
3.00	9.68	5.79	0.87	90.90	2.44	~0	100
3.50	10.69	8.76	1.15	85.36	4.72	~0	100
4.00	11.55	11.28	1.34	80.23	7.15	~0	100

*The alloy mass balance being made of some minor elements (Al, Ca and Mg) found in trace amounts in the alloy.

Table 4.4 – Thermodynamic equilibrium prediction on metal fall and alloy composition as a function of reductant mass (values of Cr, C, Fe and Si expressed as wt. %). The evaluation is done for Easterns LG concentrate.

$\frac{SiC}{Concentrate}\ ratio\ (\times 10^2)$	Metal fall %	Cr	C	Fe	Si	*Minor elements	Total
0.38	~0	0.56	0.07	99.36	0.01	~0	100
0.50	0.49	0.59	0.08	99.32	0.01	~0	100
1.00	2.44	0.75	0.10	99.14	0.01	~0	100
1.50	4.38	1.01	0.13	98.84	0.03	~0	100
2.00	6.30	1.48	0.18	98.27	0.06	~0	100
2.50	8.16	2.50	0.30	97.00	0.20	~0	100
3.00	9.79	4.82	0.57	93.80	0.82	~0	100
3.50	11.05	8.21	0.91	88.62	2.26	~0	100
4.00	12.11	11.57	1.22	83.19	4.02	~0	100

*The alloy mass balance being made of some minor elements (Al, Ca and Mg) found in trace amounts in the alloy.

From the analysis it is apparent that an increase in reductant mass will cause more oxides, particularly FeO, to reduce, thereby increasing metal fall. When reductant mass is at 0 kg, an $MgOCr_2O_3$(s) spinel forms. The stoichiometric amount of SiC required per 100 kg of LG concentrate is highlighted in Table 4.3 and Table 4.4. These amounts are determined as minimum SiC required to produce a molten metal phase, primarily being Fe, given its starting oxide concentration and ease of reduction. In both systems a molten metal phase had formed when 0.5 kg of reductant is present, emphasizing the ease of reduction of both concentrates. Almost all Cr_2O_3 is reduced to CrO, thereby increasing the solubility of Cr in the slag phase. The metal fall for respective LG concentrates will continue to rise and therefore it will become easier to recover PGMs. Somewhat better metal fall for reductive smelting of Easterns LG concentrate is expected at higher reductant to concentrate ratios since it has a marginally higher FeO concentration.

It is expected that the molten metal phase will consist primarily of Fe and other easily reduced base metals, however some Cr and Si are also expected to deport to the metal phase once the SiC / LG concentrate ratio is increased. Si and Cr start to dissolve in the molten metal at significant concentrations when reductant mass exceeds 3 kg SiC / 100 kg LG concentrate. However results from thermodynamic modelling predict metal fall and composition under ideal circumstances and base metals such as Ni and Cu were neglected in the initial concentrate input because of their ease of reduction, therefore thermodynamic modelling may slightly over estimate Fe, Cr and Si concentrations in the alloy. C concentrations in the alloy also become more significant at a higher SiC / LG concentrate ratio.

Cr solubility in the slag phase is greatly affected by the atomic state of Cr [2, 3]. Chromium in its trivalent state (spinel) has a very low solubility in the slag phase, in contrast to Chromium in its divalent state that is highly miscible in the slag phase [2]. Figure 4.2 (page 42) shows how Cr changes from a trivalent state to divalent state as function of SiC additions to Easterns LG concentrate charge.

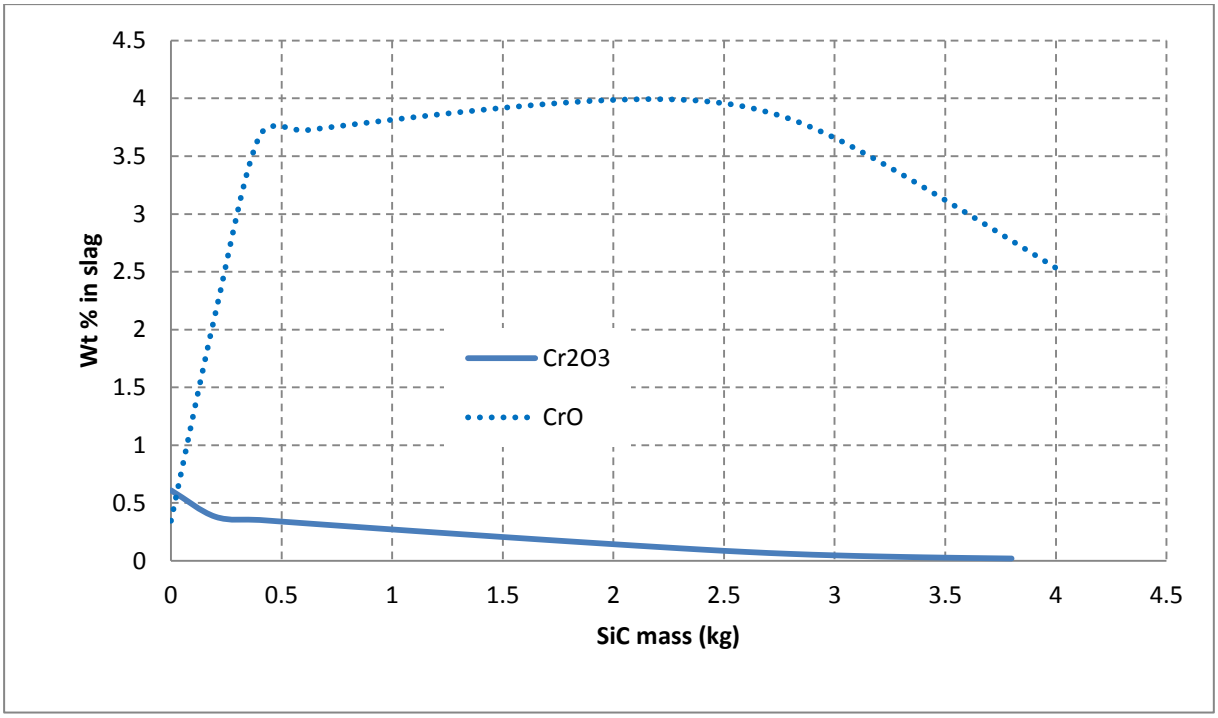

Figure 4.2 – The distribution of chromium between the phases in the system as a function of SiC additions to the charge at 1600℃.

Spinel is reduced by the SiC addition to the charge. Cr will start to dissolve into the alloy at SiC additions of 2 kg SiC / 100 kg Easterns LG concentrate or more. A very similar observation was made from SiC reduction of Rowland LG concentrate. Figure 4.2 underlines the ease of $Cr_2O_3 \rightarrow CrO$ transition through SiC reduction.

Thermodynamic modelling with the presence of chalcopyrite

The possibility of a forming matte phase should not be entirely neglected, since there is a probability that sulphide concentrations in any of the two LG concentrates were under estimated by XRD and

XFR analysis. From an ICP-MS analysis of the alloy (see section 4.3), S was found in small quantities in the alloy phase, along with Ni and Cu, which has most likely originated from the minerals pentlandite and chalcopyrite. Therefore, thermodynamic equilibrium was calculated to determine the require chalcopyrite content required to form a matte phase. Chalcopyrite was detected form XRD analysis as the only sulphide mineral; therefore it was varied to understand the effect of its presence. However the mineral pentlandite or pyrite could have also been used as an alternative to Chalcopyrite. Figure 4.3 shows the matte phase activity as a function of chalcopyrite mass. If the activity equals 1, a separate matte phase will start forming.

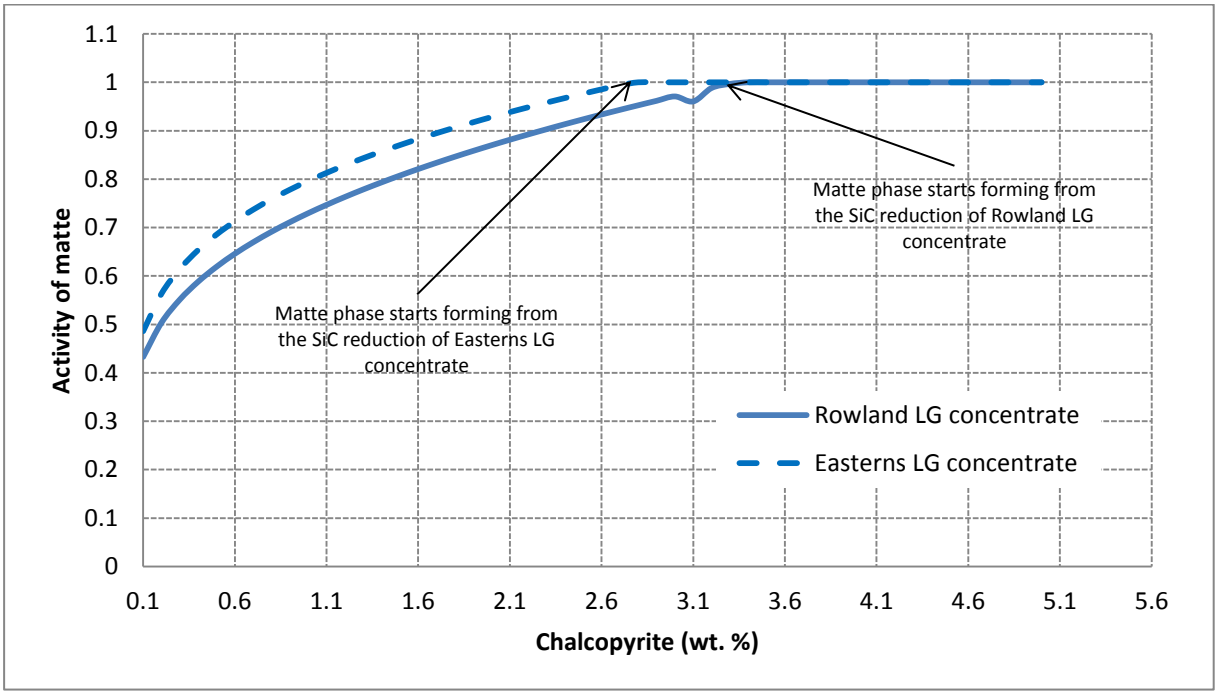

Figure 4.3 – Matte phase activity as function of Chalcopyrite wt. %. Every time the chalcopyrite wt. % was varied, other oxides were normalized to acquire a total wt. % of 100 %.

Figure 4.3 indicate that a matte phase will only coexist with an alloy, slag and gas phase when chalcopyrite in Rowland and Easterns LG concentrates are increased to 3 wt. % or more. From the XRD analysis, it was found that chalcopyrite wt. % is less than 1 %, therefore a matte phase is highly unlikely to form due to very low sulphide mineral concentrations in the respective concentrates. Although sulphide minerals could well have been under estimated or not detected at all in XRD analysis of Rowland and Easterns LG concentrates, it can at this time be assumed that a matte phase will not form during SiC reduction of Rowland and Easterns LG concentrates. A MLA of Lonmin Western Platinum Limited UG2 LG concentrates also revealed that sulphide minerals are below 3 wt. %. In these analyses, pyrite, chalcopyrite and pentlandite were the abundant sulphide minerals [50].

4.2.1 Experimental matrix

After the thermodynamic equilibrium calculations, an experimental design matrix was created. In total, 13 experiments were conducted and the results of these experiments are shown and discussed

in this section. The optimum temperature from the thermodynamic equilibrium calculations was found to be $\pm$ 1600 ℃ and the optimum reductant to concentrate ratio range was found to be 2.5 - 3.5 kg SiC / 100 kg LG concentrate. Based on some preliminary TGA experimental results conducted before any experiments in table 4.5 were conducted, it was found that no mass change occurred after $\pm$10 min of reduction time. The result from the TGA experiment was fairly reliable; therefore reduction times were ranged from 30 – 180 min to assure thermodynamic equilibrium. It was however possible to conduct only one TGA experiment due to the difficulty of the operation and fragility of the equipment. The methodology and result of the TGA experiment are found in the Appendix.

Table 4.5 – Pyrometallurgical experimental design matrix. All experiments were conducted at 1600℃.

Experiment nr.	LG Concentrate	Reductant	$\frac{SiC}{Concentrate}$ $ratio$ $(\times 10^2)$	Reduction time (min)
1	Rowland	SiC *	2.5	60
2	Rowland	SiC *	3.0	60
3	Rowland	SiC *	3.5	60
4	Rowland	SiC *	3.0	30
5	Rowland	SiC *	3.0	45
6	Rowland	SiC *	3.0	75
7	Rowland	SiC *	3.0	90
8	Rowland	SiC*	3.0	180
9	Rowland	SiC (Pure)	3.0	60
10	Easterns	SiC *	2.5	180
11	Easterns	SiC *	3.0	180
12	Easterns	SiC *	3.5	180
13	Easterns	SiC * with converter slag	3.5	180

SiC * is the reductant received from Lonmin Western Platinum Limited (Refer to section 3.4.4 for mineralogy).

In total, 13 tests were conducted in a Carbolite STF 1800 tube furnace. Figure 4.4 shows a picture of a test being conducted. The red hot alumina tube is connected to a steel tube and submerged into water to make the process air-tight. Tests were conducted at different times during the study. SiC reduction of Rowland LG concentrate was done before SiC reduction of Easterns LG concentrate and some conclusions were drawn from the results from tests with Rowland LG concentrate.

Figure 4.4 – Photo of Carbolite tube furnace used during an experiment. The tube did protrude 3- 5 mm into the water seal making the smelting operation air tight.

Reduction time of experiments

In experiments 4 – 8 the effect of reduction time on metal fall, composition and PGM recovery was investigated. By varying the time a sample spends in the furnace did investigate the effect of physical characteristics on alloy and slag separation. The result from a TGA experiment (see appendix C) indicated that thermodynamic equilibrium was reached after $\pm 10\,min$ of reduction time. The rapid equilibrium achieved is most likely from Fe reduction, given its concentration in the original concentrates. The transfer of PGMs to the alloys is inherently a non-equilibrium process dependent on time for diffusion and mass transfer, and the droplet size and settling rate through the slag and the level of motion/mixing in the slag (minimal in these experiments). These PGMs, which are locked in chromites and silicates are extremely fine grained (1 – 5 micron), therefore it is required that PGMs come into contact with the alloy droplets to be dissolved.

By varying reduction times, the amount of time required for insignificant metal fall change was determined. The reductant to concentrate ratio did remain constant at 3 kg SiC / 100 kg concentrate. Experiments exceeding ± 6 hours became inherently difficult to conduct due to the alumina rod and crucible support being exposed to the excessive high temperature, causing the materials to weaken. This led to some failed experiments and broken equipment. Consequently, the shorter experimental reduction times could restrict PGM mass transfer, as typical residence times in matte-slag industrial furnaces are 12-24 hours. However base metal recovery and overall metal fall should be adequate in making valuable conclusions from experiments.

Melts with different reductant quantities

SiC reduction of Rowland and Easterns LG concentrate with different quantities of reductant was investigated in experiments 1-3 and experiments 10-12, respectively. SiC reduction of Easterns LG

concentrate was conducted at a later time during the course of the study and results of some of the experiments with Rowland LG concentrate were already known. Therefore it was concluded that a greater metal fall and improved PGM recovery were achieved by increasing the reduction time. The reduction time for these experiments was increased to 180 min.

Melt with pure SiC

In experiment 9, Rowland LG concentrate was mixed with pure 3C-SiC (β) in order to investigate the effectiveness of SiC received from Lonmin, Marikana. Metal fall, composition and PGM recovery is used as reference to make comparison between pure 3C-SiC (β) and SiC received from Lonmin, Marikana.

Melt with converter slag addition

In experiment 13, 10 kg converter slag / 100 kg concentrate was mixed with Easterns LG concentrate and SiC reductant. The converter slag should to some extent increase metal fall (PGM collecting phase) and PGM recovery and decrease slag viscosity due to the high amount of FeO in the converter slag. The reductant to concentrate ratio was at 3.5 kg SiC / 100 kg concentrate.

4.2.2 SiC reduction of Easterns and Rowland LG concentrate

Distribution of phases

Figure 4.5 is an image of a crucible that was cut through the centre, displaying a clear alloy button surrounded by a slag phase. The sample has a reductant to concentrate ratio of 3 kg / 100 kg Rowland LG concentrate (Experiment 8). All other samples had very similar structures, a clearly visible alloy phase at the bottom of the crucible surrounded by a dark brown slag phase.

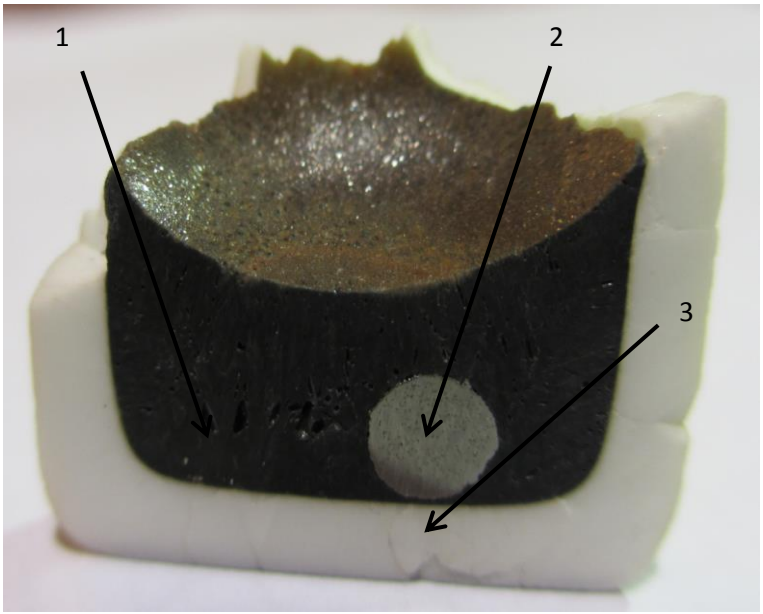

Figure 4.5 – Front view of a sample after SiC reduction of Rowland LG concentrate at 1600 ℃ , (1) – Slag phase, (2) – Alloy phase, (3) – Crucible wall

SEM analyses of the melted sample revealed two primary phases. The light grey phase is the alloy phase and the darker black phase is the slag phase. An EDX analysis on these phases is provided later in this section.

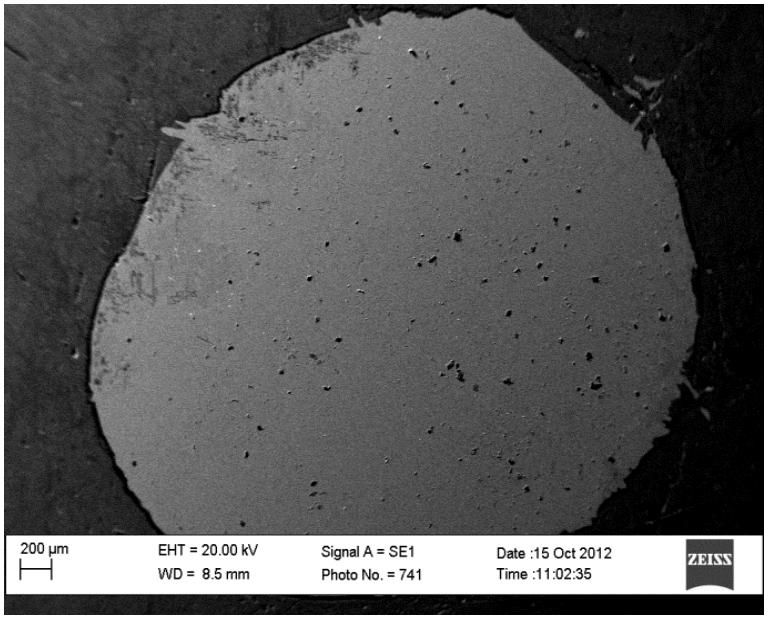

Figure 4.6 – A SEM picture of alloy produced from experiment 8 to show the distribution of the different phases.

Metal fall

An alloy from each experiment was separated from the slag phase and weighed. The metal fall for each experiment was determined from equation 3.1. The reduction time was changed for experiments conducted with Rowland LG concentrate. Metal fall from SiC reduction of Rowland and Easterns LG concentrate is shown in table 4.6 and table 4.7, respectively.

Table 4.6 – Metal fall attained for the SiC reduction of Rowland LG concentrate from all experiments conducted at 1600℃.

Experiment Nr.	$\frac{SiC}{Concentrate}\ ratio\ (\times 10^2)$	Reduction time (min)	% Metal fall
1	**2.5**	60	2.75
4	**3.0**	30	4.13
5	**3.0**	45	4.30
2	**3.0**	60	5.43
6	**3.0**	75	5.58
7	**3.0**	90	5.64
8	**3.0**	180	5.61
3	**3.5**	60	5.82
9	**3.0***	60	5.31

*Pure SiC was used as a reductant

Table 4.7 – Metal fall attained for the SiC reduction of Easterns LG concentrate from all experiments conducted at 1600℃.

Experiment Nr.	$\frac{SiC}{Concentrate}\ ratio\ (\times 10^2)$	Reduction time (min)	% Metal fall
10	**2.5**	180	3.62
11	**3.0**	180	6.80
12	**3.5**	180	7.47

The results are very clear, a longer reduction time and greater reductant to concentrate ratio will increase metal fall and is also expected to improve PGM recoveries. Work done by Andrews [28], also concluded that a longer residence time will improve settling of matte droplets. Since the results from these experiments with Rowland LG concentrate were known before any experiments with Easterns LG concentrate was conducted, reduction times were increased. Metal fall increased only marginally from 60 min to 180 min and it could therefore be assumed that any experiment with a reduction time of 60 min or longer was at physical-equilibrium. Both concentrates were sensitive to a small increase in reductant i.e. metal fall did increase by 3 % when reductant to concentrate ratio was increased from 2.5 – 3 kg SiC / 100 kg LG concentrate. This was also predicted from the thermodynamic modelling. The above experimental metal fall does however differ from that predicted from thermodynamic modelling. The largest difference in metal fall is noted at the lowest reductant to concentrate ratio, likely due to the lack of coalescence of metal prills. Less metal prills are formed at lower reductant to concentrate ratios, therefore lowering the probability to coalesce.

Increasing the amount of SiC would also cause more FeO to be reduced to Fe, causing more metal prills to form and increasing the probability to coalesce. This once again, agrees well with the work

done by Shahrokhi and Shaw [39], Saffman and Turner [40] and Ammann et al. [41]. In these studies it were concluled that sufficient matte/metal fall is required for successful coalescence to occur. Also, since more reductant was present at higher ratio's, gas bubbles rising through the slag can enhance drop growth through drop-to-drop coalescence, which was another finding by these authors. However, comparing metal fall attained from SiC reduction of Easterns LG concentrate to SiC reduction of Rowland LG concentrate at 3 kg SiC / 100 kg LG concentrate and 180 min reduction time, an almost 1 % difference is noticeable. From the thermodynamic equilibrium modeling, an almost similar metal fall % was achieved at this state of reduction.

The metal fall from an experiment conducted with pure SiC is slightly higher than that of the experiment conducted with SiC received from Lonmin. The SiC from Lonmin Western Platinum Limited is not pure and do contain some impurities (Refer to section 3.4.3 for XRD analysis on SiC received from Lonmin Western Platinum Limited). However, the difference is very small; therefore SiC received from Lonmin Western Platinum Limited could be considered as an effective reductant.

Alloy composition

In the next table, the chemical composition of the alloys attained from SiC reduction of Rowland and Easterns LG concentrate are shown in table 4.8 and table 4.9, respectively. The samples were prepared and analysed at Golden Pond 67. The results are quantitative.

Table 4.8 - Alloy composition from SiC reduction of Rowland LG as a function of % of reductant mass and reduction time (values elements expressed as wt. %).

Experiment Nr.	$\frac{SiC}{Concentrate}\ ratio\ (\times 10^2)$	Reduction time (min)	Fe	Cr	Si	Cu	Ni	S	Ir	Pt	Pd
1	2.5	60	81.2	0.24	<0.01	3.67	<0.01	<0.01	0.05	0.02	0.08
4	3	30	67.6	8.81	<0.01	2.65	<0.01	0.01	0.04	0.01	0.08
5	3	45	71.7	9.36	<0.01	2.36	<0.01	<0.01	0.06	0.01	0.06
2	3	60	81.4	2.72	<0.01	2.08	<0.01	<0.01	0.05	0.01	0.04
6	3	75	76.4	5.9	<0.01	2.25	<0.01	<0.01	0.05	0.01	0.06
7	3	90	75.1	6.12	<0.01	2.67	4.42	1.11	0.04	0.07	0.04
8	3	180	74.9	6.35	<0.01	2.71	4.51	1.13	0.05	0.08	0.06
3	3.5	60	65.1	9.59	0.01	2.02	<0.01	0.01	0.04	<0.01	0.05
9	3*	60	82.1	5.67	1.89	2.20	4.42	2.14	0.08	0.09	0.23

*Pure SiC was used as reductant

Table 4.9 - Alloy composition from SiC reduction of Easterns LG as a function of % of reductant mass and reduction time (values elements expressed as wt. %).

Experiment Nr.	$\frac{SiC}{Concentrate}\ ratio\ (\times 10^2)$	Reduction time (min)	Fe	Cr	Si	Cu	Ni	S	Ir	Pt	Pd
10	2.5	180	81.2	0.24	<0.01	3.67	<0.01	<0.01	0.34	0.02	0.08
11	3	180	84.5	1.47	0.05	1.47	4.49	2.04	0.80	0.52	1.24
12	3.5	180	88.6	1.33	0.15	1.08	2.81	1.52	0.80	0.65	1.26

Fe forms the bulk of the overall composition in all of the alloys from SiC reduction of Rowland LG concentrate. This correspond well with work done by Perry et al. [53] and Qayyam et al. [54], who also concluded that reduction of FeO will take place before the reduction of CrO. Cr concentrations increase sharply when reductant to concentrate ratio was increased. When the reductant to concentrate ratio is 3.5 kg SiC / 100 kg Rowland LG concentrate, Cr has a concentration of almost 10

% in the alloy. Cr concentrations are more than 5 % in alloys from test with different reduction times respectively. These high concentrations of Cr could cause difficulties during downstream processing, particularly during converting, BMR and PMR. Ni concentrations seem to be effected by residence time, along with S concentrations. These two elements most likely have originated from the mineral pentlandite. Pt and Pd concentrations remain very low in all of the respective alloys. However as already discussed in the materials and methods section, sample heterogeneity and assaying inconsistency may cause error in the smelting. This is seen from the variation in Fe concentration at the same SiC / Rowland LG concentrate. This will make statistical evaluation of significant deviations very difficult. PGM concentrations are also lower in Rowland LG concentrate and recoveries could be marginally more inconsistent then with Easterns LG concentrate.

Easterns LG concentrate has a higher FeO concentration than Rowland LG concentrate, justifying the higher quantity of Fe in alloy samples produced from reduction of Easterns LG concentrate. The same observation was made from the thermodynamic modelling. This correspond yet again well with work done by Perry et al. [53] and Qayyam et.al. [54], who also concluded, that reduction of FeO will take place before the reduction of CrO. The very low Cr and Si concentrations are very favourable for downstream processing, because of the difficulties in removing these elements during converting and also in the BMR and PMR plants. Pt and Pd quantities are higher in alloys from SiC reduction of Easterns LG concentrate. The better metal fall is most likely to have contributed to the higher quantities of PGMs in these alloys.

As a summary more Cr reported to the alloy where pure SiC was used as reductant. This is because pure SiC is a stronger reductant than the SiC received from Lonmin which contain some impurities. Consequently more CrO is reduced to Cr. However, the constraints of small scale experiments may overshadow any feasibility of this conclusion.

PGM recoveries

PGM recovery % (Ir, Pd and Pt) to the alloy phase for the respective concentrates are shown in Table 4.10 and Table 4.11. Recoveries are determined with the following equation:

$$\%Recovery = \frac{mass\ of\ element\ in\ alloy}{Initial\ mass\ in\ concentrate} * 100\% \qquad \text{(Eq. 4.1)}$$

Table 4.10 – Recovery % of Ir, Pd and Pt from SiC reduction of Rowland LG concentrate

Experiment Nr.	$\frac{SiC}{Concentrate}\ ratio\ (\times 10^2)$	Reduction time (min)	Fe recovery %	Ir recovery %	Pd recovery %	Pt recovery %
1	**2.5**	60	25.0	2.4	2.2	0.9
4	**3.0**	30	31.4	2.9	3.3	0.7
5	**3.0**	45	34.7	4.5	45.6	0.7
2	**3.0**	60	49.6	4.9	2.0	0.9
6	**3.0**	75	46.2	4.5	3.2	0.9
7	**3.0**	90	47.6	4.0	2.6	6.7
8	**3.0**	180	44.4	3.8	3.5	7.5
3	**3.5**	60	46.8	4.1	2.9	1.0
9	**3.0***	60	43.8	46.7	12.1	8.1

*Pure SiC was used as reductant

Table 4.11 – Recovery % of Ir, Pd and Pt from SiC reduction of Easterns LG concentrate

Experiment Nr.	$\frac{SiC}{Concentrate}\ ratio\ (\times 10^2)$	Reduction time (min)	Fe recovery %	Ir recovery %	Pd recovery %	Pt recovery %
10	**2.5**	180	24.7	11.2	1.5	0.5
11	**3**	180	57.7	69.7	62.9	35
12	**3.5**	180	66.4	94.5	86.6	59.2

It is apparent that the highest Pt and Pd recovery was achieved at a reductant to concentrate ratio of 3 kg SiC / 100 kg Rowland LG concentrate and reduction time of 180 min. The recovery of PGMs such as Ir, Pt and Pd, is very low. It is required that 90 % of PGMs should be recovered from the first melt. Fe recoveries are less than 50% from SiC reduction of Rowland LG concentrate and support the poor PGM recoveries and uncertainties from analytical analysis and small scale experiments. One factor that may significantly contribute to the low recovery of PGMs is slag viscosity and alloy-slag surface tension. The reduction time could have also been increased, however experimental constraints made this not possible. Residence times in industrial PGM collecting furnaces are 12 – 24 hours. The slag viscosity can be calculated in FactSage viscosity module that was developed from literature [55 – 62]. Section 4.3.3 evaluates the effect of slag viscosity on PGM recoveries.

The recoveries of Ir, Pd and Pt from SiC reduction of Easterns LG concentrate are significantly better. The viscosity of the slags from these tests should therefore be lower due to the higher FeO/SiO_2 ratio in the concentrate. Ir, Pd and Pt recoveries significantly increases when the quantity of reductant is increased. Overall Ir has the highest recovery, followed by Pd and Pt. The very low Cr and Si concentrations in these alloys are favourable and will allow for a further increase in reductant quantity. Therefore it should be possible to recover more than 90 % of PGMs from SiC reduction of Easterns LG concentrate. Improved Fe recovery along with better metal fall may indicate why better PGM recovery was achieved.

Characterizing and investigating the alloy phase with SEM-EDX

In order to further back-up ICP-MS results from alloys, duplicate experiments were conducted and alloys were prepared for SEM analysis. Only two alloy buttons were investigated, that of experiment 8 and 11. Other experiments could however not be conducted more than once because of limited crucibles available and other experimental constraints. Elemental composition as determined from SEM-EDX of the respective phases within the alloy is included. Figure 4.7 and Figure 4.8 show the images from SEM.

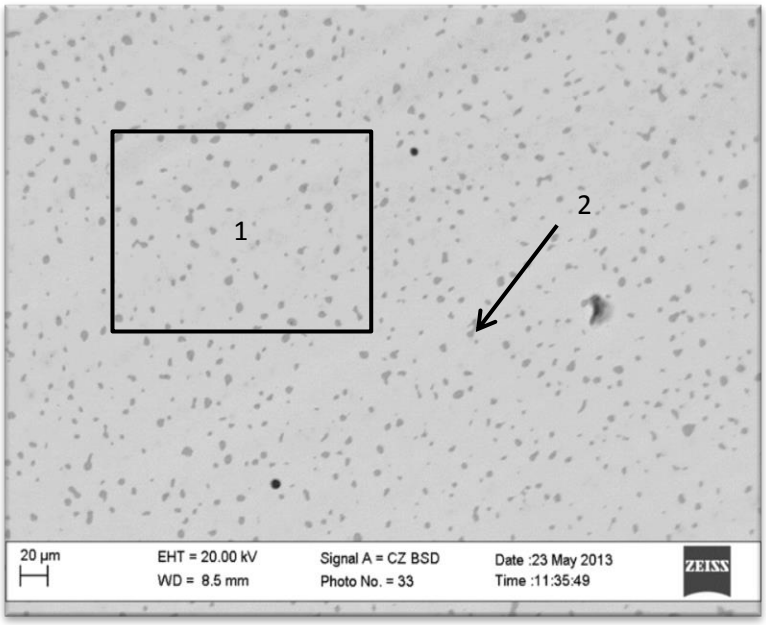

Figure 4.7 – A SEM image of an alloy button from experiment 2 (3 kg SiC / 100 kg Rowland LG concentrate – Reduction time of 180 min). The light homogeneous grey phase is a metallic phase and darker grey spots are a quaternary-Cr-Fe-Cu-S phase precipitated from slow cooling. (1) is an EDX analysis of an area, (2) is a spot EDX analysis on a sulphide phase.

Table 4.12 – EDX composition analysis of section (1) and EDX spot analysis of (2). Results are in normalized wt. %.

Element wt.%	Fe	Cr	Si	Cu	Ni	S	C	Pt	Pd	Ir	Ru	Rh
(1)	77.49	10.42	2.73	2.4	4.59	1.24	1.13	0	0	0	0	0
(2)	4.10	52.52	0.08	1.88	0	40.42	0	1.01	0	0	0	0

High Fe concentrations are detected with EDX in area (1), along with moderate to low concentrations of Cr, Si, Cu, Ni, S and C. The initial assumption that no matte phase will form during SiC reduction could however be incorrect as the S concentration in area (1) is too high for it to dissolve in a alloy phase (predicted by thermodynamic modelling), underlyning that XRD did not detect all sulphide minerals. Therefore small matte phases (quaternary-Cr-Fe-Cu-S phase) among the alloy phase are observed. However it is not expected to infleunce PGM recovery. From a spot analysis on the small quaternary-Cr-Fe-Cu-S phases, high Cr concentrations were among these phases, with low to moderate concentrations of Fe and Cu. Pt and Pd were also detected in these quaternary-Cr-Fe-Cu-S

phases. Other PGM concentrations are most likely below the detection limit (100 ppm) of the EDX. However it is not entirely conclusive why Pd and Pt is detected in close proximity to quaternary-Cr-Fe-Cu-S phases and thermodynamic modelling could not be conducted to evaluate this finding. A deeper investigation with SEM or TEM is required for this finding to be explained and conclusive.

Overall, PGMs are in very low concentrations and is assumed that most PGMs are still among the slag phase.

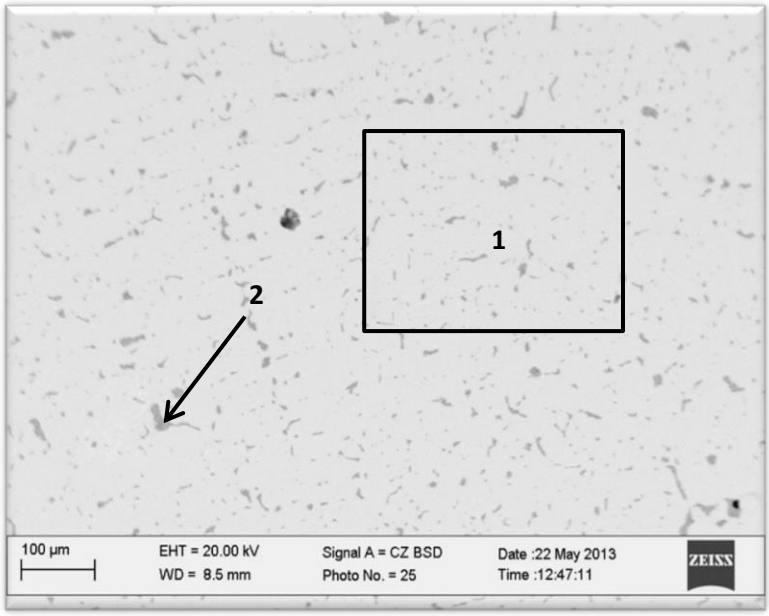

Figure 4.8 – A SEM image of an alloy button from experiment 2 (3 kg / 100 kg Easterns LG concentrate – Reduction time of 180 min). The light homogeneous grey phase is a metallic phase and darker grey spots are a quaternary-Cr-Fe-Cu-S phase precipitated from slow cooling. (1) is an EDX analysis of an area, (2) is a spot EDX analysis on a sulphide phase.

Table 4.13 – EDX composition analysis of section (1) and EDX spot analysis of (2). Results are in normalized wt. %.

Element wt.%	Fe	Cr	Si	Cu	Ni	S	C	Pt	Pd	Ir	Ru	Rh
(1)	84.9	3.64	1.27	2.25	3.49	1.44	0.75	0.62	1.31	0.33	0	0
(2)	14.86	32.06	0	12.21	0	39.32	0	0.87	0	0	0	0

High Fe concentration wasdetected with EDX in area (1), along with moderate to low concentrations of Cr, Si, Cu, Ni, S and C. Pt and Pd were detected. From a spot analysis on the small quaternary-Cr-Fe-Cu-S phases, the same finding was made as from the alloy from SiC reduction of Rowland LG concentrate. High Cr and Sconcentrations were among these phases, with low to moderate concentrations of Fe and Cu. Pt and Pd were also detected once again in this quaternary-Cr-Fe-Cu-S phaeses. The EDX analysis of elements in the alloy phased corresponded reasonable well with ICP-MS analysis, except for Si concentrations that did differ significantly. It was however reported that ICP-MS analysis had difficulties in detecting Si. Therefore it was assumed the Si concentration from the EDX analysis is accurate.

4.2.3 Investigation into the effect of slag viscosity

Slag viscosity is a function of temperature, with the viscosity decreasing as the temperature increases. It is important to keep viscosity low as this will allow the alloy phase to drain and separate. Eric [38] reported that high basicity ratios $\left(\frac{\%\ CaO+\%\ MgO}{\%\ SiO_2}\right)$ coupled with low FeO contents are detrimental to separation of two phases. It came to forth that a minimum of around 12% FeO in the slag is required for reasonable separation and settling of matte and slag. It was also found that when the iron oxide content of the slag is adequate, high basicity ratios could still cause unsatisfactory separation and settling of matte prills mainly due to the rise in liquidus temperature.

The basicity ratios of Rowland and Easterns LG concentrate are 0.516 and 0.545, respectively. These calculated values are low compared to values reported by Eric [38] in Figure 1 of the study. Therefore basicity will not have an influence because operating temperatures are at 1600℃, well above the liquidus temperatures of the slag (assuming all Cr has dissolved under reducing conditions) in contrast to the FeO content that will decrease during reduction. The SiO_2 content of the slag is also increased from the reaction of FeO with SiC. The following chemical reaction supports this finding:

$$3FeO(s) + SiC(s) = 3Fe\ (l) + SiO_2\ (l) + CO(g) \qquad \text{(Eq. 4.2)}$$

Calculating slag viscosity with FactSage viscosity module

Viscosity models have been developed [55-62] for melts and glasses and have been verified against experimental data available for for Al_2O_3-B_2O_3-CaO-FeO-Fe_2O_3-K_2O-MgO-MnO-Na_2O-NiO-PbO-SiO_2-TiO_2-Ti_2O_3-ZnO-F melts and for Al_2O_3-B_2O_3-CaO-K_2O-MgO-Na_2O-PbO-SiO_2 glasses. The viscosities of multicomponent melts and glasses are predicted by the model within experimental error limits without using any additional parameters.

The database for melts is valid for liquid and supercooled slags with viscosities which are not too high. That is when the numerical values of $\log_{10}$ (viscosity in poise) is less than 7.5. This could be considered as an accurate approximation of melt viscosities and corresponds to temperatures above about 900℃. In contrast, the database is valid for glasses at and below the transition temperature of the glass. In general, the database is valid over the whole temperature range from liquid melts to glasses; however it may be slightly less accurate for liquid slags than the first database.

Slag composition at the beginning of the melt

The viscosity module in FactSage is used to determine the viscosity at 1600℃. At a temperature of 1600℃ it can be safely assumed that the slag is a molten liquid and no solids (spinels) are present because of reducing conditions. The calculated viscosities of the slags from SiC reduction of Rowland and Easterns LG concentrate at the beginning of the melts are 3.735 and 3.065 poise, respectively. These were calculated from the initial XRF analysis of the concentrates. Already it is seen that slag viscosity is significantly higher from Rowland LG concentrate. This will make it more difficult for small metal prills to settle and coalesce.

Slag composition at the end of the melt

The composition of the slag has a large effect on the viscosity and the presence of FeO, NiO, CuO, CrO will all aid to lower the viscosity [38, 46]. Once the SiC comes in contact with these oxides, it will reduce and settle to join the alloy phase, thereby removing them from the slag phase and increasing viscosity. It is seen from table 4.14 and table 4.15 that FeO concentration in the initial concentrate feed was lowered during the reduction process.

The slag composition from the SiC reduction of Rowland and Easterns LG concentrate is shown in table 4.14 and table 4.15, respectively. Theses samples were prepared and analysed with XRF at the Central Analytical Facility, Stellenbosch University.

Table 4.14 – Slag composition of samples from SiC reduction of Rowland LG concentrate.

Experiment Nr.	$\frac{SiC}{Concentrate}\ ratio\ (\times 10^2)$	Reduction time (min)	Al_2O_3	CaO	CrO*	FeO*	MgO	SiO_2	TiO_2	Total
1	**2.5**	60	5.20	2.67	2.25	5.87	27.60	52.17	0.33	97.54
4	**3.0**	30	5.27	2.69	1.31	4.07	28.79	53.34	0.32	97
5	**3.0**	45	5.43	2.71	1.68	5.02	28.43	53.11	0.33	98
2	**3.0**	60	5.24	2.72	1.87	3.48	28.02	52.99	0.32	97.64
6	**3.0**	75	5.22	2.72	2.43	3.30	28.35	52.17	0.32	96.72
7	**3.0**	90	5.23	2.70	2.34	3.07	28.21	52.11	0.33	97.12
8	**3.0**	180	5.22	2.69	2.32	3.03	28.11	52.09	0.33	96.91
3	**3.5**	60	5.22	2.69	1.61	2.97	28.74	54.01	0.33	97.72
9	***3.0**	60	4.70	2.51	2.06	5.11	28.20	52.94	0.29	98.11

*Pure SiC was used as reductant. During XRF sample preparation, samples were fused. The gain on ignition related to the oxidation of the rock (mostly due to Fe and Cr) therefore Fe_2O_3 need be converted to FeO and Cr_2O_3 to CrO. It is assumed that most Cr_2O_3 was reduced to CrO.

Table 4.15 - Slag composition of samples from SiC reduction of Easterns LG concentrate.

Experiment Nr.	$\frac{SiC}{Concentrate}\ ratio\ (\times 10^2)$	Reduction time (min)	Al_2O_3	CaO	CrO*	FeO*	MgO	SiO_2	TiO_2	Total
10	**2.5**	180	4.75	3.08	3.11	6.51	29.11	50.17	0.33	97.61
11	**3.0**	180	4.71	3.1	3.09	5.84	30.06	49	0.33	97.61
12	**3.5**	180	4.78	3.12	3.15	3.12	29.78	51.65	0.33	97.10

Table 4.16 – Relative Standard Deviation of each oxide from the XRF analysis.

Oxide	Al_2O_3	CaO	CrO*	FeO*	MgO	SiO_2	TiO_2	Total
STDEV	0.02	0.01	0.04	0.01	0.09	0.02	0.03	0.21

The results from table 4.14 and table 4.15 shows a significant decrease in FeO concentration from the initial concentrates. Table 4.16 shows the relative standard deviation of each oxide from the XRF analysis. The lowest FeO content corresponded to the experiments which had the highest quantity

of reductant. Some inconsistencies in the results are noted, particularly for the experiment conducted with pure SiC. The FeO content was expected to be lower than that of experiment 2 where non-pure SiC was used as reductant. The scale of the experiments had most likely contributed to this finding.

The FeO content however is lower than the minimum suggested by Eric [38], who reported that a minimum of 12% FeO is required in the slag for good phase separation in a slag-matte system. However, this value should be lower for alloy-slag systems due to alloy phases being denser. Sufficient settling of alloy prills can be achieved when FeO content in the slag is marginally lower than 12 %. Table 4.16 on the next page shows viscosities of the slags at the end of the melt. The viscosities were calculated form slag compositions in Table 4.14 and Table 4.15 in the FactSage viscosity module.

Table 4.17 – Slag viscosity at the end of the melt according to FactSage modelling. The viscosity at the beginning of each melt from Rowland and Easterns LG concentrate is included in the table.

Experiment Nr.	Concentrate	$\frac{SiC}{Concentrate}\ ratio\ (\times 10^2)$	Reduction time (min)	Viscosity (poise)	
1	**Rowland**	2.5	60	3.781	
4	**Rowland**	3.0	30	3.950	
5	**Rowland**	3.0	45	3.851	
2	**Rowland**	3.0	60	4.224	
6	**Rowland**	3.0	75	3.992	3.735
7	**Rowland**	3.0	90	4.070	
8	**Rowland**	3.0	180	4.107	
3	**Rowland**	3.5	60	4.435	
9	**Rowland**	3.0*	60	4.093	
10	**Easterns**	2.5	180	3.280	
11	**Easterns**	3.0	180	3.165	3.065
12	**Easterns**	3.5	180	3.438	

Table 4.17 shows the calculated viscosities of the slags from all tests are higher than the viscosities of the melts at the beginning (indicated by the values outside the brackets in the viscosity column). This is because a significant amount of the Fe is now in the alloy. Some Cr has also deported to the alloy phase. The viscosity from slags of SiC reduction of Rowland LG concentrate is significantly higher than slags from SiC reduction of Easterns LG concentrate. This could explain why PGM recoveries are significantly lower for SiC reduction of Rowland LG concentrate.

From literature[38, 46] , PGM smelting slags have a viscosity of 1.5 – 4 poise and could restrict particles of 15 μm or less in size to settle. With gravity being the only force separating the phases in the tube furnace this value could even be higher. The FeO/SiO_2 content of such a slag seems to have a major influence on the viscosity. In such, Rowland LG concentrate under investigation has a lower FeO/SiO_2 ratio than Easterns LG concentrate. When FeO is reduced, slag viscosity will increase and valuable metal prills will not settle. The high initial slag viscosity will contribute to insufficient coalescence of metal prills and phase separation. The corresponding viscosities from these experiments conducted with Rowland LG concentrate mostly falls above the range of 1.5 – 4 poise. Therefore, it seems that a high slag viscosity is the primary factor for the low PGM recovery. Slag viscosities from SiC reduction of Easterns LG concentrate does however fall in the recommended range. The lower viscosities will aid in the coalescence of metal prills, enhance phase separation and induce good PGM recovery. Also it should be noted that experiments were conducted in a tube furnace where gravity was the only force utilized in the separation of phases. Reduction times were

also limited to 180 min. In a DC arc furnace, electromagnetic stirring will also aid in the successful coalescence of metal prills and residence times will be ranged from 12 – 24 hours.

SEM characterization of slag phases

To interpret the behaviour of metal prills in the slag phase, a picture at a high magnification from SEM is necessary. Figure 4.9 and Figure 4.10 is SEM images of the slag phases from SiC reduction of Rowland and Easterns LG concentrate. In order to be consistent the slag phases from experiments 8 and 11 were investigated. Both these experiments had a similar reductant to concentrate ratio and reduction time.

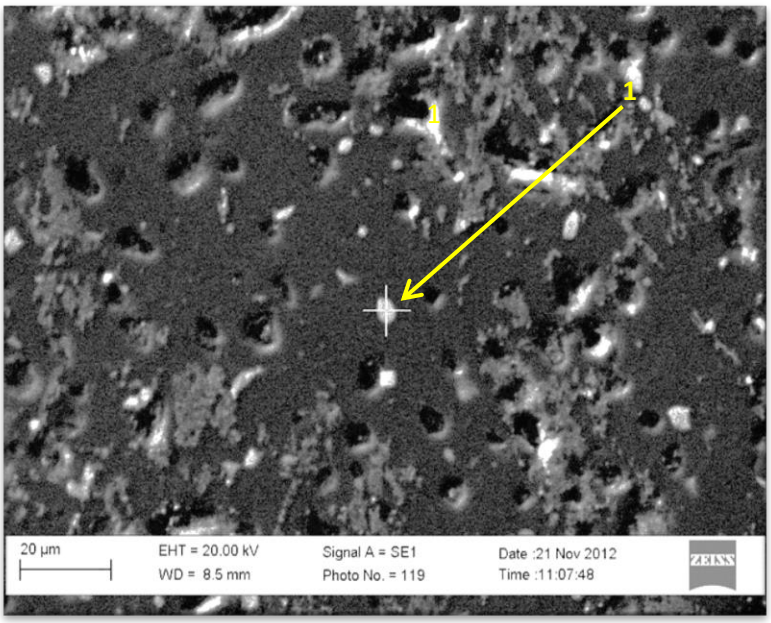

Figure 4.9 – A SEM image of a prill from the experiment conducted at 180 min and a reductant to concentrate ratio of 3 kg SiC / 100 kg Rowland LG concentrate. Darker phase is slag phase.

Figure 4.9 shows a SEM image of the slag phase from SiC reduction of Rowland LG concentrate. Metal prills are entrained in the slag. These metal prills are very small and were most likely trapped in the slag phase and will never settle or coalesce with other metal prills of similar size. Literature reported that many small metal prills (< $2\mu m$) are expected never to settle under the force of gravity alone. This phenomenon agrees well with the work done by Fagurland and Jalkanen [30] and Poggie et al. [31] who also concluded that very small droplets may either settle very slowly or may be trapped as 'rafts' of droplets floating on the top surface of the slag or as droplets suspended below small gas bubbles. However, the high viscosity of the slag is most likely restricting metal prills to coalesce and settle. From an EDX spot analysis on a metal prill (indicated by the arrow), Ir and Pd was detected to be present. The PGM recovery from Rowland LG concentrate could also increase if reduction time was increased.

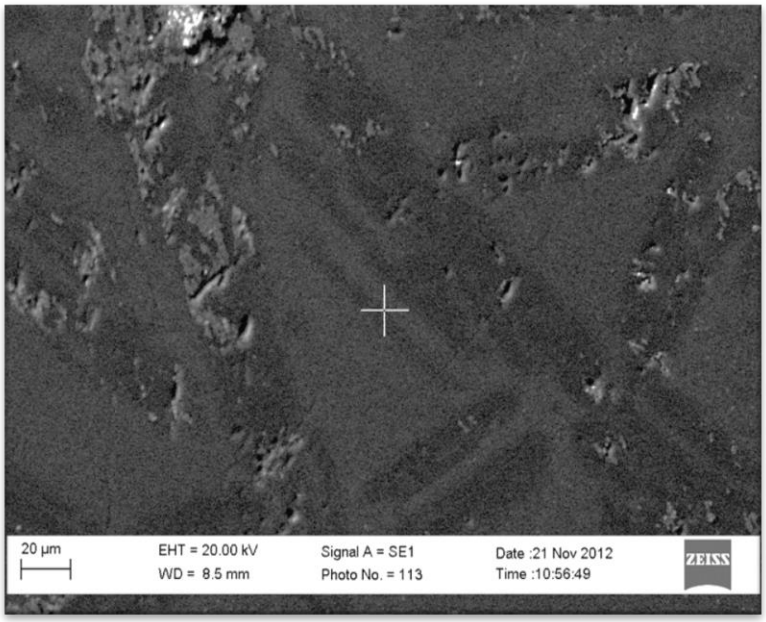

Figure 4.10 – A SEM image of the slag from the experiment conducted at 180 min and a reductant to concentrate ratio of 3 kg SiC / 100 kg Easterns LG concentrate.

Figure 4.10 shows a SEM image of the slag phase from SiC reduction of Easterns LG concentrate. A smoother slag phase, with no metal prills entrained in the slag is observed in Figure 4.4. This is an indication that metal prills coalesced and settled well within the slag phase. From these findings it is very clear that the lower slag viscosity contributes significantly in PGM recovery from SiC reduction Easterns LG concentrates. The findings revealed that a lower slag viscosity improved PGM recovery and this corresponded to similar findings in literature [39-41].

Summary of results

The recovery of PGMs from the first melt at Lonmin Western Platinum Limited is required to be more than 90%. It is however evident from the results, that poor recoveries were achieved, particularly for SiC reduction of Rowland LG concentrate. The low FeO content in the slag attributed to high slag viscosities and poor phase separation. PGM recoveries were, however, better for SiC reduction of Easterns LG concentrate mostly due to a lower slag viscosity. In order to recover more than 90 % of PGMs from Rowland and Easterns LG concentrate, the slag viscosity need to be lowered, metal fall need to be increased and reduction times need be increased. Thereby, FeO content of the initial LG concentrate charge need to be increased by introducing a source rich in FeO to the LG concentrate charge. Another option would be to melt the Easterns and Rowland LG concentrates together, with Easterns LG concentrate forming the bulk of the LG concentrate charge due to its higher FeO concentration. The two options could also be combined. The next section will evaluate these scenarios, by means of thermodynamic modelling or where possible, experimentally.

4.3 Analysis on optimum ratio of combined feed

From the results obtained from experiments, it was found that Easterns LG concentrate should form the bulk of the dry LG concentrate feed to a DC arc furnace, since it has a higher FeO/SiO_2 ratio. The latter is significant in reducing slag viscosity and increasing overall PGM recovery. The slag viscosities need to be kept in the region of ± 3.2 poise (average viscosity determined from experiments with SiC reduction of Easterns LG concentrate) or lower in order to recover PGMs. The idea would be two combine these two streams or add a source that could lower slag viscosity.

Reducing slag viscosity with a converter slag addition

The slag from a Peirce-smith converter has a high FeO/SiO_2 ratio and could be used as source to reduce the slag viscosity. The composition of this slag is found in section 4.6. Thermodynamic modelling with the help of FactSage was used to model such a scenario and a test is also conducted to back-up results from the modelling.

Figure 4.11 and Figure 4.12 were drawn up with thermodynamic modelling. The modelling was conducted at 3.5 kg SiC / 100 kg LG concentrate and 1600 ℃ . In each scenario a different amount of converter slag was added. The FactSage viscosity module was used to determine the slag viscosity.

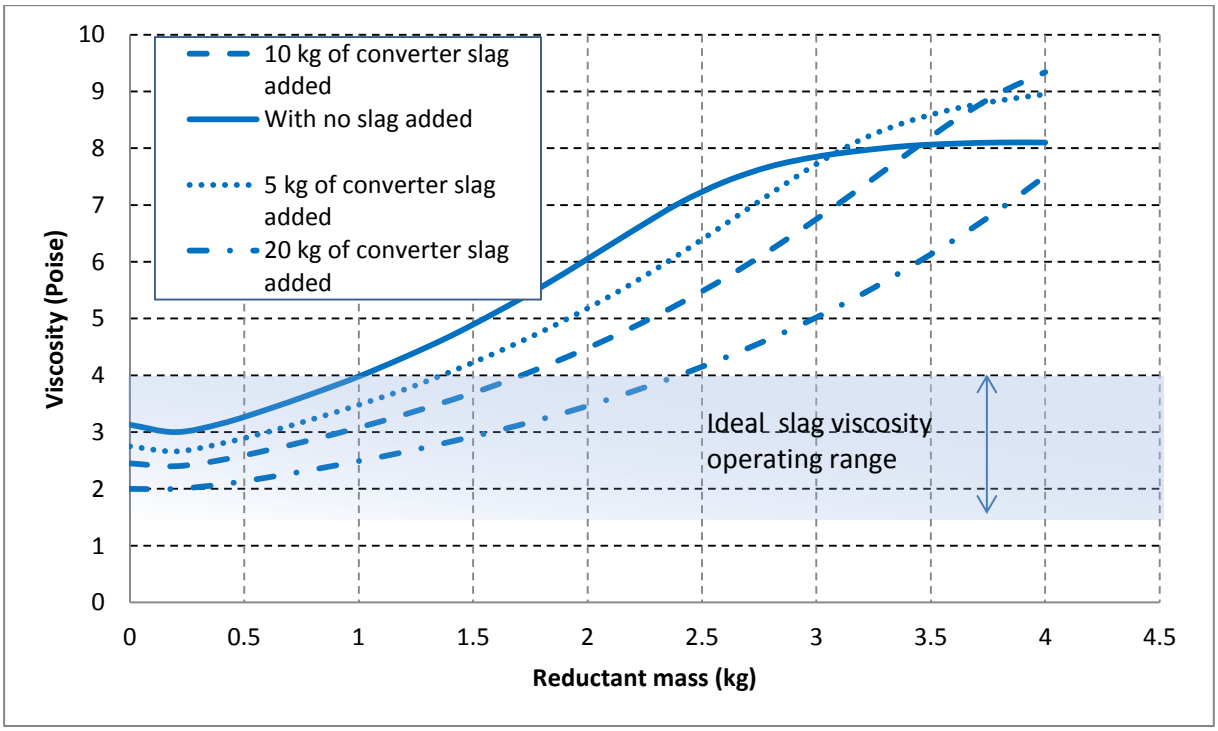

Figure 4.11 – Slag viscosity from SiC reduction of Rowland LG concentrate as a function of reductant mass and converter mass. The ideal slag viscosity operating range for PGM recovery is highlighted.

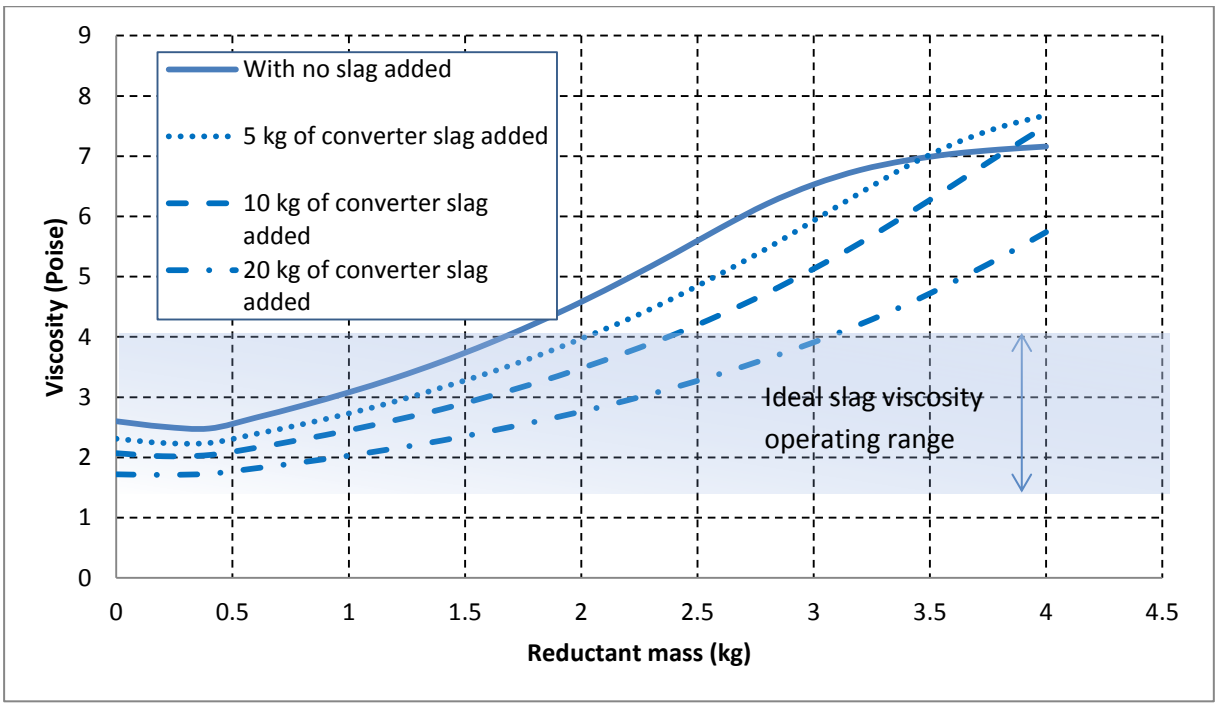

Figure 4.12 – Slag viscosity from SiC reduction of Easterns LG concentrate as a function of reductant mass and converter mass. The ideal slag viscosity operating range for PGM recovery is highlighted.

Figure 4.11 and figure 4.12 show that an addition of converter slag does decrease the slag viscosity. The converter slag is rich in FeO and thereby FeO/SiO_2 ratio is increased in the slag causing slag viscosity to decrease. However the converter slag does contain about 30 % SiO_2 in wt. %, which could increase the slag viscosity once again. The latter is evident on both figures, as an increase in reductant will cause more FeO to be reduced, consequently a system with 5 kg and 10 kg converter slag addition will have a higher slag viscosity than a system with no converter slag if the reductant additions are increased past the point of intersection. Too much converter slag could increase furnace slag quantities. This may require current furnaces to be enlarged and this could be very costly from an economic point of view. Another problem is that the conductivity and viscosity properties of the slag are opposite to each other. The decrease in viscosity will increase the conductivity of the slag (increasing iron oxide serves to depolymerize the slag and creates sites for electronic conduction) [2, 38]. An alloy with a very high Fe, Ni and Cu concentration could ultimately dilute PGMs and other base metals.

However higher slag viscosities were calculated from the thermodynamic modelling results than that of experimental slag viscosities at the same conditions. The FeO/SiO_2 ratio is lower in the slags from thermodynamic equilibrium calculations. The thermodynamic equilibrium state calculated is an ideal state and it is assumed that no physical characteristics constrain the reduction process. This approximation made with thermodynamic modelling is still however a good indication of the effect of an addition of converter slag on slag viscosity.

From the thermodynamic modelling it was found that around 10 kg of converter slag addition to a 100 kg concentrate sample will decrease slag viscosity and not increase furnace slag quantities by more than 10% compared to a thermodynamic model with no converter slag additions. The alloy is also expected to have a good PGM grade. A test was conducted (experiment 13 from the

experimental matrix) and Table 4.18 shows the results from experiment and also thermodynamic modelling results at the same conditions.

Table 4.18 – Comparison between experimental results and FactSage modelling results.

Experimental with Peirce-Smith converter slag		**Thermodynamic modelling with Peirce-Smith converter slag**	
Metal fall %	**8.82**	**Metal fall %**	**12.42**
Alloy	**Wt. %**	**Alloy**	**Wt. %**
Fe	85.30	Fe	94.44
Cr	4.13	Cr	1.74
Si	2.73	Si	0.13
Cu	1.10	Cu	1.32
Ni	2.59	Ni	1.65
S	1.53	S	Not included in feed
Ir	0.81	Ir	Not included in feed
Pd	1.21	Pd	Not included in feed
Pt	0.65	Pt	Not included in feed
Slag	**Wt. %**	**Slag**	**Wt. %**
Al_2O_3	4.40	Al_2O_3	5.47
CaO	2.95	CaO	3.21
CrO	3.88	CrO	3.88
FeO	7.66	FeO	4.72
MgO	28.85	MgO	24.00
SiO_2	49.75	SiO_2	58.18
TiO_2	0.32	TiO_2	Not included in feed
Alloy	**Recovery %**	**Alloy**	**Recovery %**
Ir	97.9	Ir	100
Pd	97.0	Pd	100 *
Pt	69.1	Pt	100
Fe from concentrate	75.5	Fe from concentrate	97.9

*If PGMs were included in a feed it was found from thermodynamic equilibrium calculations that all PGMs report to the alloy phase.

Table 4.18 shows an improved PGM recovery with a converter slag addition. The improvement is likely to have come from the decrease in slag viscosity which aided in more metal prills coalescing and separating from the slag phase. The Pd and Ir recovery is nearly 100%, compared to Pd and Ir recoveries of 94.5 and 86.3 % obtained from an experiment with no slag addition (experiment 12). Pt recovery has also improved from 59.2 % to almost 70 %. It is expected that Pt recovery should improve if the metal fall increases. More reductant could be added to increase metal fall and thereby increase the Pt recovery from the initial concentrate. Overall, this is a significant finding. Therefore a portion of converter slag can be recycled and melted again along with any LG concentrate to increase metal fall and PGM recoveries. The ultimate aim would be to achieve a metal fall of > 10 %. The next section will deal with finding an optimum ratio between a combined feed of Easterns and Rowland LG concentrate with the addition of converter slag.

From Table 4.18 it is apparent that thermodynamic modelling predicts a slag with similar composition. The marginally lower FeO/SiO_2 ratio in the slag from thermodynamic modelling will cause the viscosity to be somewhat higher than the slag from the experiment. Mentioned previously, calculations from thermodynamic equilibrium do not take into account any physical characteristics of the melt. Easily reduced base metals were also neglected from the concentrate feed. SiO_2 concentration from the initial feed would have been more than that of the actual

concentrate. In order to make any good predictions from the thermodynamic modelling, an assumption is required on slag viscosity. Therefore the average between the slag composition from the experiment and predicted slag composition from thermodynamic modelling is used to develop a simplified model in calculating the optimum feed ratio between Rowland and Easterns LG concentrate in the next section. The average yielded a viscosity of $\pm$**3.5 poise** and in this region, metal prills are expected to coalesce and settle, which will increase the PGM and easily reduced base metal recoveries to almost 100%.

Establishing an optimum feed ratio between Rowland LG concentrate, Easterns LG concentrate and converter slag

PGM recovery from SiC reduction of Rowland LG concentrate was below 10%. It was found that the high slag viscosity restricted metal prills to settle and coalesce. The metal prills became entrained in the slag and phase separation was not good. However, improved PGM recovery was achieved from SiC reduction of Easterns LG concentrate and PGM recovery improved further when a converter slag was added to increase FeO/SiO_2 ratio and therefore decrease slag viscosity. Thereby thermodynamic modelling was used to predict an optimum ratio of feed between Rowland and Easterns LG concentrate. The reductant to concentrate ratio was fixed at 3.5 kg SiC / 100 kg LG concentrate and temperature was fixed at 1600℃. Figure 4.13 shows the viscosity as a function of fraction of Easterns LG concentrate in the feed and quantity of converter slag in the feed.

The quantity of converter slag addition is constrained by alloy to slag ratio (slag quantities), slag resistivity and PGM grade in the alloy. Table 4.19 shows the percentage of alloy to slag as a function of the LG concentrate (100 kg bases) in the feed and slag additions. The FeO/SiO_2 ratios as a function of fraction of Easterns LG concentrate in the feed and slag additions are shown in Table 4.20.

Table 4.19 – Thermodynamic modelling results of alloy to slag ratio as a function of fraction of Easterns LG concentrate in the feed and slag additions. A is the quantity of slag in kg. Optimum values/zone is highlighted.

Fraction of Easterns LG concentrate in feed = 0		Fraction of Easterns LG concentrate in feed = 0.2		Fraction of Easterns LG concentrate in feed = 0.4		Fraction of Easterns LG concentrate in feed = 0.6		Fraction of Easterns LG concentrate in feed = 0.8		Fraction of Easterns LG concentrate in feed = 1	
A	$\frac{alloy}{slag}(\times 10^2)$	A	$\frac{alloy}{slag}(\times 10^2)$	A	$\frac{alloy}{slag}(\times 10^2)$	A	$\frac{alloy}{slag}(\times 10^2)$	A	$\frac{alloy}{slag}(\times 10^2)$	A	$\frac{alloy}{slag}(\times 10^2)$
0	11.95	0	12.04	0	12.12	0	12.19	0	11.95	0	12.30
10	12.98	10	12.91	10	12.83	10	12.75	10	12.66	10	12.58
20	12.31	20	12.22	20	12.13	20	12.04	20	11.95	20	11.86
30	11.59	30	11.50	30	11.42	30	11.34	30	11.25	30	11.17
40	10.95	40	10.87	40	10.80	40	10.72	40	10.65	40	10.58
50	10.39	50	10.32	50	10.25	50	10.19	50	10.12	50	10.05

Table 4.20 – Thermodynamic results of FeO/SiO_2 ratios (in percentages) as a function of fraction of Easterns LG concentrate in the feed and slag additions. A is the quantity of slag in kg. Optimum values/zone is highlighted.

Fraction of Easterns LG concentrate in feed = 0		Fraction of Easterns LG concentrate in feed = 0.2		Fraction of Easterns LG concentrate in feed = 0.4		Fraction of Easterns LG concentrate in feed = 0.6		Fraction of Easterns LG concentrate in feed = 0.8		Fraction of Easterns LG concentrate in feed = 1	
A	$\frac{FeO}{SiO_2}(\times 10^2)$	A	$\frac{FeO}{SiO_2}(\times 10^2)$	A	$\frac{FeO}{SiO_2}(\times 10^2)$	A	$\frac{FeO}{SiO_2}(\times 10^2)$	A	$\frac{FeO}{SiO_2}(\times 10^2)$	A	$\frac{FeO}{SiO_2}(\times 10^2)$
0	0.72	0	0.83	0	0.95	0	1.08	0	1.23	0	1.38
10	5.42	10	5.91	10	6.42	10	6.96	10	7.51	10	8.07
20	14.64	20	15.26	20	15.88	20	16.52	20	17.15	20	17.80
30	23.66	30	24.31	30	24.96	30	25.62	30	26.29	30	26.97
40	31.97	40	32.64	40	33.31	40	33.99	40	34.68	40	35.38
50	39.61	50	40.29	50	40.98	50	41.67	50	42.37	50	43.08

The optimum zone had been identified as an area where thermodynamic modelling predicted a slag viscosity in a 10 % proximity of 3.5 poise, a metal fall of > 10% and the feed contains at least 20-40 % Rowland LG concentrate. An ideal ratio of alloy to slag is not known, however the zone identified should be adequate in not increasing furnace slag quantities that will require modifications to enlarge current furnaces.

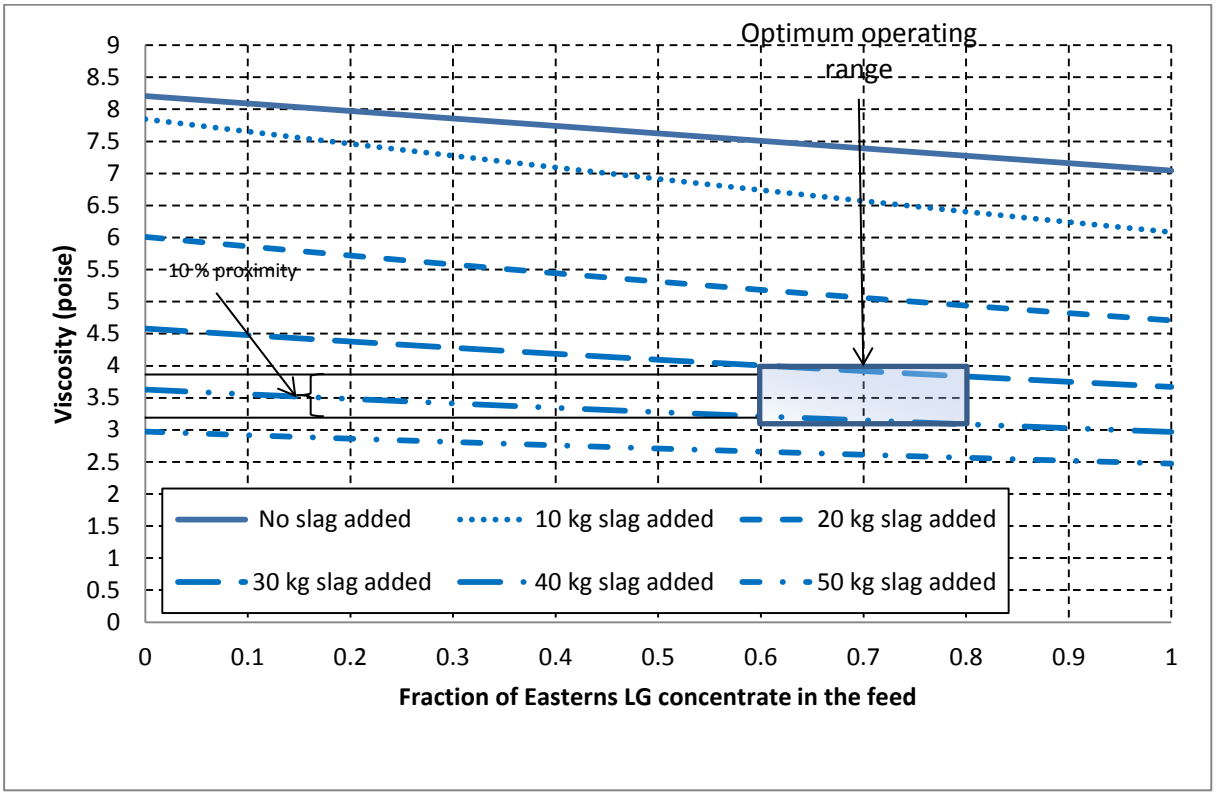

Figure 4.13 – Slag viscosity as a function of fraction of Easterns LG concentrate in the feed and quantity of Peirce-Smith converter slag in the feed. The required slag viscosity for PGM recovery as predicted from an average slag composition calculated between experiment 13 and slag composition predicted from thermodynamic modelling. The optimum operating range is highlighted.

Results from Thermodynamic modelling indicates a decrease in the fraction of Easterns LG concentrate in the feed required to sustain a low enough slag viscosity for good PGM recovery if the quantity of Peirce-Smith converter slag is increased. The Peirce-Smith converter slag has a high FeO

content and will decrease the slag viscosity along with increasing metal fall. Therefore, to maintain the slag viscosity in a 10 % proximity of 3.5 poise, the fraction of Easterns LG concentrate need be increased or the quantity of Peirce-Smith converter slag in the feed need by increased. The optimum operating range is highlighted. Thermodynamic modelling predicts that adding more than 40 kg converter slag / 100 kg LG concentrate decreases alloy to slag ratio. Slag quantities significantly increases and metal fall is restricted to reductant quantity. Therefore a 0.6-0.8 fraction of Easterns LG concentrate in the feed, 30 - 40 kg converter slag / 100 kg LG concentrate, should not significantly increase furnace slag quantities and FeO/SiO_2 ratio should be adequate to sustain a slag viscosity in a 10 % proximity of 3.5 poise with at least 20 % Rowland LG concentrate in the initial LG concentrate feed. At these operating conditions more than 90% of PGMs should be recovered from a LG concentrate feed in an alloy with a high PGM grade. Cr and Si concentrations in the alloy are less than 1 % in total and C concentrations are less than 1 % in the alloy.

4.4 Comparison between SiC and C as reductant

The aim of the project is to conclude whether or not SiC is an effective and feasible reductant. The effectiveness is a function of more than one variable, including **energy requirements for reduction**, **acceptable metal fall and composition for PGM recovery**, **gas emissions**, **slag quantities and economics**. In this section, SiC will be compared to C (most frequently used reductant), in order to determine feasibility of SiC as reductant. Thermodynamic modelling with the help of FactSage will once again be utilized for predictions. The optimum feed conditions from section 4.4 are used in the comparison. Thereby, it is assumed that slag viscosity will be low enough to insure good phase separation and PGM recovery. In retrospect, the feed input is as following:

- Concentrate → 70 % Easterns LG concentrate and 30 % Rowland LG concentrate (100 kg basis)
- Reductant quantity → 0 - 4 kg reductant / 100 kg LG concentrate
- Temperature → 1600°C.
- Converter slag addition → 35 kg Converter slag / 100 kg LG concentrate
- Type of reductant → Pure C and pure SiC
- Normal system

It should be noted that C reduction of Rowland and Easterns LG concentrate will require less converter slag additions. C reduction does not produce SiO_2 during its reaction with FeO. This is shown in the following chemical reaction:

$$FeO(s) + C(s) = Fe(l) + CO(g) \qquad \text{(Eq. 4.3)}$$

However, the feed conditions will remain the same for the comparison.

Comparison of metal fall

The metal fall is predicted in FactSage and shown as function of reductant mass in figure 5.13.

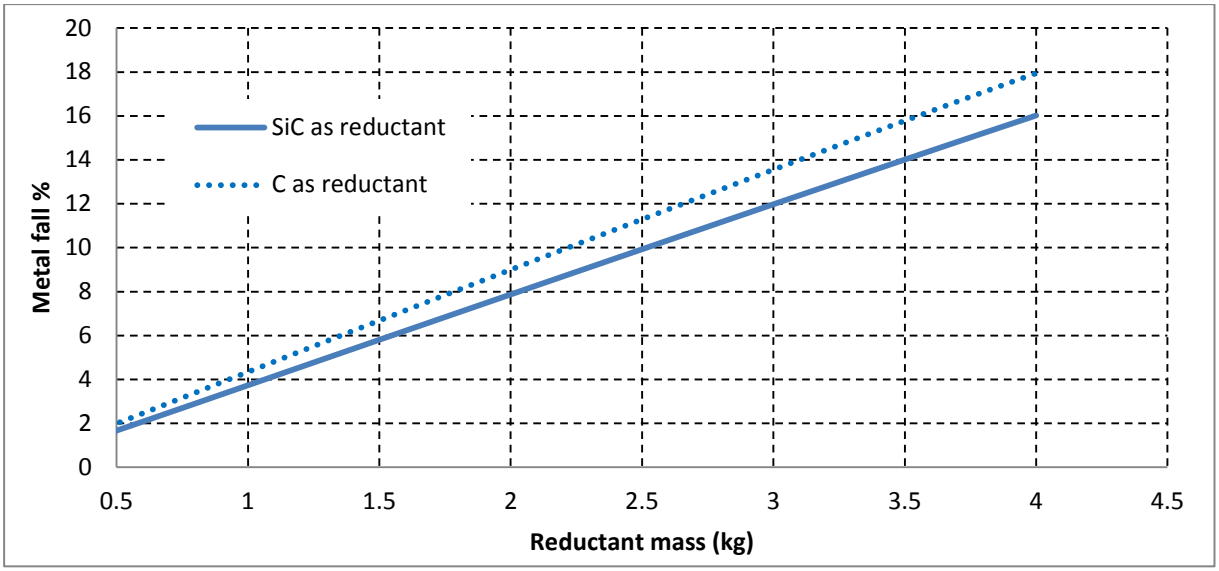

Figure 4.14 – Metal fall from C and SiC reduction of a mixed LG concentrate feed as a function of reductant mass.

Figure 4.14 show that C reduction of a mixed LG concentrate feed has a marginally higher metal fall than SiC reduction of a mixed LG concentrate feed. Therefore the metal fall is roughly the same and SiC is effective in producing an alloy for PGM collection.

Comparing alloy composition

Alloy composition is shown in Table 4.21 at 0.5,1, 1.5, 2, 2.5, 3, 3.5, 4 kg reductant / 100 kg mix feed.

Table 4.21 - FactSage prediction on alloy composition as a function of reductant to feed ratio (values of Cr, C, Cu Fe, Ni and Si expressed as wt. %).

	SiC as reductant						C as reductant					
$\frac{SiC}{Concentrate}\ ratio\ (\times 10^2)$	C	Cr	Cu	Fe	Ni	Si	C	Cr	Cu	Fe	Ni	Si
0.5	0.01	0.16	7.91	62.35	29.58	0.00	0.01	0.17	7.15	67.62	25.04	0.00
1.0	0.03	0.22	4.94	81.23	13.57	0.00	0.03	0.24	4.43	83.60	11.70	0.00
1.5	0.04	0.28	3.68	87.22	8.77	0.01	0.04	0.30	3.30	88.73	7.63	0.01
2.0	0.05	0.34	2.97	90.15	6.49	0.01	0.05	0.37	2.66	91.23	5.68	0.01
2.5	0.06	0.42	2.50	91.86	5.15	0.01	0.06	0.47	2.24	92.68	4.53	0.01
3.0	0.08	0.52	2.17	92.94	4.27	0.02	0.08	0.63	1.95	93.55	3.77	0.02
3.5	0.10	0.68	1.92	93.61	3.65	0.03	0.11	0.88	1.73	94.00	3.24	0.04
4.0	0.14	0.93	1.73	93.95	3.19	0.06	0.17	1.34	1.56	93.99	2.85	0.09

The thermodynamic modelling determined an alloy with very similar composition. Only small differences are observed in elements such as Cr. C is by a very small degree a stronger reductant as SiC and thereby at the same reductant mass it will reduce more CrO. However, Cr and Si concentrations are very low and will not be problematic for downstream processing.

Gas emissions and slag quantities

Gas emissions and slag quantities determined from thermodynamic modelling are shown as a function of reductant mass in Figure 4.15 and Figure 4.16, respectively.

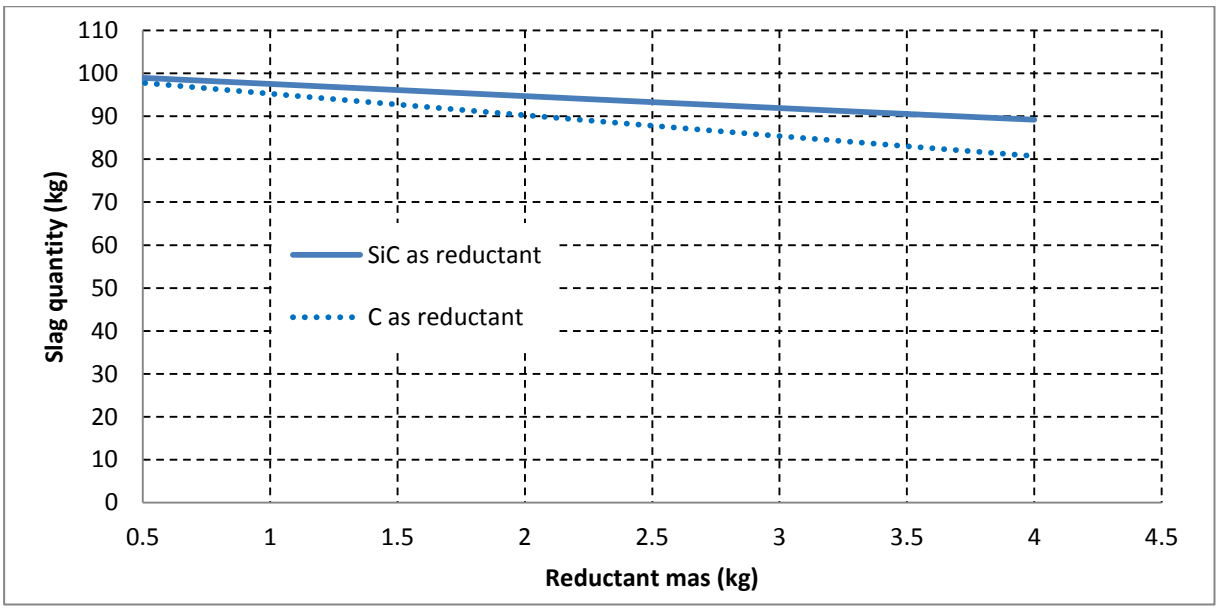

Figure 4.15 – Slag quantity as a function of reductant mass.

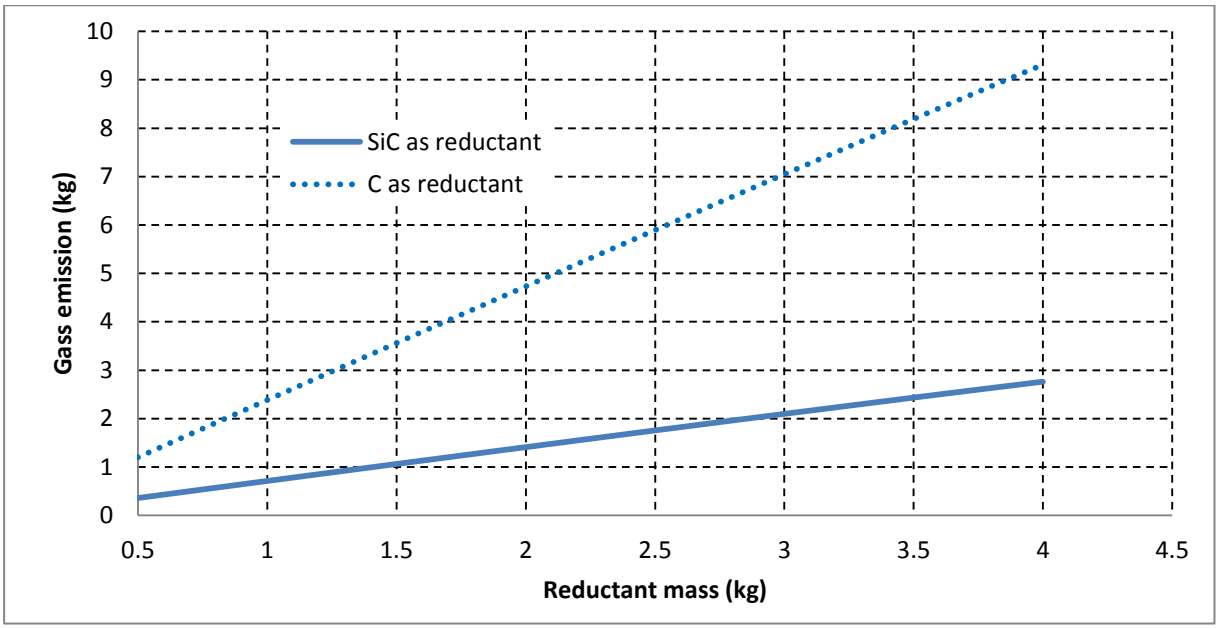

Figure 4.16 – Gas emission as a function of reductant mass.

From the thermodynamic modelling it was found that SiC reduction of a LG concentrate produces a larger quantity of slag. However, at the same time it produces less gas than C reduction of LG concentrate. The reason is that C will react with FeO, to form largely Fe (l) and CO (g) as product species, while SiC will react with FeO(l) to form largely Fe(l), SiO_2(l) and CO(g) as product species. Adding more reductant will increase the reduction of FeO and thereby the difference in slag quantities and gas emissions from the respective reductants.

Gas emissions from arc furnaces need to be kept to a minimum in order adhere to strict pollution control legislation and thereby production costs will increase to remove and clean gas. Therefore SiC could be used in such a degree to reduce gas emissions.

Energy required for smelting

The energy required to smelt 1 ton of LG concentrate feed is shown in figure 4.16 as function of reductant mass. The reductant to concentrate ratio is fixed at 30, 35 and 40 kg reductant / ton LG concentrate.

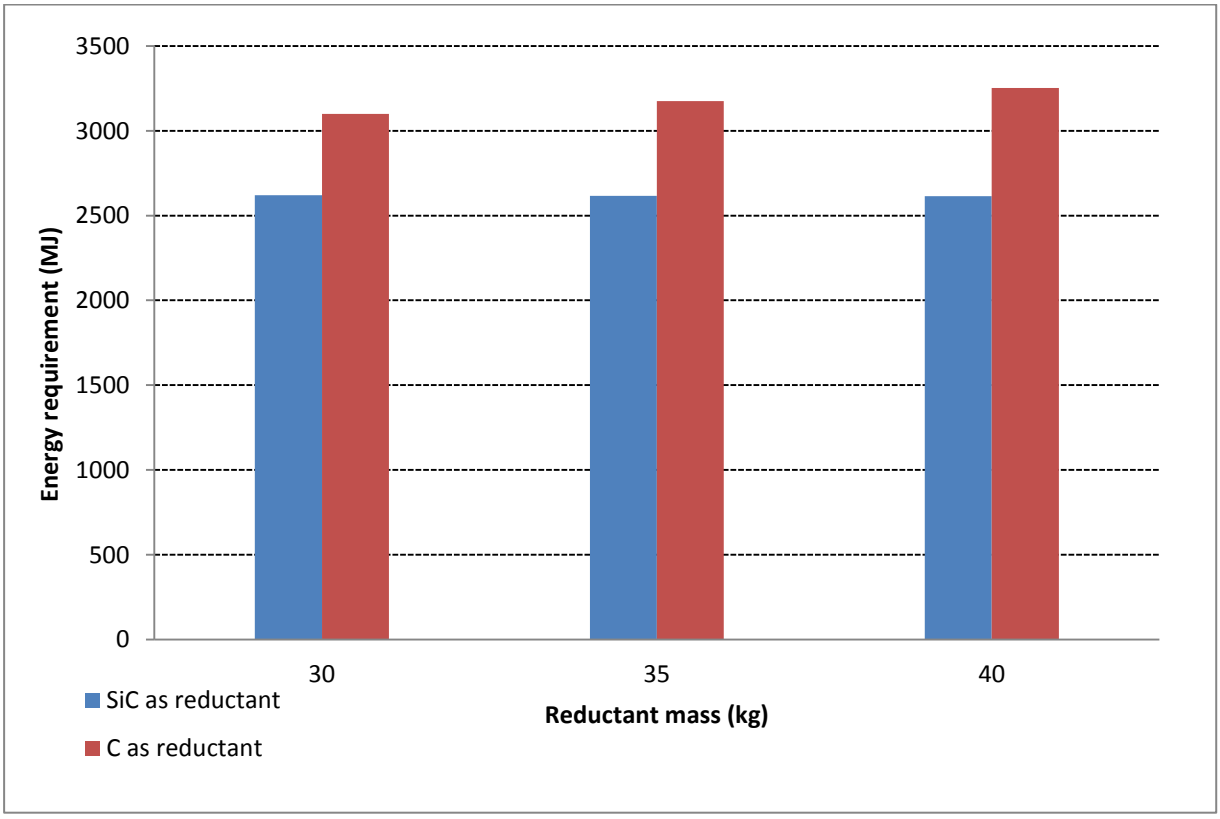

Figure 4.17 – Energy required to smelt 1 ton of LG concentrate (30 % Rowland and 70 % Easterns) as a function of reductant mass.

Figure 4.17 shows that C reduction of a LG concentrate requires more energy than SiC reduction of LG concentrate. The thermodynamic modelling results also predict that the energy difference between SiC and C as reductant systematically increases when more reductant is added. This is attributed to C reacting **endothermically** with FeO, in contrast to SiC reacting **exothermically** with FeO. Thereby the energy required to increase metal fall does not increase with SiC as reductant. The finding is very significant with regard to economic aspects, since a higher energy requirement will increase process operational costs. However it was mentioned previously that C reduction will require less Peirce-Smith converter slag additions and this will reduce the energy required for smelting.

Advantages and disadvantages of SiC and C as reductants

The predictions made from FactSage thermodynamic modelling is used to construct table 4.22 and table 4.23.

Table 4.22 and Table 4.23 compare advantages and disadvantages of both reductants:

Table 4.22 – Advantages and disadvantages of SiC as reductant

Silicon carbide (SiC)	
Advantages	**Disadvantages**
Low Gas emissions – Less pollution and costs for cleaning of gas.	During reduction of iron oxide, SiO_2 is formed as product specie. Higher concentration of SiO_2 in the slag increases slag viscosity, which could hinder settling of metal prills.
Reduced energy requirements because of SiC reacting exothermically with FeO.	Downstream processes (Slag plant) need to be modified to handle larger quantities of slag.
Acceptable metal fall can be achieved for sufficient PGM recovery. Proven in this study by good Ir, Pd and Pt recoveries achieved from reductive smelting of Easterns LG concentrate with converter slag additions.	Not been tested on large practical scale.
Downstream processing requires little to none adjustments, for the reason that the alloy will be robust and can be easily treated by existing processes for PGM and base metal recovery.	The energy costs in producing SiC could attribute in increased overall operational costs when purchased from a supplier.

Table 4.23 – Advantages and disadvantages of C as reductant

Carbon (C)	
Advantages	**Disadvantages**
Tested and used on regular basis for reductive smelting processes i.e. ConRoast Process	High energy requirements at furnace because of C reacting endothermically with FeO
Acceptable metal fall can be achieved for sufficient PGM recovery	High gas emissions that require regulation and control to avoid pollution and other related facets such as safety.
By product gas species could be used as reactant species in producing other valuable products.	
Downstream processing requires little to none adjustments, for the reason that the alloy will be robust and can be easily treated by existing processes for PGM and base metal recovery.	
C (coal, coke or graphite) is manufactured and purchased on large scales making it an inexpensive reductant.	

5. Integrating reductive smelting route into current matte-based collection route

Proposed alternative route

Integrating a reductive smelting of LG concentrates into current matte-based collection route would be beneficial for PGM recovery from LG concentrates. From the results obtained from experiments and thermodynamic modelling, it was found that Easterns LG concentrate should form 60 – 80% of the dry LG concentrate feed to a DC arc furnace, since it has higher FeO/SiO_2 ratio. After converting, a small portion of converter slag could be recycled to the furnace where LG concentrates are smelted in order to reduce slag viscosity. The best PGM recovery was obtained when converter slag was added to an Easterns LG concentrate sample. Converter slag is not discarded as it still contains valuable base and precious metals. Thereby adding 30 - 40 kg converter slag / ton LG concentrate was found to be an optimum. Converter slag addition will further increase FeO/SiO_2 ratio and decrease slag viscosity to enhance phase separation and PGM recovery.

The alloy produced could be mixed with a matte stream from a melted blended UG2 concentrate and send to a converter in order to remove Fe. A typical feed composition of a UG2 blend at Lonmin Western Platinum Limited is shown in table 5.1. Fe may either be present in an oxide or in a sulphide mineral, however for simplification; it is assumed that all Fe in the feed will be in an oxide form. Therefore matte fall may be under predicted. PGMs are not included in the thermodynamic modelling. Thermodynamic modelling is used to predict matte and slag composition.

Table 5.1 – Typical feed composition of a UG2 blend at Lonmin in wt. %, Marikana

Al_2O_3	CaO	Cr_2O_3	Cu	FeO	MgO	Ni	SiO_2	S	PGM
3.7	4.3	1.8	1.9	21.6	17.8	3.0	39.9	6.8	257 ppm

- Feed → 1 ton basis
- Temperature → 1600°C.

Figure 5.1 is a proposed process flow diagram for integrating reductive smelting of LG concentrates into the current matte-based collection route. The LG concentrate feed can be varied by increasing or decreasing $\frac{Rowland\ LG\ concentrate}{Easterns\ LG\ concentrate}\ ratio$ in conjunction with Peirce-Smith converter slag additions within the limits that were set in section 4.3. The thermodynamic equilibrium modelling results of three scenarios are discussed:

The LG concentrate (see section 3.6 for normalized feed compositions) feed investigated in this study has the following feed variations and is found in Table 5.2:

Table 5.2 – Feed conditions investigated with thermodynamic modelling.

Scenario	Temperature	SiC / LG concentrate ratio ($\times$ **10**)	Fraction of Easterns LG concentrate in the LG concentrate feed	Converter slag / LG concentrate feed ratio ($\times$ **10**)
1	1600	3.5	0.6	40
2	1600	3.5	0.7	35
3	1600	3.5	0.8	30

The lowest fraction of Easterns LG concentrate in the feed corresponds to the highest Peirce-Smith converter slag additions. These conditions were predicted to be optimal (see section 4.3) for recovery of PGMs from LG concentrates with SiC as reductant. Temperature and SiC / LG concentrate ratio will remain constant.

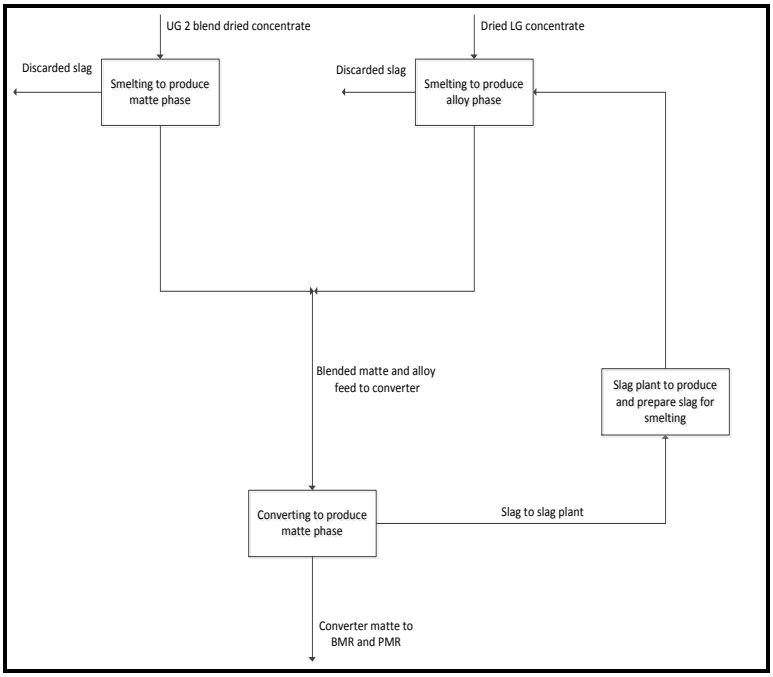

Figure 5.1 – Block flow diagram of the proposed pyrometallurgical process that can be implemented to recover PGMs from LG concentrates.

The proposed method starts with two separate streams, a UG 2 blend feed and a LG concentrate consisting of 60 - 80 % Easterns LG concentrate and 20 - 40 % Rowland LG concentrate. The high temperatures of the UG2 blend smelting step allow a matte phase to separate from a slag phase. The matte phase will recover > 90% of PGMs [1, 2, 38]. SiC reduction of a LG concentrate will produce an alloy that will settle and separate from the slag phase. The alloy phase, as predicted in this study should recover > 90% of PGMs. Slags from both furnaces contain very low PGM concentrations ($< 5\ ppm$) and can mostly be discarded. Table 5.3 – 5.6 shows the phase quantities and composition of the matte phase and alloy phase, respectively.

Table 5.3 – Thermodynamic modelling results of matte, slag and gas quantities from the smelting of UG2 blended concentrate.

Matte fall (%)	Total slag produced (kg)	Total gas emissions (kg)
9.80	863.39	40.433

Table 5.4 – Thermodynamic modelling results of alloy, slag and gas quantities for 3 different LG concentrate melts. Slag viscosities are also shown.

Scenario	Metal fall (%)	Total slag produced (kg)	Total gas emissions (kg)	Slag viscosity (poise)
1	14.34	1267	24.63	3.506
2	14.14	1219	24.57	3.825
3	13.94	1171	24.50	4.203

The metal fall from all 3 scenarios are sufficient to recover more than 90 % of PGMs. The slag viscosity of scenario 3 was calculated to be above 4 poise (Typical PGM slags have a slag viscosity of 1.5 – 4 poise [38]); however it is assumed that electrocapillary motion in a DC furnace should support coalescence of metal prills and overcome limitations imposed by slag viscosity.

Table 5.5 – Thermodynamic modelling results of matte composition (values of Cu, Fe and S expressed as wt. %).

Cu	Fe	Ni	S	Total
17.47	25.24	28.063	29.226	100

Table 5.6 – Thermodynamic modelling results of alloy composition (values of Cu, Cr, Fe, Ni and Si expressed as wt. %).

Scenario	Cu	Cr	Fe	Ni	Si	Minor elements*	Total
1	2.775	0.331	91.123	5.703	0.012	0.056	100
2	2.485	0.400	91.979	5.061	0.014	0.061	100
3	2.184	0.488	92.833	4.402	0.017	0.076	100

*The alloy mass balance being made of some minor elements (Al, Ca and Mg) found in trace amounts in the alloy.

Separation of the slag and matte/alloy phases can be achieved by tapping the two phases on different elevations. There after it can be granulated or casted into sand moulds to break it up. The lumps will then be added to ladles of molten furnace matte where it will dissolve. An alloy phase is highly miscible in a matte phase at high temperatures. Thermodynamic modelling is again used to predict the final composition of the blended stream.

From the thermodynamic modelling results, the following conclusions could be drawn:

- At 1600℃ the alloy phase is highly miscible in the matte phase.
- A combined stream has a new matte phase and has the composition is shown in Table 5.7. It makes up more than 99 % of the total mass of the combined stream.

Table 5.7 – Thermodynamic modelling predictions on combined stream (matte) composition (values of Cr, C, Fe and Si expressed as wt. %).

New matte phase				
Scenario	**Cu**	**Fe**	**Ni**	**S**
1	8.762	64.529	14.816	11.893
2	8.644	64.841	14.518	11.997
3	8.524	65.149	14.220	12.107

- Small quantities of solids, including CrS(s), Cr_3Si(s) and FeSi(s) have emerged among the matte phase. However these solids make up less than 1 % of the total mass of the combined stream. These unwanted solid phases stress out the importance in keeping Cr and Si as low as possible in the alloy phase from SiC reduction of the LG concentrate charge.
- A liquid metallic phase has started to emerge and makes up less than 1 % of the combined stream. This is an indication that the matte phase is saturated with the alloy phase. Thereby the ratio of alloy to matte needs to be controlled to avoid immiscibility of the alloy in the matte.

The combined stream can then be converted in order to remove most of the iron through oxidation. The slag from the converter is recycled and prepared to be melted with the LG concentrate. The matte from the converter is then treated in the BMR and PMR plants.

Energy requirements

In this part, an energy requirement comparison between alloy PGM collection (from this study) and matte-based PGM collection will be made. There will be specifically looked at energy consumptions of the respective evaluations in order to make a general conclusion on operation costs.

The same feed compositions from the proposed process flow diagram is used in calculating energy requirements for smelting a UG2 blended concentrate and 3 possible feeds of LG concentrate. The results from thermodynamic evaluation of respective routes are shown in Figure 5.2:

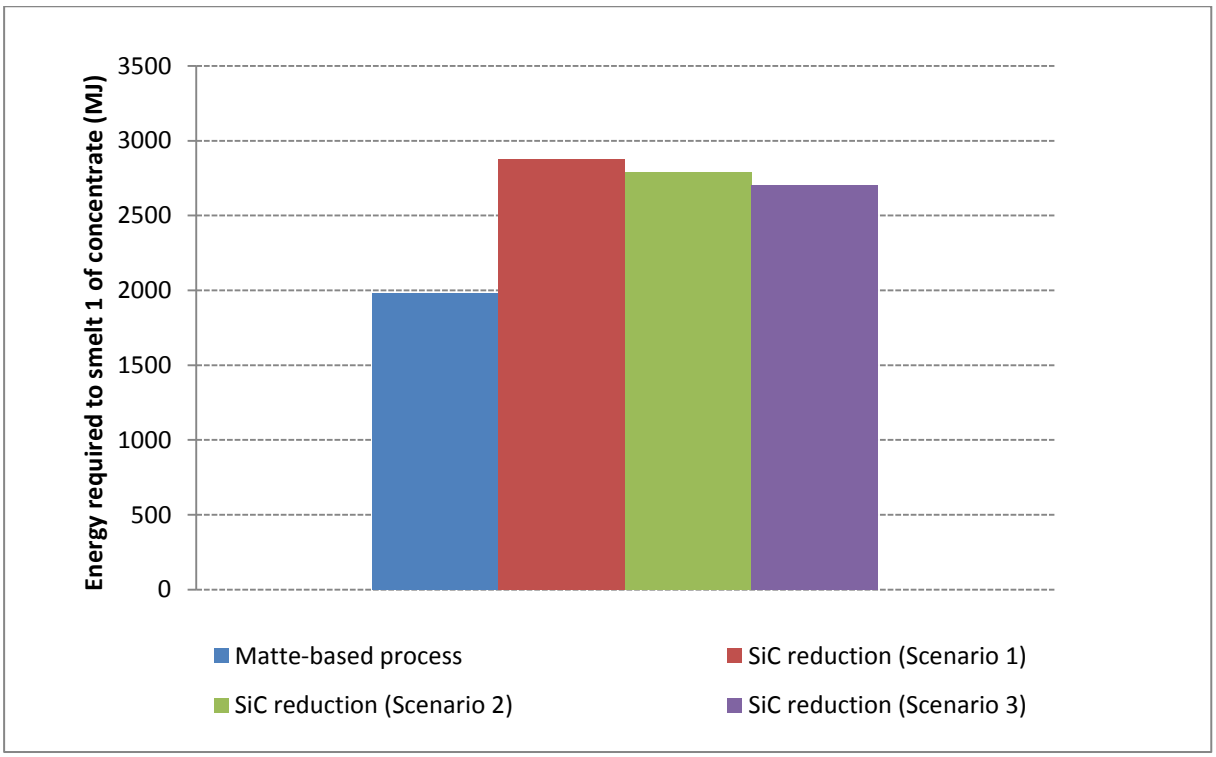

Figure 5.2 – Energy required to smelt 1 ton of UG2 blend concentrate and LG concentrate (3 scenarios).

From Figure 5.2 it is seen that SiC reduction does however require more energy to smelt 1 ton of concentrate. Consequently, operational costs of furnaces are expected to be higher. Reductive smelting does however produce less gas and is a positive attribute in reducing scrubbing and cleaning costs. CO forms 99 % of the gas composition from reductive smelting, while SO_2 and S_2 makes up the gas composition (58 % and 37 %) from matte-based smelting. Scenario 1 from SiC reduction requires the most energy, however, at this process conditions, metal fall was highest, Cr and Si concentrations in the alloy were lowest and slag viscosity was lowest. However, all 3 scenarios are expected to recover $> 90\ \%$ of PGMs.

Even though more energy is required for reductive smelting than for matte-based smelting, SiC reduction of LG concentrates still need to be considered as a feasible alternative for smelting LG concentrates. Subsequently PGM containing concentrates are becoming more enriched with UG 2 concentrates, it is expected to be integrated or replaced with a reductive smelting process. With respect to reductants, from this study it was found that SiC is an adequate reducing agent and could be recommended as an alternative reductant to C.

6. Conclusions

In this study, SiC reduction of Rowland and Easterns LG concentrates was investigated. The purpose of the study was to investigate the feasibility of using SiC as reductant with respect to metal fall, PGM grade in the alloy, slag composition (specifically looking at Cr solubility) and overall PGM recovery and if possible, the integration of such in the current matte-based collection process. Thermodynamic modelling with the help of FactSage is used to predict the effect of reductant to concentrate ratio and temperature on metal fall, alloy grade and Cr solubility in the slag. The experimental work was conducted in MgO crucibles using a vertical tube furnace. The Analytical techniques including ICP-MS, XRF, XRD and SEM-EDX were utilized throughout the course of the study. On the basis of the experimental and modelling results, the main conclusions of this study are listed in this section. It will also conclude on the hypothesis and objectives that was set in section 1 of the thesis.

In the light of aims and objectives, thermodynamic modelling was used to establish that a reductant to concentrate ratio of 2.5 – 3.5 kg SiC / 100 Kg LG concentrate yield a good metal fall (8 -12 %) and a good PGM grade in the alloy (Cr and Si concentrations below 10 % in total). Thermodynamic modelling calculations also predicted a slag liquidus temperature of $\pm$1420°C when the reductant to concentrate ratio was fixed at 3 kg SiC / 100 kg Rowland or Easterns LG concentrate. Thereby it was determined that an equilibrium temperature of 1600 °C should be adequate to support reduction, avoid spinel solid phases and not cause a superheated molten liquid. The results also indicated that it is highly unlikely that a matte phase will coexist with an alloy, slag and gas phase at thermodynamic equilibrium because of the low sulphur concentration in the LG concentrates.

Very poor PGM recovery (less than 10 %) was attained from SiC reduction of Rowland LG concentrate. Sample heterogeneity did contribute to uncertainty in PGM recovery, given its low concentration in the LG concentrates. Therefore Fe recovery was determined to support findings from PGM recovery due it being the most abundant base metal. Fe recoveries were less than 50 % and metal fall was low (< 6 %). An XRF analysis on the composition of the slag yielded a very low FeO/SiO_2 ratio. The FactSage viscosity module predicted slag viscosities higher than 4 poise. From literature [2, 38], it was found that slag viscosities of PGM bearing concentrates were typically in the range of 1.5 - 4 poise and in this range good phase separation was generally achieved. However, even in these range particles smaller than 15 μm may not settle. SEM images revealed metal prills, rich in Ir, Pd and Pt, entrained in the slag phase. A reduction time beyond 60 min had little effect on metal fall and PGM recovery. Cr and Si concentration in the alloy became very significant at a reductant to concentrate ratio of 3.5 Kg SiC / 100 kg Rowland LG concentrate. The latter made up more than 10 % of the alloy composition.

SiC reduction of Easterns LG concentrate had significantly better metal fall and PGM recoveries. At a reductant to concentrate ratio of 3.5 kg SiC / 100 kg Easterns LG concentrate more than 85 % of Ir and Pd was recovered and more than 60 % of Pt was recovered. The highest Fe recovery (66.4 %) corresponded to the highest PGM recovery. The higher FeO/SiO_2 ratio and thereby lower slag viscosity (below 4 poise) is most likely to have contributed to the improvement of PGM and Fe recoveries. A SEM image from a slag from SiC reduction of Easterns LG concentrate showed few to no metal prills entrained in the slag. This is an indication that most metal prills had coalesced and settled. Cr and Si concentrations are below 2 % in total in all alloys.

In order to further improve on PGM recoveries, the FeO content of the initial charge had to be increased. Thereby, Peirce-Smith converter slag from Lonmin was used as an addition to increase FeO/SiO_2 ratio. Thermodynamic modelling predicted that 10 kg converter slag / 100 kg Easterns LG concentrate was acceptable to increase FeO/SiO_2 and therefore decrease slag viscosity. The reductant to concentrate ratio was 3.5 kg SiC / 100 kg Easterns LG concentrate. In order to confirm these findings from the thermodynamic modelling, an experiment was conducted and yielded the followings:

- Metal fall (PGM collecting phase) increased with more than 1% from a test without converter slag.
- The higher FeO/SiO_2 ratio, compared to a test without converter slag, decreased slag viscosity and improved metal fall.
- More than 95 % of Ir and Pd were recovered from the initial Easterns LG concentrate charge and about 70 % of Pt was recovered from the initial Easterns LG concentrate charge.
- Fe recovery from the LG concentrate was 75.5 %.

The improved results from an addition of converter slag were utilized during thermodynamic modelling to find an optimum feed ratio between Rowland LG concentrate, Easterns LG concentrate and converter slag. Results from thermodynamic modelling indicated that Easterns LG concentrate should make up 60 – 80 % of the LG concentrate charge and 30 – 40 kg / 100k kg LG concentrate should be added to a LG concentrate charge to attain a low viscosity for good phase separation. Reductant to concentrate ratio was fixed at 3.5 kg SiC / 100 kg LG concentrate. Converter slag additions are however limited by slag quantities, slag resistivity and PGM grade in the alloy. Below follow a concise summary of the major conclusion on an optimum LG concentrate charge:

- Cr and Si concentrations in the alloy are below 1 %.
- Metal fall is > 10 %.
- Slag viscosity was in 10 % proximity of 3.5 poise. According to the test conducted with a slag addition and literature [2, 38], this will allow good coalescence of metal prills and ultimately good phase separation.
- It is expected that > 90 % of PGMs should be recovered from the LG concentrate charge in conjunction with a good PGM grade in the alloy.

Although this optimum LG concentrate charge was not experimentally explored it could however be assumed that $> 90\ \%$ PGMs should be recovered in a DC furnace. The electrocapillary motion in a DC furnace will greatly contribute to reduce metal prill entrainment in the slag. The latter was not experienced in the tube furnace used for experiments in this study. Using this optimum LG concentrate charge, the effectiveness of SiC as a reductant was also compared to a frequently used reductant such as C through thermodynamic modelling. Below follow a concise summary of the major conclusions from thermodynamic modelling results of SiC and C as reductants:

- C reduction of a LG concentrate charge has a marginally higher metal fall at the same reductant to concentrate ratio than SiC reduction of a LG concentrate charge.
- Alloy composition was very similar and only small differences in Fe, Cr and Si concentrations were noted.

- Gas emissions and energy requirements are higher for C reduction of a LG concentrate charge. This is mostly due to C reacting endothermically with FeO to produce Fe(l) and CO(g) in contrast to SiC reacting exothermically with FeO to produce Fe(l), SiO_2(l) and CO(g).

From the evidence, it was clear that SiC is an extremely effective reductant. Thereby, integrating or even replacing the present matte-based collection process with an alloy collection process could be considered. A proposed process flow diagram for integrating an alloy collection process into current matte-based collection process was developed on the basis of the evidence from experiments and thermodynamic modelling results. 1 ton of UG2 blended concentrate and 1 ton of LG concentrate (60 - 80 % Easterns LG concentrate, 20 - 40% Rowland LG concentrate and 300 – 400 kg converter slag addition) were evaluated through thermodynamic modelling. Below follow a concise summary of the major conclusions from the proposed integrated process flow diagram:

- SiC reduction of a LG concentrate charge requires more energy than melting of UG2 blended concentrate. Thereby, operational costs are increased and reductant requirements could further increase process costs. The alloy collection process does however produce less gas, but more slag than the matte-based collection process.
- Both processes are expected to recover > 90% of the PGMs from the initial concentrate charge.
- The alloy is dissolved in the matte phase and a combined stream is converted to remove Fe. The amount of alloy introduced as lumps into the matte should be carefully controlled to avoid a separate liquid phase or any solid phases to form.
- Converter slag is prepared and recycled to be smelted along with the LG concentrate charge.

Finally, from the overall findings of this study, it is conclusive that base metals and PGMs could be recovered in an iron alloy from reductive smelting of LG concentrates with SiC as reductant. Therefore integrating such a process into the matte-based collection process could be considered as a future alternative to smelting UG2 LG concentrates.

7. Recommendations for future work

Opportunities for future work lie in two main areas:

1.) The integration of the alloy collection process into a current matte-based collection process needs to be further investigated from a practical and economical point of view. Therefore, a further study on the proposed process flow diagram might be required.

2.) The findings from SEM need to be further investigated. For instance, a Transmission Electron Microscope (TEM) could be used to give a more clear understanding on physical PGM distribution in the alloy phase. The alloy samples from this project could be used for such particular study.

8. References

1. Jones R.T. and Kotze I.J., DC arc smelting of difficult PGM-containing feed materials. SAIMM, 2004: pp.33 - 36.
2. Nell J., Melting of platinum group metal concentrates in South Africa. The Journal of The South African insitute of Mining and Metallurgy, 2004: p. 423-428.
3. Jones R.T., Towards commercialisation of Mintek's Conroast process for platinum smelting, in Pyrometallurgy of Nickel and Cobalt 48th Annual conference of Metallurgists of CIM2009. pp. 159-168.
4. Jones R.T. ConRoast: DC are smelting of dead-roasted sulphide concentrates. 2011; Available from: www.pyromeallurgy.co.za/Mintek/ConRoast.
5. Phillips R.E., Jones R.T., and Chennells P., Commercialization of the ConRoast process, in Third international platinum conference, The Southern African Institute of Mining and Metallurgy, B.R. plc, Editor 2008, Mintek: South Africa. pp. 141-148.
6. Koretsky M.D., Engineering and chemical thermodynamics. Vol. 1. 2004, Oregan state.
7. N.A., General methods for extraction of metals, 1998.
8. Chakraborty D., Ranganatha S. and Sinha S., Corbothermic reduction of chromite ore under different flow rates of inert gas. Metallurgical and Materials transactions B, 2010. 41B: p. 10-18.
9. Haque R. and H.S. Ray, Carbon contact and direct reduction in the reduction of iron oxide by carbon. Metallurgical and Materials transactions B, 1995. vol 26B.
10. Murti N.S.S. and V. Seshadri, Reduction of synthetic chromite by carbon. Trans. Iron stell Inst. Jpn., 1982. 22: pp. 925-933.
11. Nafziger R.H., Tress J.E. and Paige J.I., The reduction of chromite ores under different reductants and temperatures. Metallurgical transactions B, 1979. 10B: pp. 5-14.
12. R.H. Eric, A.A Hejja and D.D. Howat, Metal losses to the slag and matte-slag separation in electric smelting of copper-nickel concentrates. The Minerals, Metals & Materials Society, 1994: pp. 641-656.
13. Choi N and Cho W.D, Distribution behaviour of cobalt, selenium and tellurium between nickel-coppper-iron matte and silica-saturated iron silicate slag. Metallurgical and Materials transactions B, 1997. vol 28B pp. 429-438.
14. R.W Ruddle, B. Taylor, and A.P. Bates, The solubility of copper in iron silicate slags. Inst. Min. Metall, 1966: pp. C1-C12.
15. Fontana A, Properties of ferrous silicate slags associated with copper flash smelting and electric furnace processes, in Proceedings of Extraction Metallurgy 1989: London: IMM. pp. 147-164.
16. Chen C, Zhang L, and Jahanshahi S, Review and thermodynamic modelling of CoO in iron silicate-based slag and calcium ferrite-based slags, in Proceedings of the 7th Int. Conf. on molten slags, Fluxes and Salts 2004: Cape town: SAIMM. p. 509-515.
17. Takeda Y., Copper solubility in SiO_2-CaO-FeO slag equilibrated with matte, in Proc. 6th Int. Conf. on molten slags, Fluxes and Salts2000: Stockholm/Helsinki: ISBN. p. 18 pp.
18. Shimpo R., Goto S., Ogawa O. and Asakura I., A study on the equilibrium between copper matte and slag. Can. Metall. Quaterly, 1986. 25 (no. 2): pp. 113-121.
19. Kim H.G. and Sohn H.Y., Effects of CaO, Al_2O_3 and MgO additions on the copper solubility, ferrc/ferrous ratio, and minor element behaviour of iron silicate slags. Metallurgical and Materials transactions B, 1998. 29B: p. 583-590.

20. Wang S.S., Santander N.H. and Toguri J.M., The solubility of nickel and cobalt in iron silicate slags. Metall. Trans, 1974(5): pp. 261-265.
21. Barnett S.C.C. and Jeffes J.H.E., Recovery of nickel from Thompson smelter electric furnace slag. Trans. Inst. Min. Metall., 1977. vol C(86): pp. 155-157.
22. Ngamori M. and Mackey. P.J, Thermodynamics of copper matte converting: Part 1. Fundamentals of the Noranda Process. Metallurgical and Materials transactions B, 1978. 9B: pp. 255-265.
23. Tan P. and Neushutz D., A thermodynamic model of nickel smelting and direct high-grade nickel matte smelting processes: Part 1. Model development and validation. Metallurgical and Materials transactions B, 2001(32B): pp. 341-351.
24. Holzheid A., Palme H., and Chakraborty S., The activities of NiO, CoO and FeO in silicate melts. Chemical Geology, 1997. 139: pp. 21-38.
25. Floyd J.M. and Mackey P.J., Developments in the pyrometallurgical treatment of slag: a review of current technology and physical chemistry., in Proceedings of extraction metallurgy 1981: London: IMM. pp. 345-371.
26. Sahoo P. and Reddy R.G., Activity coefficient of nickel oxide in FeO-NiO-$FeO_{1.5}$-$AlO_{1.5}$-SiO_2 slag at 1573 K, in Proc. 2nd Int. Symp. on metallurgical slags and fluxes 19841984: Metall. Soc. of AIME. pp. 533-545.
27. Li G. and Tsukihashi. F., Distribution equilibria of Fe, Co and Ni between MgO-saturated FeO-MgO-SiO_2 slag and Ni alloy. ISIJ international, 2001(41): pp. 1303-1308.
28. Andrews L., Base metal losses to furnace slag during processing of platinum-bearing concentrates, Faculty of materials and minerals engineering, 2008, University of Pretoria: Pretoria.
29. Minto R. and Davenport W.G., Discussion of Entrapment and flotation of matte in molten slags. Trans. Inst. Min. Metall., 1973. 82: pp. C59-C62.
30. Fagurland K.O. and Jalkanen H., Some aspects on matte settling in copper smelting, in Proc. Copper 99 Int. Conf.1999. pp. 539-551.
31. Poggie D., Minto R. and Davenport W.G., Mechanisms of metal entrapment in slags. Journ. Metals, 1969: pp. 40-45.
32. Rhodes M., Intoduction to particle technology. second ed 2008, England: John Wiley & Sons Ltd.
33. Clift R., Grace J.R. and Weber M.E., Bubbles, drops and particles, in Academic Press1978: London. pp. 30-46.
34. Minto R. and Davenport W.G., Entrapment and flotation in molten slags. Trans. Inst. Min. Metall., 1972. 82: pp. C59-C62.
35. Ip S.W. and Toguri J.M., Entrianment behaviour of copper and copper matte in copper smelting operations. Metall. Trans B, 1992. vol 23B: pp. 303-311.
36. IP S.W. and Toguri J.M., Surface and interacial tension of the Ni-Fe-S, Ni-Cu-S and fayalite slag systems. Metall. Trans B, 1993. vol 24B: pp. 657 - 668.
37. Hamuyuni, J., Measurement of surface tension in base metal sulfide mattes by an improved Sessile drop method, in Faculty of Engineering 2012, Stellenbosch university: Stellenbosch.
38. Eric R.H., Slag properties and design issues pertinent to matte smelting electric furnaces. The Journal of The South African Institute of Mining and Metallurgy, 2004 (October 2004): pp. 499-510.
39. Shahrokhi H. and Shaw J.M., Fine drop recovery in batch gas-agitated liquid-liquid systems. Chem. Eng. Sci., 2000. 55: pp. 4719-4735.

40. Saffman P.G. and Turner J.S., On the collision of drops in turbulent clouds. Journ. Fluid Mechanics, 1956. 1: p. 16-30.
41. Ammann P.R., Kim J.J., and Loose T.A., The Kennecott Process for nickel slag cleaning. Journ. Metals, 1979. 1(2): pp. 20-25.
42. Yazawa A., Thermodynamic evaluations of extractive metallurgical processes. Metall. Trans. B, 1979. 10B: pp. 307-321.
43. Mackey P.J., The physical chemisty of copper smelting slags - a review. Metall . Quarterly 1982. 21(3): pp. 221-260.
44. Maruyama T., Furui N., Hamamoto M. and Sunamoto T., The copper loss in slag of flash smelting furnace in Tamano Smelter, in The Minerals, Metals & Materials Society 2003. pp. 337-347.
45. Ip S.W. and Toguri J.M., Entrainment of matte in smelting and converting operations., in J.M. Toguri Symp. Fundamentals of Metallurgical Processing, Pickles G., Utigard T., and Vahed A., Editors. 2000: Ottowa, Canada: Met. Soc. pp. 291-302.
46. Eric R.H. and A.A. Hejja, Dimensioning, scale up and operating considerations for six electrode elctric furnaces. Part 2: Design and scale-up considerations for furnaces treating PGM-containing copper-nickel concentrates, in Proc. EPD Congress, G.W. In Warren, Editor 1995. pp. 239-257.
47. Warczok A. and Utigard T.A., Settling of copper in molten slags. Metall. Trans. B, 1995. 26B: pp. 1165-1173.
48. Warczok A., Riveros G., Echeverria P, Diaz C.M., Schwarze H. and Sanchez G., Factors governing slag cleaning in an electric furnace. Can. Met. Quarterly, 2002. 41(4): pp. 465-474.
49. Warczok A. and Riveros G., Slag cleaning in crossed electric and magnetic fields. Minerals Engineering, 2007. 20: pp. 34-43.
50. Smith S. and Bezuidenhout R., Mineralogical analysis of concentrate samples: Lonmin Process Division, 2010, ALS Laboratory Group.
51. Lutterotti, L. Introduction to diffraction and the Rietveld method. 2012; Available from: www.ing.unitn.it/~luttero/laboratoriomateriali/RietveldRefinements.pdf.
52. Sikilitsky V. Properties of Silicon Carbide. 2009; Available from: www.ioffe.ru/SVA/NSM/Semisond/SiC/.
53. Perry K.P.D., Finn C.W.P., and King R.P., Metallurgical transactions B, 1988. 19B: p. 677-684.
54. Qayyam M.A., Can. Met. Quarterly, 1976. 15: pp. 193-200.
55. S. A. Decterov, A. N. Grundy, I.-H. Jung and A. D. Pelton, “Modeling the Viscosity of Aluminosilicate Melts”, In: Computation in Modern Science and Engineering, (Proc. Int. Conf. on Computational Methods in Sciences and Engineering), AIP (American Institute of Physics) Conference Proceedings, Vol. 963, Issue 2, Pt B, Eds. T. E. Simos and G. Maroulis, pp. 404-407 (2007).
56. Grundy A.N., H.-C. Liu, I.-H. Jung, S.A. Decterov and A.D. Pelton, "A Model to Calculate the Viscosity of Silicate Melts. Part I.: Viscosity of Binary SiO_2-MeO_x Systems (Me = Na, K, Ca, Mg, Al)". Int. J. Mat. Res., 2008, vol. 99 (11), pp. 1185-1194.
57. Grundy A.N., I.-H. Jung, A.D. Pelton and S.A. Decterov, "A Model to Calculate the Viscosity of Silicate Melts. Part II.: Viscosity of the Multicomponent $NaO_{0.5}$-MgO-CaO-$AlO_{1.5}$-SiO_2 System". Int. J. Mat. Res., 2008, vol. 99 (11), pp. 1195-1209.
58. Kim W.-Y., A.D. Pelton and S.A. Decterov, "A Model to Calculate the Viscosity of Silicate Melts. Part III: Modification of the model for melts containing alkali metals". Int. J. Mat. Res., 2010, submitted.

59. Brosh E., A.D. Pelton and S.A. Decterov, "A Model to Calculate the Viscosity of Silicate Melts. Part IV: Borosilicate melts". Int. J. Mat. Res., 2010, submitted.
60. Brosh E., A.D. Pelton and S.A. Decterov, "A Model to Calculate the Viscosity of Silicate Melts. Part V: Borosilicate melts containing alkali oxides". Int. J. Mat. Res., 2010, submitted.
61. S. A. Decterov, A. N. Grundy and A. D. Pelton, “A Model and Database for the Viscosity of Molten Slags”, Proc. VIII Int’l Conf. on Molten Slags, Fluxes and Salts, Santiago, Chile, pp. 423-431 (2009).
62. Kim W.-Y., A.D. Pelton and S.A. Decterov, "Modeling the Viscosity of Silicate Melts Containing Lead Oxide". Metall. Mater. Trans., 2010, submitted.
63. Kinsley, G, 2001, Properly Purge and Inert Storage Vessels, CEP Feb 2001
64. Bale C.W., Belisle E., Chartrand P., Decterov S.A., Eriksson G., Hack G., Jung, I-H, Kang Y-B., Melancon, J., Pelton A.D., Robelin C., Petersen S., Bale P., FactSage Thermochemical Software and Databases - Recent Developments, CalPhad J., vol. 32, pp. 189-228, 2008
65. Eksteen J.J., Van Beek B. and Bezuidenhoud G.A., Cracking a hard nut: An overview of Lonmin's operations directed at smelting of UG2-rich concentrate blends, SAIMM, 2011 (Oct). 11: pp. 681 - 690

Appendix A – Tables and Figures

Table A1 – Chemical formulas of minerals detected from XRD in Rowland and Easterns LG concentrates

Mineral	Formula	Mineral Group
Actinolite	$Ca_2(Mg,Fe)Si_8O_{22}(OH)_2$	Alteration silicates
Augite	$(Ca,Na)(Mg,Fe,Al,Ti)(Si,Al)_2O_6$	Alteration silicates
Biotite	$K(Mg,Fe)_3(AlSi_3O_{10})(OH, F)_2$	Alteration silicates
Calcite	$CaCO_3$	Carbonates
Chalcopyrite	$CuFeS_2$	Sulphides
Chlorite	$(Mg, Fe)_5Al(Si_3Al)O_{10}(OH)_8$	Alteration silicates
Chromite	$FeCr_2O_4$	Oxides
Enstatite	$MgSiO_2$	Alteration silicates
Kaolinite	$Al_2Si_2O_5(OH)_4$	Alteration silicates
Plagioclase	$(Na,Ca)(Al,Si)_4O_8$	Feldspar
Pentlandite	$(Fe,Ni)_9S_8$	Sulphides
Quartz	SiO_2	Quartz
Talc	$Mg_3Si_4O_{10}(OH)_2$	Alteration silicates

The cumulative percent passing graphs are presented in Figures A1 – A2. All size distribution data for mineral phases are presented as weight percent passing.

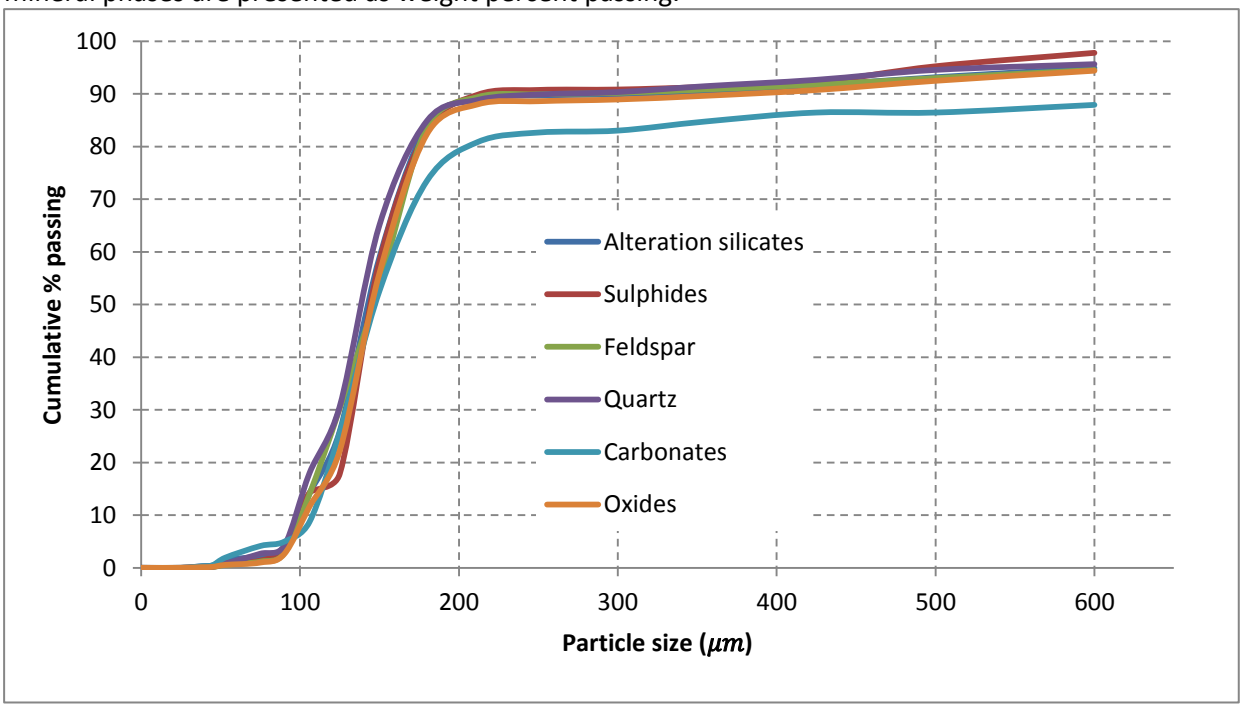

Figure A1 – Cumulative % passing of minerals of interest in Rowland LG concentrate

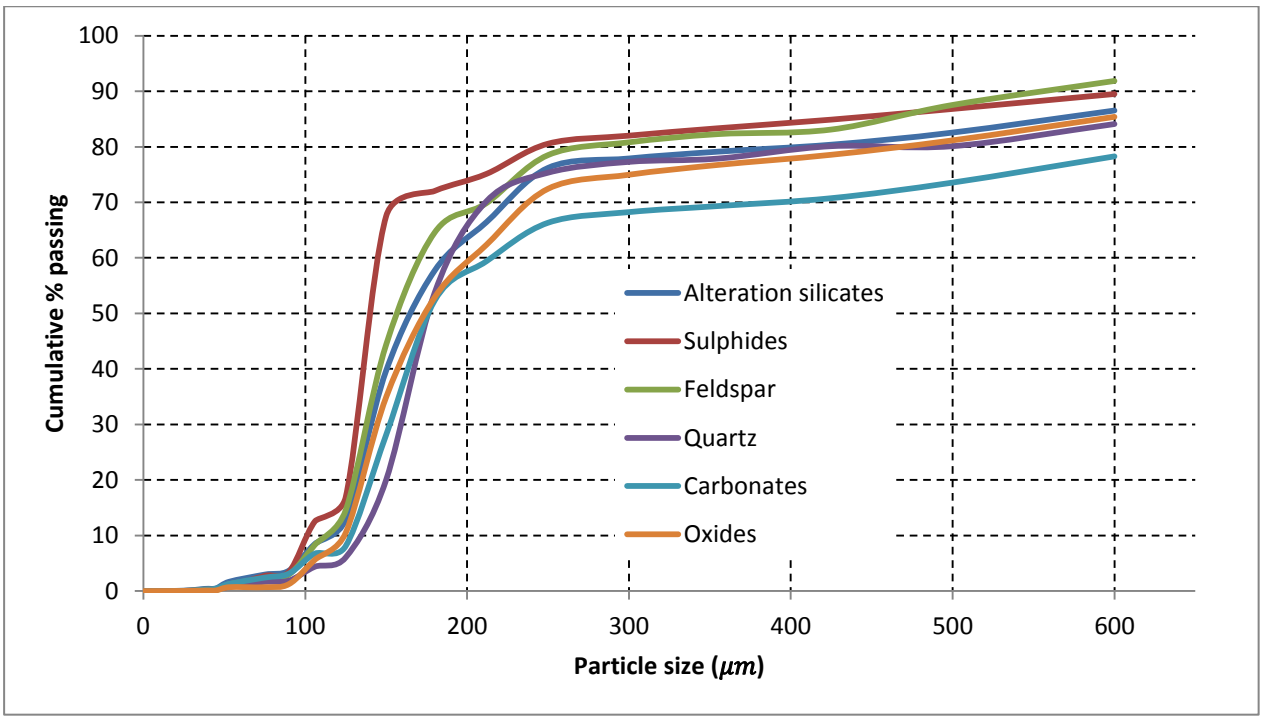

Figure A2 – Cumulative % passing of minerals of interest in Easterns LG concentrate

The P-Values from figure A1 and figure A2 are shown in the following tables:

Table A2 – P 20 value for minerals of interest.

P 20		
Mineral	**Rowland LG concentrate - microns**	**Easterns LG concentrate - microns**
Alteration silicates	115	132
Sulphides	127	125
Feldspar	117	129
Quartz	108	150
Carbonates	119	141
Oxides	122	134

Table A3 – P 60 value for minerals of interest.

P 60		
Mineral	**Rowland LG concentrate - microns**	**Easterns LG concentrate - microns**
Alteration silicates	150	188
Sulphides	152	145
Feldspar	155	170
Quartz	145	190
Carbonates	159	217
Oxides	153	205

Table A4 – P 80 value for minerals of interest.

P 80		
Mineral	**Rowland LG concentrate - microns**	**Easterns LG concentrate - microns**
Alteration silicates	171	400
Sulphides	172	242
Feldspar	173	280
Quartz	169	420
Carbonates	340	600
Oxides	176	460

Table A5 – XRD results of Rowland LG concentrate for respective screen sizes

Mineral	25 - 38 µm	3 sigma error	38-45 µm	3 sigma error	45-53 µm	3 sigma error	53-75 µm	3 sigma error	75-90 µm	3 sigma error	90-106 µm	3 sigma error	106-125 µm	3 sigma error	125-150 µm	3 sigma error	150-180 µm	3 sigma error
Actinolite	1.36	0.36	2.37	0.48	3.97	0.54	2.41	0.48	0.99	0.45	4.68	0.81	2.28	0.54	4.17	0.84	1.13	0.51
Augite	2.19	0.6	2.69	0.57	2.23	0.42	2.72	0.54	4.6	0.57	4.29	0.54	3.85	0.51	4.26	0.54	5.12	0.54
Biotite	4.87	0.69	6.35	0.6	7.07	0.54	6.4	0.75	5.48	0.69	4.69	0.69	5.07	0.6	4.09	0.69	5.29	0.72
Calcite	0.46	0.21	0.66	0.19	0.71	0.19	1.26	0.39	0.22	0.15	0.17	0.3	0.65	0.27	0.38	0.23	0.38	0.22
Chalcopyrite	0.16	0.08	0.1	0.07	0.17	0.07	0.13	0.13	0.33	0.14	0.24	0.13	0.07	0.06	0.29	0.13	0.23	0.14
Chlorite	8.35	0.81	9.81	0.81	10.87	0.63	7.88	0.96	4.9	0.93	4.88	0.75	5.22	0.78	6.86	0.81	7.51	0.81
Chromite	2.23	0.25	1.94	0.3	2.1	0.27	2.74	0.3	4.83	0.36	4.51	0.36	4.51	0.42	5.28	0.39	5.33	0.33
Enstatite	62.85	1.8	54.8	1.5	49.72	1.26	39	2.1	46.78	1.32	38.3	2.28	34.05	2.67	42.2	2.07	41.44	1.35
Kaolinite	3.43	0.54	3.92	0.51	3.64	0.42	4.26	0.6	4.35	0.66	5.1	0.6	4.02	0.57	3.96	0.63	4.57	0.6
Plagioclase	1.8	0.42	1.85	0.36	2.49	0.36	4.34	0.48	5.3	0.6	6.18	0.54	7.63	0.81	4.01	0.48	6.71	0.54
Quartz	0.53	0.14	0.59	0.12	0.8	0.12	3.03	0.36	1.11	0.22	1.73	0.21	1.35	0.23	1.35	0.22	1	0.18
Talc	11.78	2.01	14.91	1.98	16.22	1.71	25.8	3.3	21.1	1.32	25.2	3.9	31.3	4.8	23.1	3.3	21.28	1.56

Table A5 (continued) – XRD results of Rowland LG concentrate for respective screen sizes

Mineral	180-212 µm	3 sigma error	212-250 µm	3 sigma error	250-300 µm	3 sigma error	300-355 µm	3 sigma error	355-425 µm	3 sigma error	425-500 µm	3 sigma error	500-600 µm	3 sigma error	> 600 µm	3 sigma error
Actinolite	1.77	0.69	1.32	0.66	5.86	0.96	2.6	0.63	2.66	0.69	4.92	0.75	3.72	0.87	2.26	0.63
Augite	5	0.6	5.1	0.6	6.54	0.63	5.23	0.51	5.43	0.48	4.64	0.57	4.66	0.54	5.14	0.72
Biotite	4.74	0.75	4.22	0.75	2.24	0.36	6.89	0.72	6.78	0.69	6.16	0.87	5.68	0.63	4.09	0.72
Calcite	0.64	0.3	1.57	0.39	0.64	0.25	1.3	0.29	0.7	0.33	0	0	0.38	0.21	1.08	0.33
Chalcopyrite	0.3	0.13	0.4	0.16	0.07	0.06	0.19	0.08	0.19	0.1	0.47	0.14	0.34	0.11	0.1	0.08
Chlorite	7	0.87	7.78	1.38	7.06	0.78	8.7	0.9	8.69	0.93	5.57	0.84	6.28	0.87	6.33	0.96
Chromite	5.42	0.42	5.73	0.39	6.3	0.33	5.82	0.33	5.01	0.29	5.94	0.29	5.58	0.36	5.54	0.63
Enstatite	41.25	2.16	36.38	1.47	35.99	1.23	38.71	1.08	41	1.14	39.68	1.23	41.12	1.26	37.8	4.2
Kaolinite	4.45	0.66	4.33	0.69	4.71	0.57	4.19	0.57	4.04	0.54	4.92	0.63	3.91	0.6	4.24	0.72
Plagioclase	6.02	0.63	5.63	0.57	5.65	0.45	5.99	0.51	4.55	0.51	4.67	0.63	4.93	0.57	5.96	0.81
Quartz	0.96	0.2	2.49	0.48	2.21	0.42	2.34	0.36	1.38	0.18	1.61	0.22	0.79	0.18	1.08	0.22
Talc	22.5	3.3	25.05	2.25	22.73	1.62	18.03	1.05	19.55	0.96	21.43	1.29	22.6	1.44	26.3	8.1

Table A6 – XRD results of Easterns LG concentrate for respective screen sizes

Mineral	<25 µm	3 sigma error	25-38 µm	3 sigma error	38-45 µm	3 sigma error	45-53 µm	3 sigma error	53-75 µm	3 sigma error	75-90 µm	3 sigma error	90-106 µm	3 sigma error	106-125	3 sigma error	125-150 µm	3 sigma error
Actinolite	2.3	0.51	2.66	0.45	2.91	0.6	2.9	0.45	2.62	0.51	3.61	0.54	3.32	0.63	2.47	0.54	3.32	0.63
Augite	5.45	0.63	4.17	0.51	2.86	0.48	3.67	0.57	2.78	0.84	5.4	0.57	4.67	0.72	5.58	0.57	4.67	0.72
Biotite	4.22	0.63	4.11	0.9	3.88	0.63	6.2	0.6	6.46	0.78	6.13	0.66	4.9	0.57	3.99	0.72	4.9	0.57
Calcite	1.66	0.36	1.4	0.27	2.89	0.29	1.27	0.36	1.66	0.48	1.78	0.39	1.3	0.57	0.53	0.3	1.3	0.57
Chalcopyrite	0.23	0.11	0.2	0.1	0.34	0.07	0.11	0.07	0.46	0.16	0.3	0.11	0.54	0.21	0.28	0.12	0.54	0.21
Chlorite	4.17	1.44	8.08	0.72	6	0.57	6.75	0.51	8.23	0.84	4.93	0.66	7.83	0.87	10.43	1.05	7.83	0.87
Chromite	3.78	0.33	1.73	0.22	1.37	0.3	3.34	0.19	0	0	5.23	0.29	6.03	0.33	7.21	0.42	6.03	0.33
Enstatite	56.55	1.83	60.25	1.65	57.12	1.41	49.55	1.29	53.9	1.59	51.12	1.11	50.93	1.35	48.83	1.26	50.93	1.35
Kaolinite	2.43	0.48	2.28	0.51	2.35	0.51	3.03	0.42	0.82	0.54	2.33	0.48	2.07	0.6	0.63	0.48	2.07	0.6
Plagioclase	1.25	0.36	1.28	0.39	1.53	0.36	3.64	0.96	3.24	0.51	3.97	0.45	4.25	0.51	5.36	0.6	4.25	0.51
Quartz	0.24	0.19	0.24	0.1	4.22	0.45	0.74	0.2	0.82	0.36	0.43	0.17	0.72	0.28	0.52	0.19	0.72	0.28
Talc	17.73	1.92	13.6	1.62	14.53	1.68	18.8	1.29	19.01	1.62	14.76	0.72	13.44	1.11	14.17	1.23	13.44	1.11

Table A6 (continued) – XRD results of Easterns LG concentrate for respective screen sizes

	150-180 µm	3 sigma error	180-212 µm	3 sigma error	212-250 µm	3 sigma error	250-300 µm	3 sigma error	300-355 µm	3 sigma error	350-425 µm	3 sigma error	425-500 µm	3 sigma error	500-600 µm	3 sigma error	> 600 µm	3 sigma error
Actinolite	1.86	0.63	3.6	0.54	1.95	0.39	2.72	0.45	0.43	0.54	3.31	0.63	3.53	0.63	2.37	0.57	2.08	0.48
Augite	3.99	1.14	5.17	0.45	4.84	0.51	8.58	0.6	5.65	0.54	5.38	0.78	5.51	0.75	5.11	0.87	6.64	0.69
Biotite	7.47	2.04	3.76	0.51	4.08	0.6	6.64	0.63	4.51	0.69	3.74	0.45	6.13	0.72	6.47	0.81	7.81	0.84
Calcite	2.27	0.66	1.4	0.29	1.24	0.36	1.85	0.33	1.49	0.36	1.89	0.57	2.13	0.45	2.03	0.54	2.77	0.54
Chalcopyrite	0.07	0.07	0.1	0.06	0.16	0.09	0.23	0.11	0.3	0.12	0.34	0.21	0.24	0.12	0.19	0.14	0.22	0.16
Chlorite	6.65	1.86	3.64	0.69	5.22	0.84	3.49	0.63	5.32	0.87	11.57	1.14	5.25	0.99	11.42	1.17	5.39	0.84
Chromite	6.41	1.65	7.12	0.33	6.86	0.51	9.28	0.42	9.18	0.42	9.25	0.63	7.49	0.42	6.91	0.42	7.08	0.45
Enstatite	45.5	11.7	42.02	1.56	43.15	2.88	39.38	1.17	47.05	1.2	43.83	1.5	41.99	1.5	46.22	1.41	46.48	1.65
Kaolinite	2.29	0.78	2.68	0.51	2.02	0.48	3.6	0.51	4.11	0.6	2	1.08	3.32	0.6	0.53	0.66	2.97	0.72
Plagioclase	4.16	2.58	2.3	0.29	3.4	0.45	4.88	0.51	4.43	0.51	2.4	0.57	7.38	1.14	4.08	0.42	2.28	1.32
Quartz	2.51	0.72	2.59	0.25	0.73	0.22	1.5	0.16	0.64	0.26	2.36	0.51	0	0	1.36	0.39	1.61	0.33
Talc	16.9	21	25.64	2.25	26.3	4.5	17.84	1.65	16.91	0.87	13.93	1.74	17.02	1.8	13.3	1.38	14.66	1.83

Table A7 - XRD results of SiC for respective screen sizes

Mineral	<25 µm	3 sigma error	25-38 µm	3 sigma error	38-45 µm	3 sigma error	45-53 µm	3 sigma error	53-75 µm	3 sigma error	75-90 µm	3 sigma error	90-106 µm	3 sigma error	106-125 µm	3 sigma error	125-150 µm	3 sigma error
CA6 Hibonite	10.39	0.57	8.63	0.57	8.95	0.54	5.44	0.36	3.81	0.39	3.06	0.54	3.5	0.36	4.47	0.39	3.67	0.54
Corundum	4.14	0.72	3.56	0.33	4.41	0.81	3.57	0.29	2.44	0.26	3.54	0.36	2.57	0.26	2.57	0.23	2.05	0.33
Cristobalite	4.98	0.72	3.35	0.39	3.53	0.28	2.29	0.29	1.72	0.22	1.44	0.29	1.44	0.19	1.14	0.21	1.35	0.36
Graphite C	13.5	0.78	24.01	1.05	23.62	0.72	35.29	0.72	42.75	0.84	48.24	1.2	44.19	0.72	14.63	0.69	16.98	1.32
SiC4H	57.59	1.02	46.17	0.9	55.4	0.9	45.98	0.75	37.77	0.75	32.05	0.84	39.89	0.66	63.5	0.87	55.31	1.2
SiC6H	9.4	0.66	14.28	0.72	4.07	0.51	7.43	0.51	11.51	0.6	11.66	0.72	8.41	0.48	13.69	0.63	20.63	0.81

Table A7 (continued) - XRD results of Easterns LG concentrate for respective screen sizes

Mineral	150-180 µm	3 sigma error	180-212 µm	3 sigma error	212-250 µm	3 sigma error	250-300 µm	3 sigma error	300-355 µm	3 sigma error	355-425 µm	3 sigma error	425-500 µm	3 sigma error	500-600 µm	3 sigma error	> 600 µm	3 sigma error
CA6 Hibonite	3.55	0.9	4.37	0.75	5.1	0.57	3.44	0.45	2.99	0.51	2.85	0.36	3.74	0.48	2.83	0.36	1.87	0.72
Corundum	0.98	0.39	1.74	0.48	1.29	0.23	1.33	0.25	0.91	0.36	0.59	0.2	1.02	0.25	0.85	0.21	0.08	0.15
Cristobalite	1.35	0.39	2.32	0.54	1.08	0.21	0.98	0.21	0.76	0.22	0.99	0.23	0.77	0.18	0.55	0.16	0.64	0.28
Graphite C	38.4	2.94	18	1.86	7.67	0.66	6.53	0.63	6.39	0.75	7.07	0.51	5.69	0.57	9.42	0.51	2.22	1.08
SiC4H	39.03	1.98	39.46	1.23	68.76	0.9	68.27	0.93	62.85	1.14	73.66	0.84	69.87	0.9	72.27	0.84	76.83	1.29
SiC6H	16.69	1.5	34.12	1.29	16.11	0.69	19.46	0.87	26.1	1.02	14.83	0.66	18.91	0.81	14.08	0.69	9.7	0.51

The phases identified in the LG concentrate samples are shown using the scan most representative of all scans and then again showing all scans in one graph.

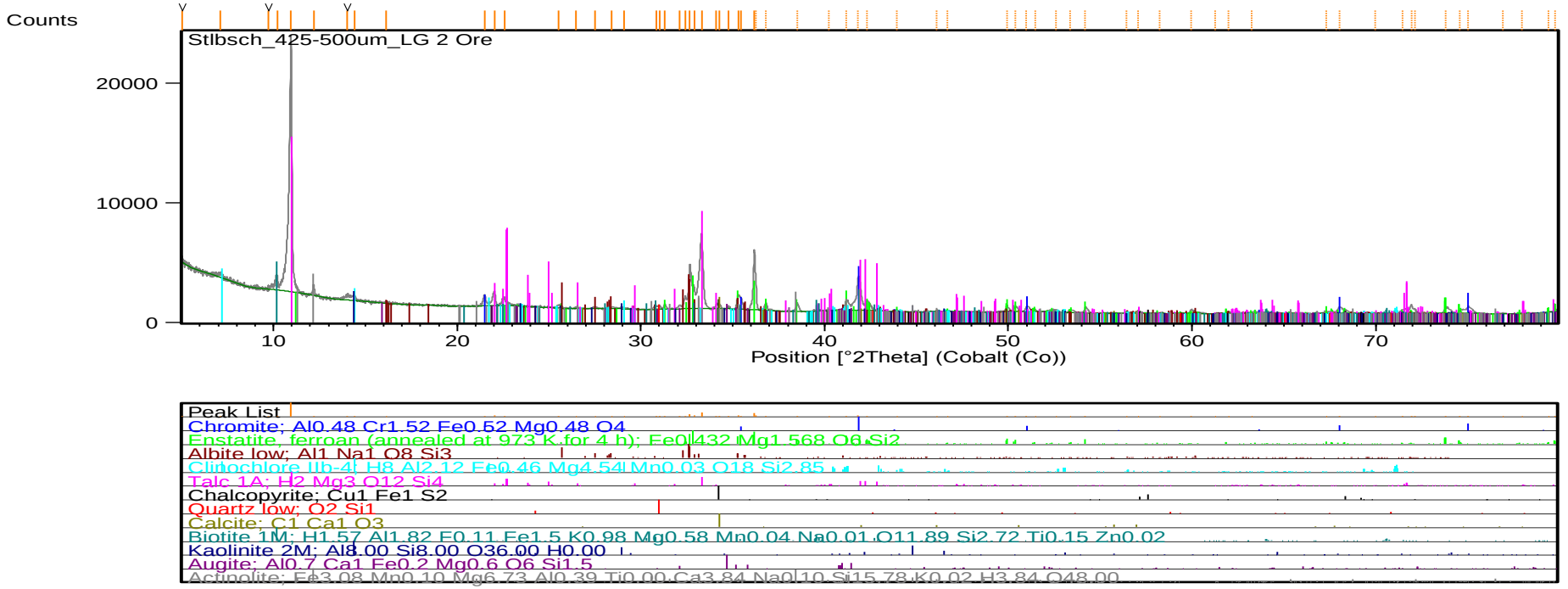

Figure A3 – Peak intensity graphs from XRD of Easterns LG concentrate (425 μn – 500 μn)

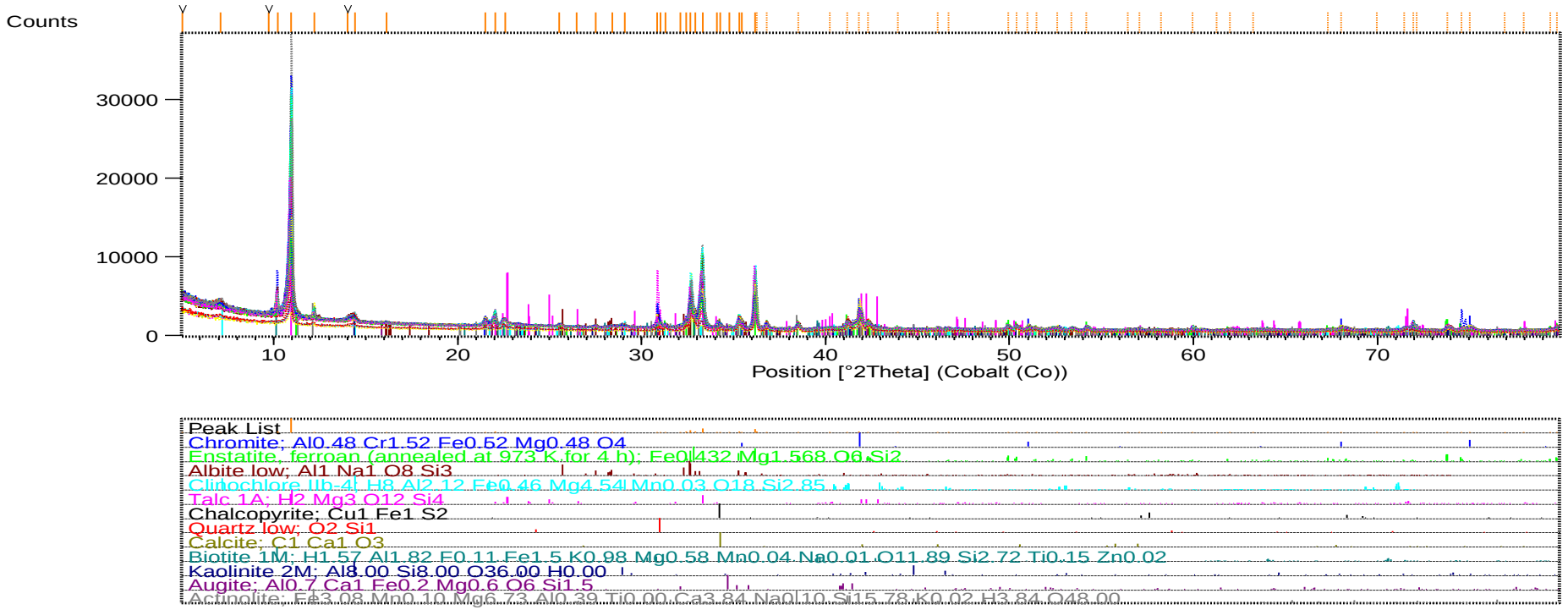

Figure A3 – Peak intensity graphs from XRD of Easterns and Rowland LG concentrates for all respective screen sizes

The SiC samples are shown in the graphs below grouped based on a statistical cluster analysis, grouping samples together based on similarities of the scans – traces of other polymorphs may be present.

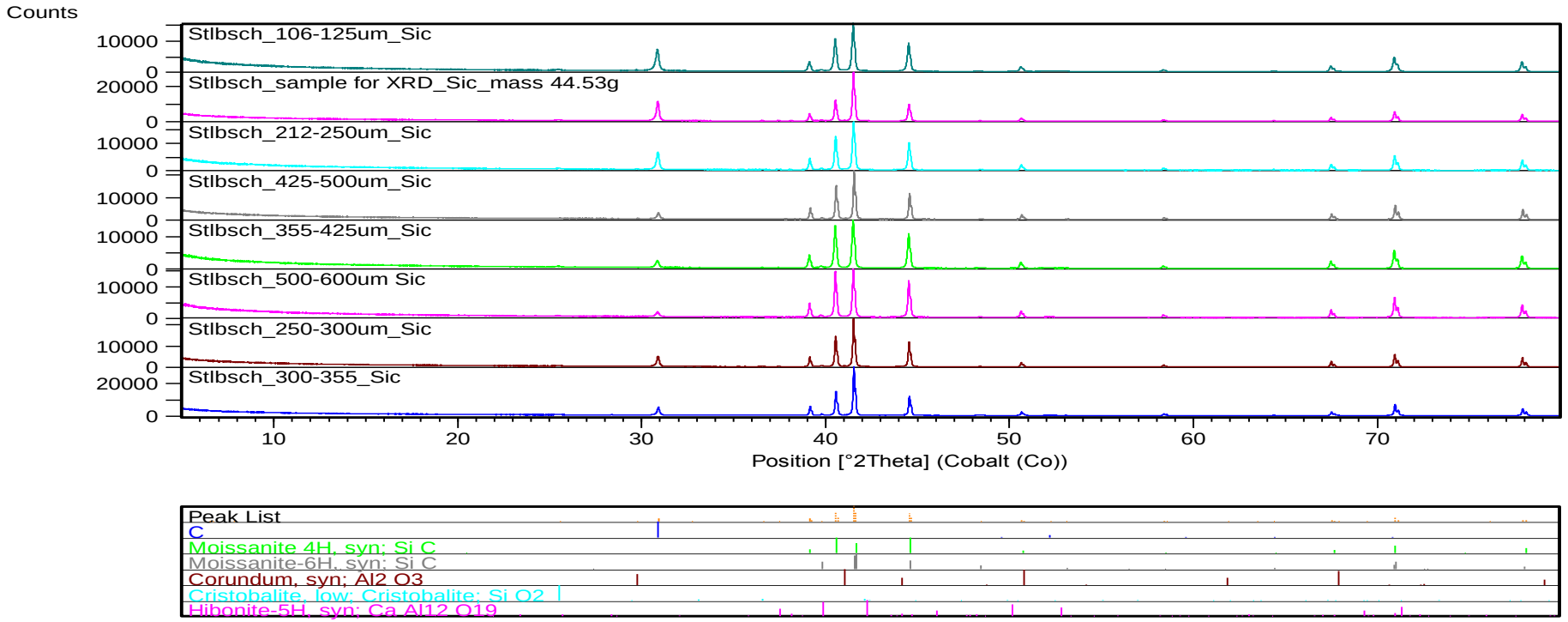

Figure A4 - Peak intensity graphs from XRD of SiC reductant

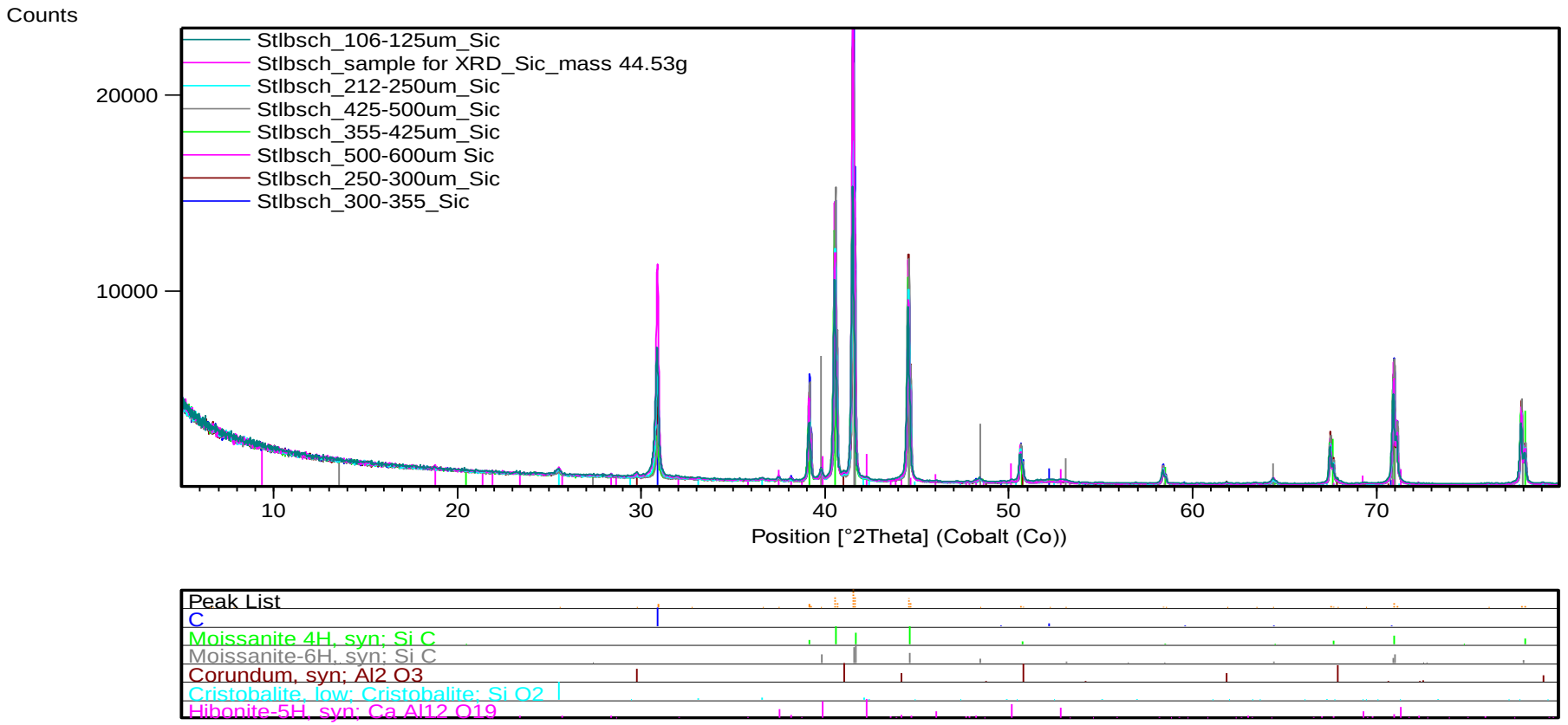

Figure A5 - Peak intensity graphs from XRD of SiC reductant (continued)

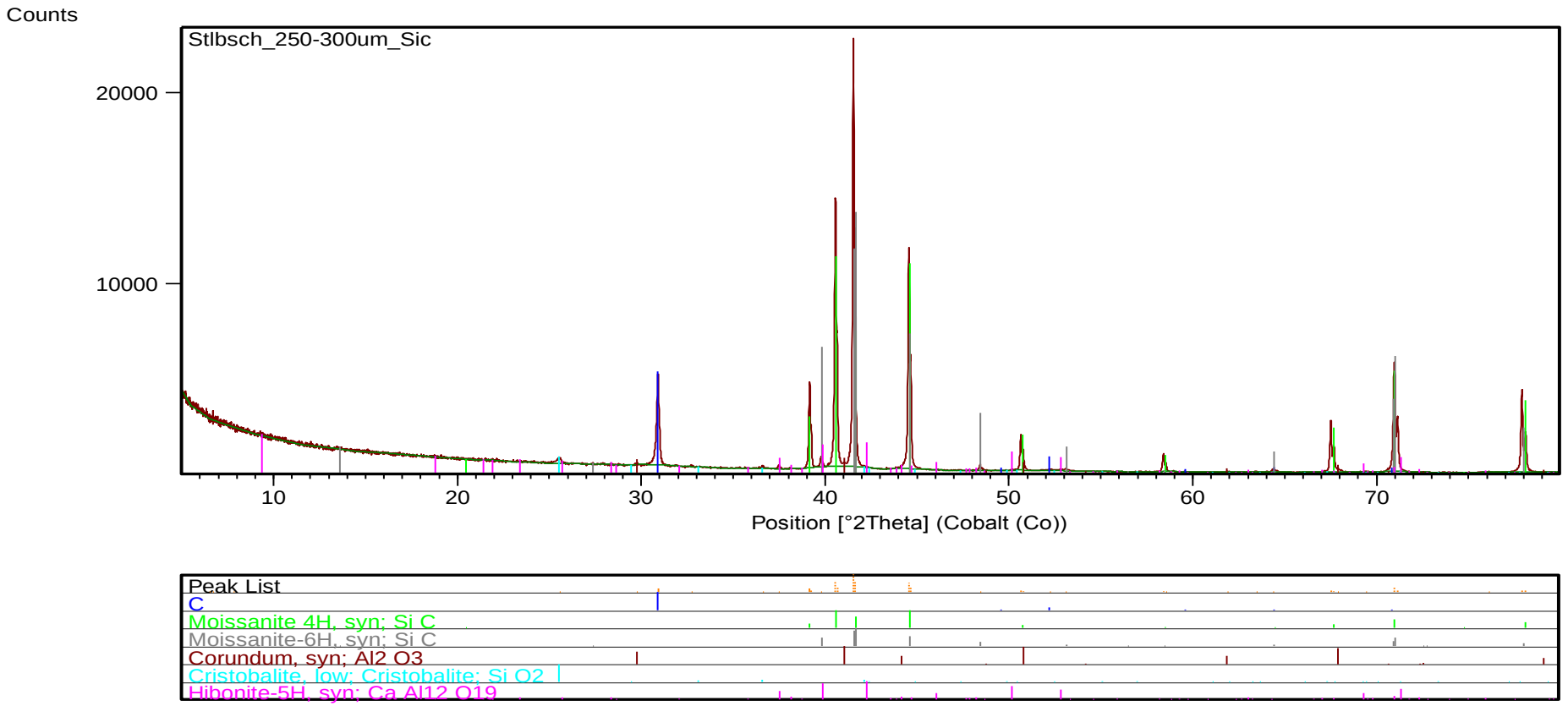

Figure A6 - Peak intensity graphs from XRD of SiC reductant (continued)

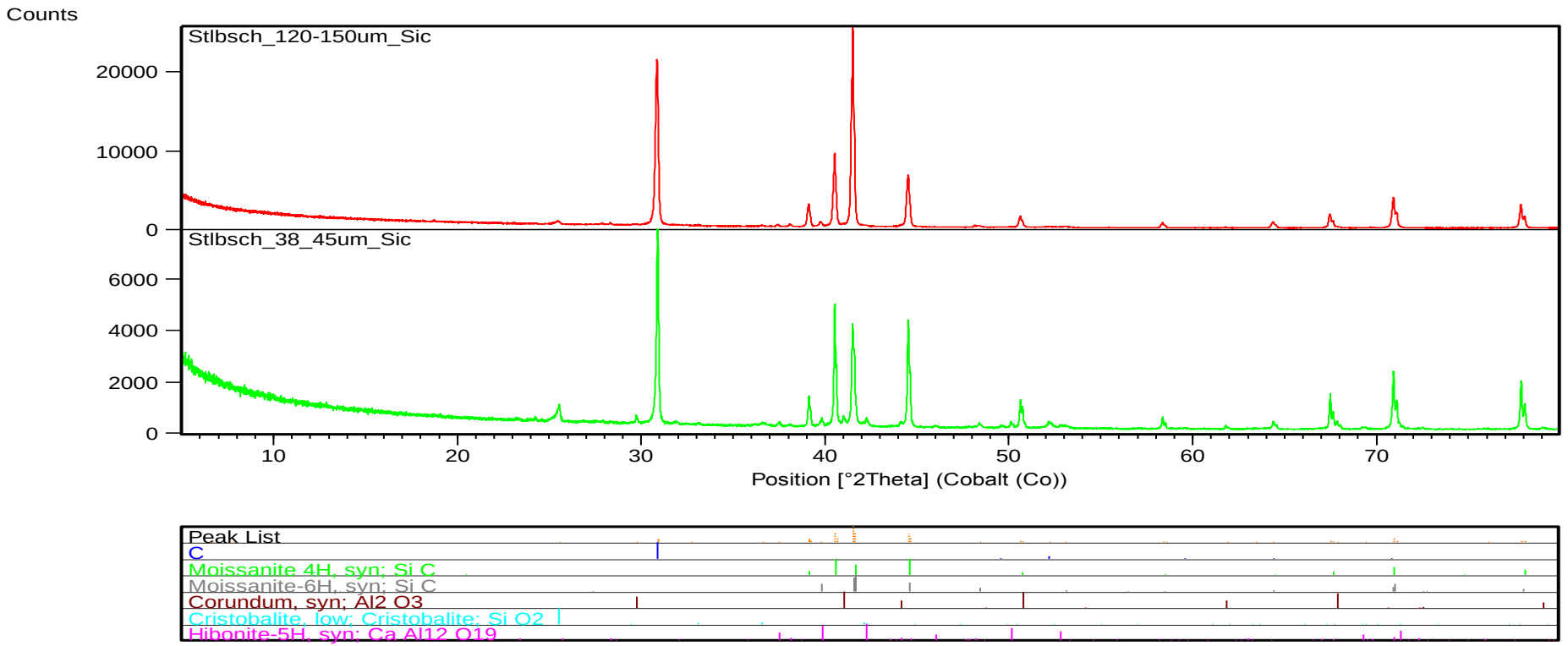

Figure A7 - Peak intensity graphs from XRD of SiC reductant (continued)

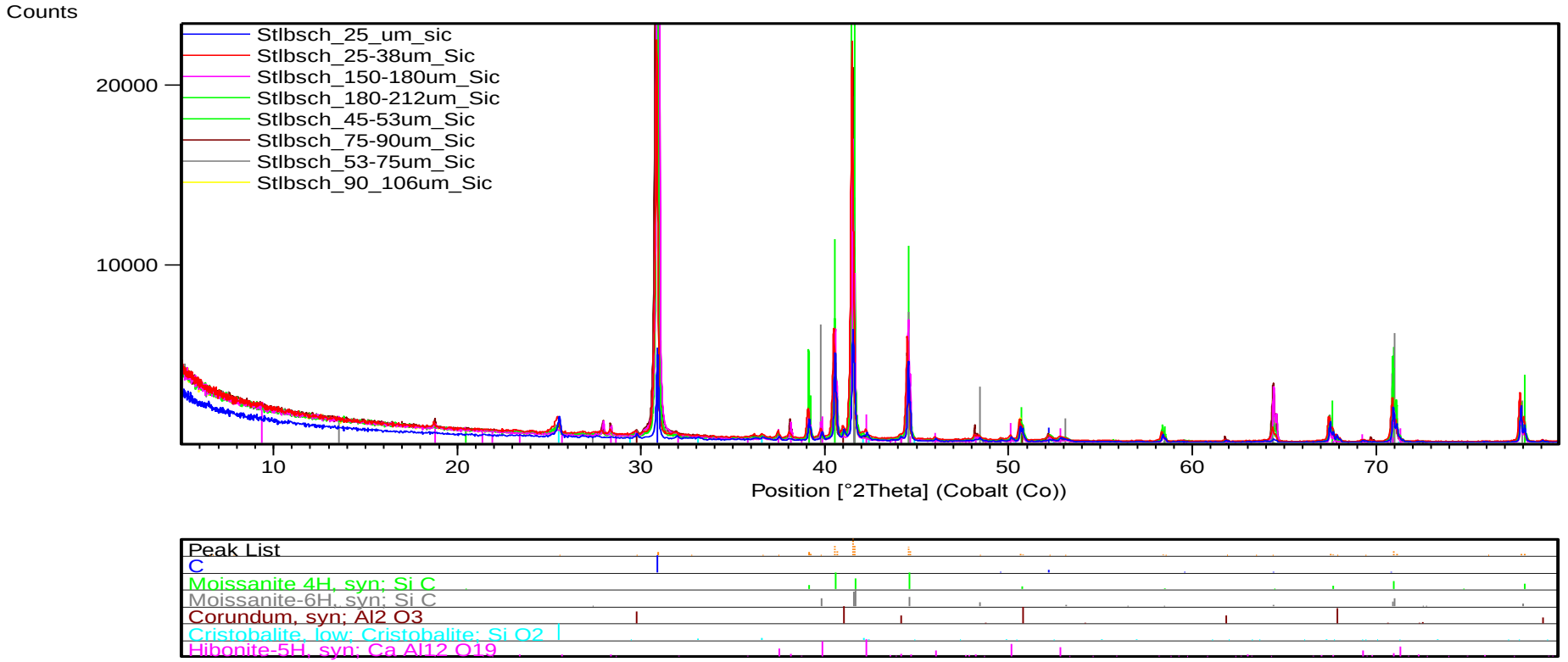

Figure A8 - Peak intensity graphs from XRD of SiC reductant (continued)

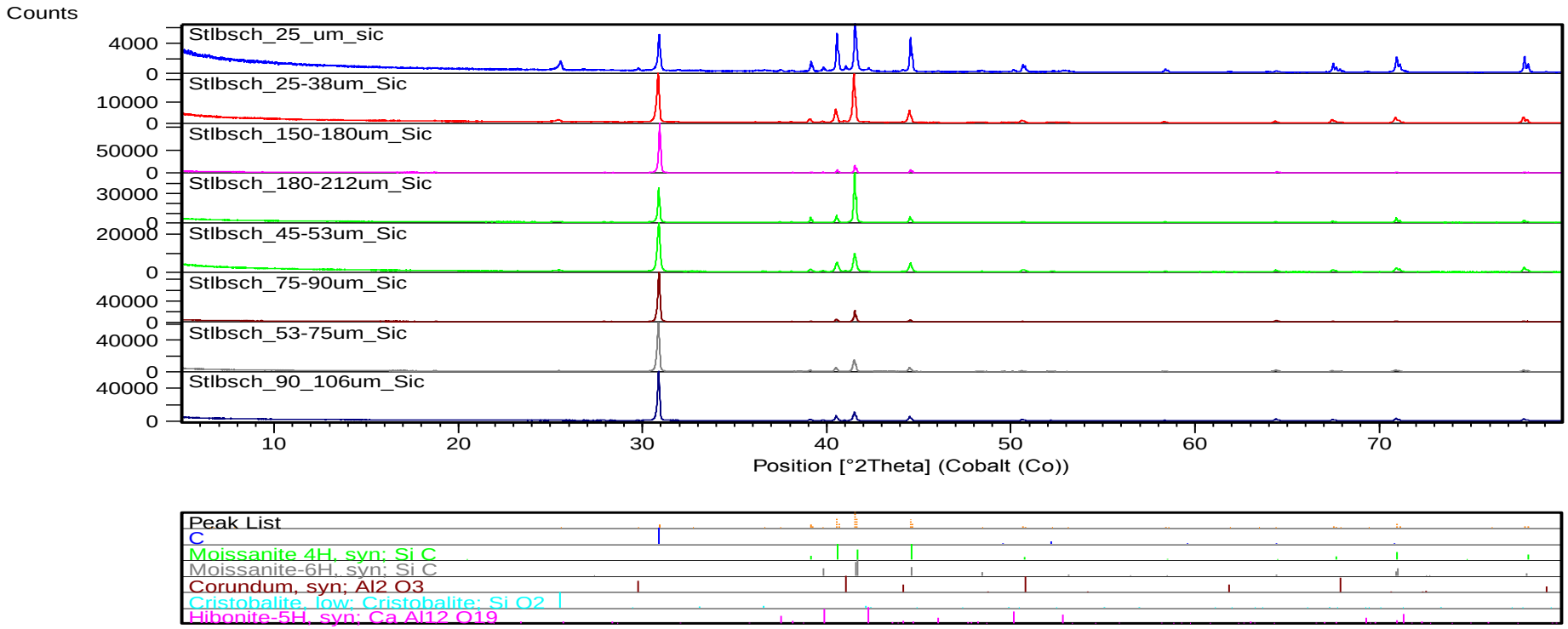

Figure A9 - Peak intensity graphs from XRD of SiC reductant (continued)

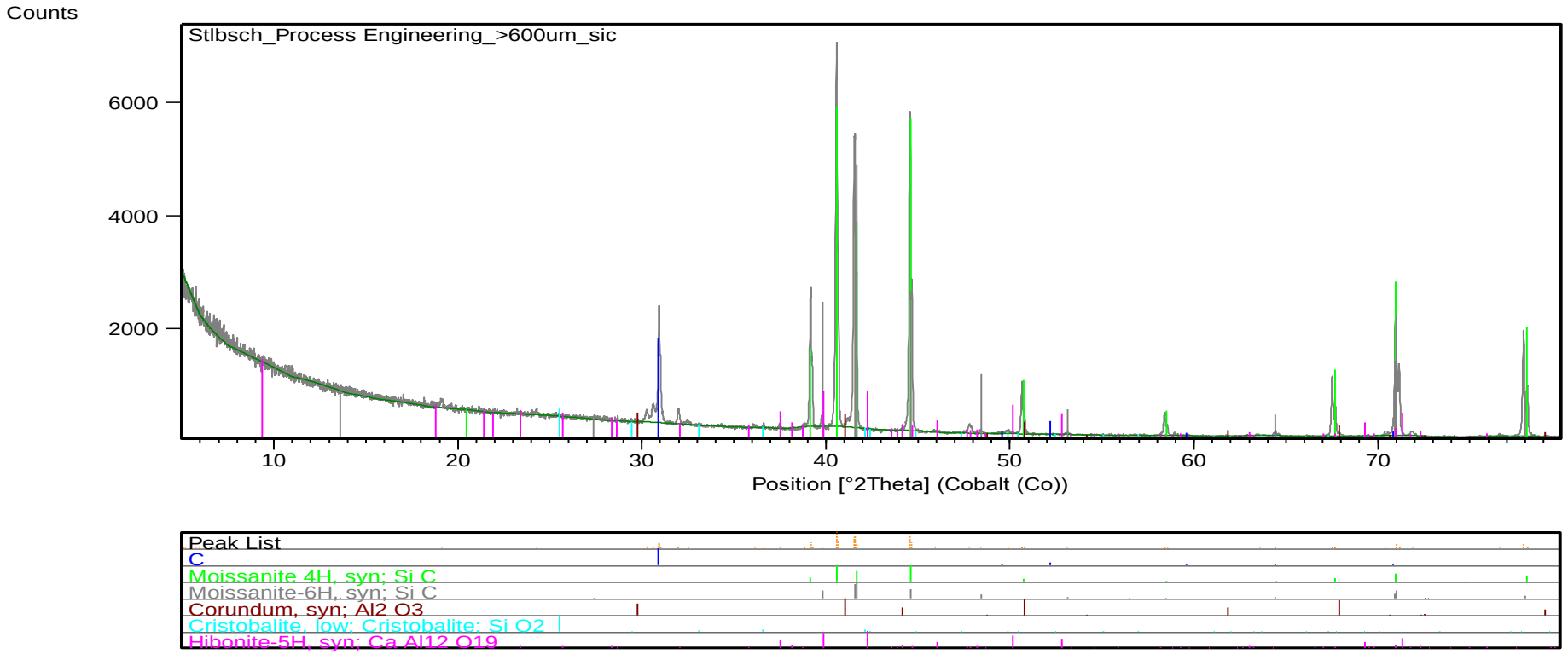

Figure A10 - Peak intensity graphs from XRD of SiC reductant (continued)

Table A8 – XRF results of Rowland LG concentrate for respective screen sizes

	Al2O3	**CaO**	**Cr2O3**	**Fe2O3**	**K2O**	**MgO**	**MnO**	**Na2O**	**P2O5**	**SiO2**	**TiO2**	**LOI**	**Sum Of Conc.**
Microns	(%)	(%)	(%)	(%)	(%)	(%)	(%)	(%)	(%)	(%)	(%)	**(%)**	(%)
< 25	N/A	N/A	N/A	N/A	N/A	N/A	N/A	N/A	N/A	N/A	N/A	N/A	N/A
25-38	4.12	2.24	2.16	12.53	0.07	24.62	0.17	0.22	0.01	51.05	0.34	2.77	100.30
38-45	N/A	N/A	N/A	N/A	N/A	N/A	N/A	N/A	N/A	N/A	N/A	N/A	N/A
45-53	N/A	N/A	N/A	N/A	N/A	N/A	N/A	N/A	N/A	N/A	N/A	N/A	N/A
53-75	5.14	2.33	2.88	12.73	0.09	23.20	0.16	0.27	0.02	50.00	0.29	3.06	100.15
75-90	N/A	N/A	N/A	N/A	N/A	N/A	N/A	N/A	N/A	N/A	N/A	N/A	N/A
90-106	5.33	2.63	2.89	12.69	0.10	23.16	0.16	0.33	0.03	49.99	0.30	3.05	100.65
106-125	5.37	2.65	2.95	12.72	0.09	23.13	0.16	0.32	0.02	49.88	0.31	3.06	100.65
125-150	5.39	2.62	2.85	12.61	0.10	22.80	0.16	0.33	0.02	49.66	0.30	3.01	99.85
150-180	5.69	2.82	2.97	12.69	0.11	22.40	0.15	0.37	0.02	49.18	0.30	3.15	99.86
180-212	5.66	2.82	2.93	12.68	0.11	22.36	0.15	0.36	0.02	49.20	0.30	3.23	99.83
212-250	6.39	3.08	3.69	13.70	0.12	20.94	0.14	0.44	0.02	47.18	0.31	4.01	100.02
250-300	N/A	N/A	N/A	N/A	N/A	N/A	N/A	N/A	N/A	N/A	N/A	N/A	N/A
300-355	N/A	N/A	N/A	N/A	N/A	N/A	N/A	N/A	N/A	N/A	N/A	N/A	N/A
425-500	N/A	N/A	N/A	N/A	N/A	N/A	N/A	N/A	N/A	N/A	N/A	N/A	N/A
500-600	N/A	N/A	N/A	N/A	N/A	N/A	N/A	N/A	N/A	N/A	N/A	N/A	N/A
> 600	5.99	2.70	3.07	12.62	0.11	22.46	0.15	0.35	0.02	49.55	0.31	3.12	100.44

Table A9 – XRF results of Easterns LG concentrate for respective screen sizes

	Al2O3	**CaO**	**Cr2O3**	**Fe2O3**	**K2O**	**MgO**	**MnO**	**Na2O**	**P2O5**	**SiO2**	**TiO2**	**LOI**	**Sum Of Conc.**
Microns	(%)	(%)	(%)	(%)	(%)	(%)	(%)	(%)	(%)	(%)	(%)	**(%)**	(%)
< 25	N/A	N/A	N/A	N/A	N/A	N/A	N/A	N/A	N/A	N/A	N/A	N/A	N/A
25-38	4.12	2.50	3.65	13.88	0.08	23.77	0.18	0.18	0.01	48.60	0.30	2.36	99.63
38-45	4.51	2.81	4.07	14.18	0.09	23.52	0.19	0.26	0.01	48.03	0.31	2.25	100.22
45-53	N/A	N/A	N/A	N/A	N/A	N/A	N/A	N/A	N/A	N/A	N/A	N/A	N/A
53-75	N/A	N/A	N/A	N/A	N/A	N/A	N/A	N/A	N/A	N/A	N/A	N/A	N/A
75-90	N/A	N/A	N/A	N/A	N/A	N/A	N/A	N/A	N/A	N/A	N/A	N/A	N/A
90-106	4.69	2.97	3.75	13.72	0.10	23.34	0.18	0.27	0.01	48.26	0.30	2.23	99.82
106-125	4.81	2.94	4.18	14.14	0.10	23.36	0.18	0.25	0.01	48.11	0.31	2.22	100.61
125-150	4.87	3.00	3.95	13.94	0.11	23.20	0.18	0.29	0.01	48.25	0.31	2.28	100.39
150-180	N/A	N/A	N/A	N/A	N/A	N/A	N/A	N/A	N/A	N/A	N/A	N/A	N/A
180-212	5.00	2.91	4.20	14.10	0.11	22.89	0.18	0.23	0.02	47.54	0.30	2.35	99.82
212-250	4.97	2.71	4.29	14.19	0.10	22.74	0.18	0.23	0.02	47.26	0.31	2.32	99.31
250-300	5.43	2.88	5.57	15.52	0.10	22.17	0.18	0.26	0.02	45.60	0.34	2.39	100.45
300-355	N/A	N/A	N/A	N/A	N/A	N/A	N/A	N/A	N/A	N/A	N/A	N/A	N/A
425-500	5.18	2.90	4.99	15.05	0.10	22.48	0.18	0.32	0.02	46.57	0.33	2.35	100.47
500-600	5.02	2.92	4.67	14.69	0.10	22.72	0.18	0.26	0.02	47.11	0.31	2.40	100.41
> 600	5.08	2.88	4.75	14.71	0.09	22.63	0.17	0.28	0.02	46.74	0.31	2.49	100.14

Appendix B - Calculations

Table A10 – Specifics of pyro-metallurgical experiments conducted.

Experiment	Mass of concentrate (g)	Mass of reductant (g)	Combined mass after being mixed (g)	Mass of alloy button after experiment (g)
1	8.118	0.21	8.273	0.223
2	8.141	0.245	8.318	0.442
3	8.166	0.287	8.408	0.475
4	8.06	0.245	8.316	0.333
5	8.109	0.247	8.356	0.349
6	8.203	0.253	8.203	0.442
7	8.069	0.247	8.322	0.532
8	5.209	0.169	5.378	0.275
9	5.175	0.161	5.353	0.275
10	5.250	0.139	5.372	0.190
11	5.145	0.162	5.307	0.287
12	5.289	0.189	5.425	0.400
13*	5.175	0.161	5.854	0.460

- Experiment 13 was conducted with the addition of some converter slag. The amount added was 0.5175 g.

Calculations - metal fall % and recovery % of Fe and Pd is calculated as an example. Experiment 12 is used in this illustration.

$$\%\ metal\ fall = \frac{Alloy\ mass}{Initial\ concentrate\ mass} \times 100 = \frac{0.400}{5.289} = 7.463\ \%$$

$$\%\ Pd\ recovery = \frac{Pd\ in\ alloy}{Pd\ in\ initial\ concentrate} \times 100 = \frac{0.0126 * 0.400}{0.0011 * 5.289} \times 100 = 86.63\ \%$$

Conversion of Fe_2O_3 to FeO in concentrate :

$$Mass\ of\ FeO\ in\ Rowland\ LG\ concentrate = \frac{Mass\ of\ Fe_2O_3}{MM\ Fe_2O_3} \times 2\ \times MM\ FeO = \frac{12.730\ g}{159.697\ {}^{g}/_{mol}} \times 2\ \times 71.849\ {}^{g}/_{mol} = 11.457\ g$$

$$Mass\ of\ FeO\ in\ Easterns\ LG\ concentrate = \frac{Mass\ of\ Fe_2O_3}{MM\ Fe_2O_3} \times 2\ \times MM\ FeO = \frac{14.240\ g}{159.697\ {}^{g}/_{mol}} \times 2\ \times 71.849\ {}^{g}/_{mol} = 12.882\ g$$

Conversion of FeO to Fe in concentrate :

$$Mass\ of\ Fe\ in\ Easterns\ LG\ concentrate = \frac{Mass\ of\ FeO}{MM\ FeO}\ \times MM\ Fe = \frac{11.457\ g}{71.849\ {}^{g}/_{mol}} \times 2\ \times 55.85\ {}^{g}/_{mol} = 8.906\ g$$

$$Mass\ of\ Fe\ in\ Easterns\ LG\ concentrate = \frac{Mass\ of\ FeO}{MM\ FeO}\ \times MM\ Fe = \frac{12.882\ g}{71.849\ {}^{g}/_{mol}} \times 2\ \times 55.85\ {}^{g}/_{mol} = 9.956\ g$$

Note: The conversion of Fe_2O_3 and Cr_2O_3 to FeO and CrO in the slag samples are done similar to the above calculations.

Appendix C – TGA experiment methodology and result

TGA Methodology

A TGA experiment was conducted to establish a range of reduction times. The alumina pedestal with the attached crucible and its containing LG concentrate charge and SiC reductant were placed on a scale. The scale was connected to a computer with A VGA cable to acquire the change in mass of the concentrate charge. It was assumed that the mass of the crucible, refractory support material and alumina pedestal remained constant throughout the experiment. Therefore the only change in mass was that of the concentrate and reductant charge. The operation was made air tight and mass changes on the scale were noted every 0.5 s on a computer. Figure A11 shows the TGA experiment being conducted in the Carbolite STF1800 furnace. The reductant to concentrate ratio was 3 g SiC / 100 g Rowland LG concentrate and the temperature was 1600°C.

Figure A11 – A TGA experiment being conducted in a carbolite STF 1800 furnace at the Department of Process Engineering, Stellenbosch University. (1) – Tube furnace, (2) – Scale placed within an enclosed/air tight box made with plastic. (3) – Laptop computer connected to the scale to take mass readings from the scale every 0.5 s.

Purging calculations

By applying equation C1, it was possible to calculate the time required to reduce $pO_2 \leq 10^{-12}\ atm$ from the plastic box with Ar purging. The method that was used is known as sweep through purging. The method introduces a purge gas into a vessel at one opening and withdraws the mixed gas at another opening and vents in to the atmosphere, thus sweeping out residual gasses. The following equation was used to calculate the time required for purging [63]:

$$Q_t = \frac{V}{K} ln\left(\frac{C_1}{C_2}\right) \qquad \text{(Eq. C1)}$$

Where,

Q = Volume of Ar required for desired purging conditions

V = Volume of the area to be purged
K = Mixing correction factor (assumed to be 0.25)
C_1 = Initial O_2 concentration
C_2 = Required O_2 concentrate ($pO_2 \leq 10^{-12}\ atm$)

In order to reduce the volume of the box (Height = 144 mm, Length = 398 mm and width = 300 mm) which was calculated as 17.19 L, sealed plastic air bags inflated with Ar were place within the enclosed box. This reduced the volume to $\pm$ 1 L. The box is water sealed on the walls and therefore no air could have entered the system once the experiment was being conducted. Figure A12 was constructed with Eq. C1. The system was evaluated at 1 L, 2 L and 6 L of total volume.

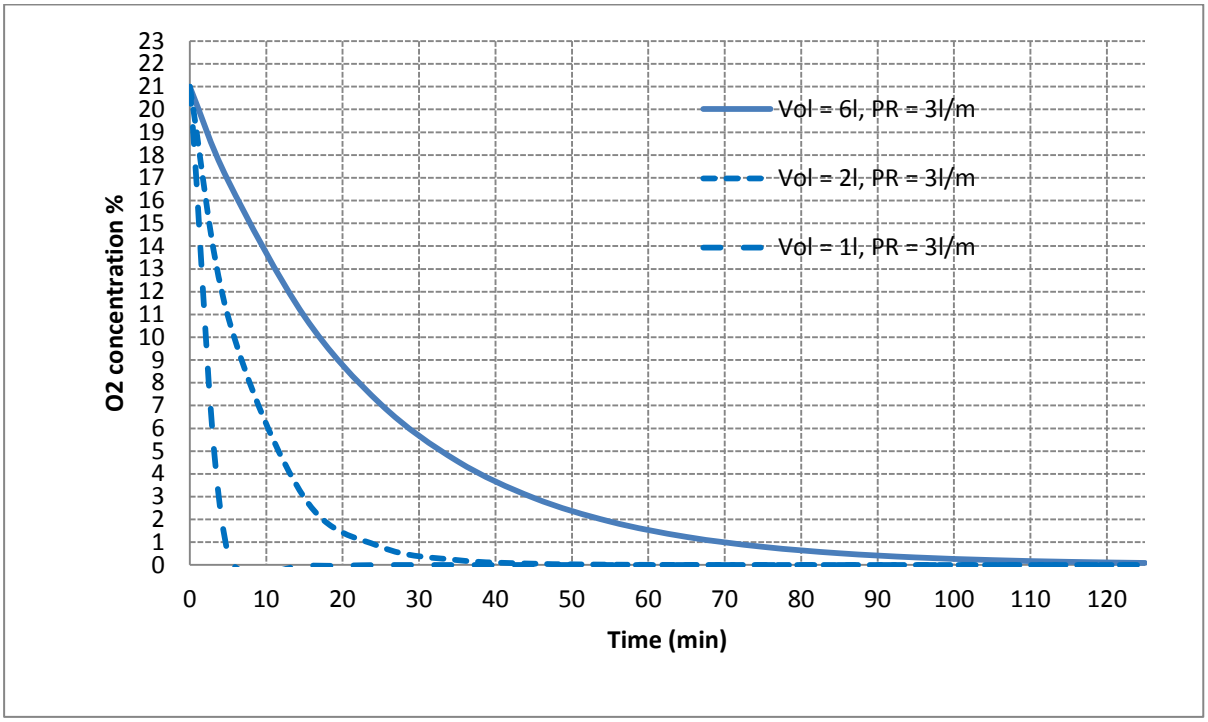

Figure A12 – The reduction of O_2 concentration as a function of time and purge volume (Vol = volume and PR = Purge rate).

It was therefore assumed that 30 min of Ar purging at 3 L/min will reduce the $pO_2 \leq 10^{-12}\ atm$. After 30 min, the Ar flow rate was reduced to 500 mL/min and the experiment was conducted.

TGA results

After the TGA experiment was conducted a graph of mass vs. time was constructed.

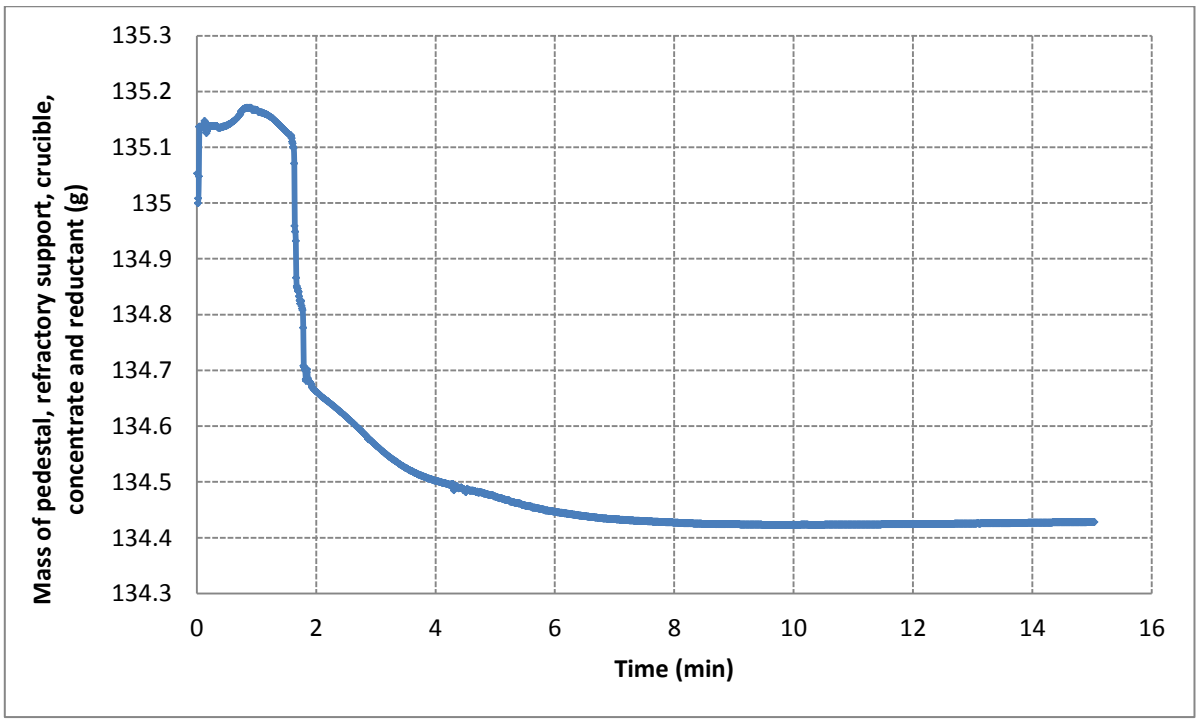

Figure A13 – The TGA experiment showing the change in mass as a function of time.

Figure A11 shows that no significant mass changes occurred after $\pm$ 10 min of reduction time. Therefore it is assumed that thermodynamic equilibrium should be reached for any experiment after 30 min.

Reader Notes: